INSTITUTO DE QUÍMICA

PROGRAMA DE PÓS-GRADUAÇÃO EM GEOCIÊNCIAS-GEOQUÍMICA

OMOTAYO ANUOLUWAPO FADINA

MERCURY DEPOSITION ON SOUTH AMERICAN AND AFRICAN MARGINS DURING THE LAST GLACIAL-INTERGLACIAL CYCLE- *EVALUATING THE IMPACTS OF EXTREME GLOBAL CLIMATE CHANGE ON THE MERCURY BIOGEOCHEMICAL CYCLE*

NITERÓI
2019

OMOTAYO ANOLUWAPO FADINA

MERCURY DEPOSITION ON SOUTH AMERICAN AND AFRICAN MARGINS DURING THE LAST GLACIAL - *A COMPARISON OF PALEOCLIMATIC DYNAMICS ON EITHER SIDES OF THE ATLANTIC OCEAN*

Tese apresentada ao Curso de Pós-Graduação em Geociências da Universidade Federal Fluminense, como requisito parcial para o obtenção do **Grau de Doutor**. Área de concentração: **Geoquímica Ambiental.**

Orientadora

PROF^{A}. ANA LUIZA SPADANO ALBUQUERQUE

Co-orientador

PROF. EMMANOEL VIEIRA SILVA-FILHO

NITERÓI
2019

OMOTAYO ANOLUWAPO FADINA

MERCURY DEPOSITION ON SOUTH AMERICAN AND AFRICAN MARGINS DURING THE LAST GLACIAL- ***A COMPARISON OF PALEOCLIMATIC DYNAMICS ON EITHER SIDES OF THE ATLANTIC OCEAN***

Tese apresentada ao Curso de Pós-Graduação em Geociências da Universidade Federal Fluminense, como requisito parcial para a obtenção do **Grau de Doutor**. Área de concentração: **Geoquímica Ambiental.**

Aprovada em 8 de Agosto, 2019

BANCA EXAMINADORA

PROF[A]. DRA. ANA LUIZA SPADANO ALBUQUERQUE
ORIENTADORA/UFF

PROF.DR. EMMANOEL VIEIRA DA SILVA FILHO
CO-ORIENTADOR/UFF

PROF. DR OLAF MALM
UNIVERSIDADE FEDERAL DO RIO DE JANEIRO

PROF. DR. JÚLIO WASSERMAN
UFF

PROF[A]. DR[A]. RUT AMELIA DIAZ RAMOZ
UFF

DR. IGOR MARTINS VENANCIO P DE OLIVEIRA
INSTITUTO NACIONAL DE PESQUISA ESPACIAL

NITERÓI
201

DEDICATION

To the King eternal, Immortal, Invisible, the God only wise.

ACKNOWLEDGEMENT

To Almighty God be all the glory for the successful completion of this work.

I would like to first express my gratitude to my supervisor, Profª. Ana Luiza Spadano Albuquerque, who afforded me this golden opportunity to embark on the Doctor of Philosophy degree under her tutelage. I cannot imagine having a more knowledgeable, understanding and kind supervisor than you, ma. I also appreciate the support of my co-supervisor, Prof. Emmanoel Vieira Silva-Filho in the course of the Ph.D. study and research. I am thankful to you both.

My very special gratitude goes to Coordenação de Aperfeiçoamento de Pessoal de Nível Superior - Brasil (CAPES) for providing the funding for this Ph.D. research. I profoundly thank the members of staff of Petrobras Core Repository (Macaé/Petrobras) and the International Ocean Discovery Program (IODP) Bremen Core Repository (BCR) for supplying the sediments used in this study.

I appreciate the Ph.D. thesis examiners for their insightful remarks and suggestions. I equally thank all members of staff of the Department of Geochemistry, Fluminense Federal University. My sincere appreciation goes to Profª. Carla Seminaris who gave access to her laboratory for part of this research. I am also grateful to Prof. Andre for his stimulating discussions, suggestions, and support.

I sincerely appreciate the help of LOOP research group members. In particular, I thank Catarina, Camila, Diego, Giselly, and Thais, for their support while working in the laboratory. I thank the Post-doc researchers; Bruna, Douglas, Lu, Manuel and Thiago, you welcomed me warmly into the department and gave me all the support I needed academically and in settling into the Brazil system. I thank my entire classmates, especially my co-researchers; Jojo, Alicia, and Paty. It was great working with you all. A very special gratitude goes to Igor for his immense and unfailing support in consolidating the ideas of this thesis.

I am grateful to my amazing parents, Prince and Dr. (Mrs.) O. Fadina, as well as my siblings Femi and Tosin, for their love and rock-solid support throughout this period, and life in general. I am also thankful to my other family members and friends who have supported me all-the-way. Agba, Funmi, Hamdia, Hendrika, Labake, Mariana and Shakirat, thank you all for believing in me. I thank my dear Uncle David Goriola for his love and support.

I appreciate Pastors Ijaopo for their constant prayers and love. I am immensely grateful to my Brazilian parents, Anthony and Miriam, as well as Edimilson and Rute, for their inestimable love and support. I also appreciate the leadership and members of Igreja Methodist Vital Brasil, for their warm reception and kindness.

And finally, last but by no means least, to my dear daughter, Oluwatamilore (TAMMY), with whom I embarked on this journey at a tender age of seven (7) months, I simply lack words to express how much you mean to me. Thank you for being my ‘sunshine’. I love you to the moon and back, a million times and more.

"God created everything by number, weight and measure."

"I have a fundamental belief in the Bible as the Word of God, written by those who were inspired. I study the Bible daily."

"In the absence of any other proof, the thumb alone would convince me of God's existence."

—***Sir Isaac Newton***

RESUMO

Nesta pesquisa de doutorado, testemunhos sedimentares marinhos coletados nas margens continentais oeste e leste do Atlântico Sul foram utilizados para reconstruir as variações no conteúdo de mercúrio (Hg) durante o último ciclo glacial / interglacial. Nesse sentido, o testemunho GL-1248 coletado na margem continental do nordeste do Brasil cobriu os últimos 128 ka, enquanto que o testemunho ODP1077 recuperado da área de leques do Rio Congo (África) cobriu os últimos 130 ka, e ambos foram estudados com o intuito de entender e comparar os principais mecanismos impulsionadores da acumulação de Hg. Os resultados mostraram que as concentrações de Hg no GL-1248 variaram entre 14,95 e 69,43ng/g, e variando em periodicidades de 56 ka e 900 anos, sugerindo a presença de alterações glacial-interglaciais, como também de variabilidade da escala milenar. Tendências paralelas observadas nos diagramas de Hg e XRF-Fe sugerem que, após a deposição de Hg atmosférico no continente, o Hg foi incorporado à compostos com Fe e posteriormente transportados, com eventual imobilização no talude continental do Nordeste do Brasil. Já na margem Africana, as concentrações de mercúrio medidas no ODP1077 variaram significativamente com concentrações entre 23,12 ng/g e 256 ng/g, demonstrando um padrão antifásico com a relação a razão Fe/Ca, o que distingue entre períodos de aumento de aporte de material terrígeno. Essa tendência inversa observada entre o conteúdo de Hg e a razão Fe/Ca indica que, durante os períodos de maior (menor) aporte de material terrígeno, com menores (maiores) acumulações de mercúrio nos sedimentos marinhos. A concentração de mercúrio se correlaciona positivamente com dados semiquantitativos de Calcio (XRF-Ca), sugerindo que a matéria orgânica marinha controla o sequestro de mercúrio nos sedimentos marinhos nessa região. Embora ambos os testemunhos marinhos tenham sido recuperados na região tropical e cubram os mesmos períodos glaciais / interglaciais, suas concentrações de mercúrio e os principais impulsionadores das concentrações de mercúrio são diferentes. Esse estudo conclui que os processos climáticos regionais e as condições geoquímicas regionais são essenciais controlar as variações de Hg nos arquivos ambientais. Além disso, esse estudo também demonstrou que a fonte de carbono orgânico sedimentar é determinante como parâmetro-chave controlador da acumulação de mercúrio, devido a sua grande afinidade.

PALAVRAS-CHAVE
Acumulação de mercúrio; Sedimentos marinhos; Ciclo Glacial / Interglacial, Eventos milenares; nordeste do Brasil; Leque do Rio Congo

ABSTRACT

In this PhD research, sediment cores collected from the Western and Eastern South Atlantic continental margins are used to reconstruct mercury (Hg) variations over the last glacial/interglacial cycle. Using marine sediment cores GL-1248 collected from the continental slope off northeastern Brazil and dating to 128 ka, as well as ODP1077 retrieved from the Congo deep-sea fan area and covering the last 130 ka, this study aims to reconstruct mercury (Hg) variations over the last glacial/interglacial cycle. Alongside relevant paleo-proxies, the main drivers of Hg accumulation in both marine sediment cores are established and compared. This work pays special attention to understanding the processes that control mercury remobilization, transportation and eventual accumulation in marine sediments. Hg concentrations in GL-1248 ranged between 14.95 and 69.43ng/g, and varied with periodicities of 56 ka and 900 yr suggesting the presence of glacial-interglacial changes and millennial-scale variability respectively. Parallel trends of Hg and XRF-Fe plots suggest that following atmospheric Hg deposition onto the continent, Hg is incorporated with Fe-compounds before transportation and eventual immobilization at the NE Brazil continental slope. Mercury concentrations in ODP1077 varied significantly having concentrations between 23.12 ng/g and 256 ng/g, and its plot exhibits an anti-phase pattern with the Fe/Ca ratio plot that distinguishes between periods of increased and decreased terrigenous material delivery. This inverse trend in the plots of mercury concentration and Fe/Ca ratio shows that during periods of increased (decreased) terrigenous material delivery, less (more) mercury accumulates in the marine sediment. However, mercury concentration correlates positively with XRF-Ca implying that marine organic matter controls mercury sequestration into marine sediments. Although both marine sediment cores were retrieved from the tropics and cover the same glacial/interglacial periods, their mercury variations and the main drivers of mercury concentrations are dissimilar. The outcome of this study shows that regional climate processes and geochemical conditions are essential to Hg variations in environmental archives. Another obvious finding from this study is that the source of sedimentary organic carbon is a key determinant of their affinity for mercury.

KEYWORDS
Mercury accumulation; Marine sediments; Glacial/Interglacial climate, Millennial-scale events; northeastern Brazil; Congo deep-sea fan

ABBREVIATIONS
(in alphabetical order)

AC	Angola current
Al	Aluminium
AMS	Accelerator Mass Spectrometry
BC	Benguela Current
BCC	Benguela Coastal Current
BOC	Benguela Oceanic Current
Ca	Calcium
Cdb	citrate-dithionate-bicarbonate
Fe	Iron
GICO	Greenland Ice Core Chronology
HCl	Hydrochloric acid
Hg	Mercury
HS	Heinrich Stadials
ICP-AES	Inductively Coupled Plasma Atomic Emission Spectroscopy
ITCZ	Intertropical Convergence Zone
ka	Thousand years
Kv	Kilo volts
LGM	Last Glacial Maximum
M	meters
MIS	Marine Oxygen Isotope Stage
NBC	North Brazil Current
Nd	Neodymium
NE	Northeast
NECC	North Equatorial Countercurrent
NGRIP	North Greenland Ice Core Project
NRCC	National Research Council Canada
º	Degrees
ODP	Ocean Drilliing program
OM	organic matter
RSL	Relative Sea-Level
S	South
SEC	South Equatorial Current

SECC	South Equatorial Countercurrent
TOC	Total Organic Carbon
USA	United States of America
W	West
WHO	World Health Organization
XRD	X-ray powder Diffractometer
XRF	X-ray Fluorescence
$\delta\ ^{13}C$	Carbon stable isotope
$\delta\ ^{15}N$	Nitrogen stable isotope

LIST OF FIGURES AND TABLE

TABLE OF CONTENT

1. INTRODUCTION

Mercury (Hg) is a volatile, bioaccumulating trace metal. It is deleterious to the human health and the environment, and is emitted into the environment from both natural and anthropogenic sources. Mercury can be transported from point sources to remote locations (Schoroeder and Munthe, 1998), where it travels through the atmosphere-soil-water distribution cycles and can remain in circulation for years (Rice et al., 2014). Natural sources of mercury include volcanoes, cinnabar (ore), forest fires, geothermal vents, and rock weathering, and anthropogenic sources are agriculture, landfill, manufacturing and industrial processes, power generation as well as coal and fuel combustion (Amos et al., 2013). Mercury is volatile at room temperature and has a complex and an unpredictable behaviour in the environment, with the ability to exist in the liquid and gaseous states of matter. In the atmosphere, it exists mainly as Gaseous Elemental Mercury (GEM). Surface waters are generally supersaturated with this gaseous form of mercury (Morel et al., 1998; Fitzgerald et al., 2007) due to their exposure to the atmosphere. Elemental mercury (Hg^{o}) can be oxidized into divalent mercury (Hg II), in the atmosphere, and washed out by rainfall (Hall, 1995).

The interactions of mercury in the environment is intriguing, making the mercury biogeochemical cycle one of the 'most scientifically challenging' on the Earth's surface (Fitzgerald and Lamborg, 2003). Atmospheric deposition is the main source of Hg to both land and water bodies. Its deposition occurs both by dry and wet deposition, with the oceans as its largest recipient. Its sources and post-depositional fluxes within different reservoirs (atmosphere, soils, sediments, oceans, ice, etc) constitute the global Hg biogeochemical cycle [Figure 1] (Mason and Sheu, 2002; Sunderland and Mason, 2007; Selin et al., 2008; Holmes et al., 2010; Smith- Downey et al., 2010; Driscoll et al., 2013), with the global ocean being its largest sink (Pirrone et al., 2010). Asides its function as a Hg sink, the oceans play an essential role in the global Hg cycle because over 70% of the Hg deposited in the ocean is re-

emitted to the atmosphere (Mason and Sheu, 2002; Soerensen et al., 2010; Corbitt et al., 2011), therefore operating also as a source of atmospheric Hg (Mason et al., 1994; Mason et al., 2001). Irrespective of its source, deposited Hg can be emitted back into the atmosphere from the oceans, soils and vegetation, as well as through biomass burning (Mason et al., 2012), or remobilized to secondary locations. Furthermore, its deposition and recycling within the ecosystem have been found to be controlled by environmental factors.

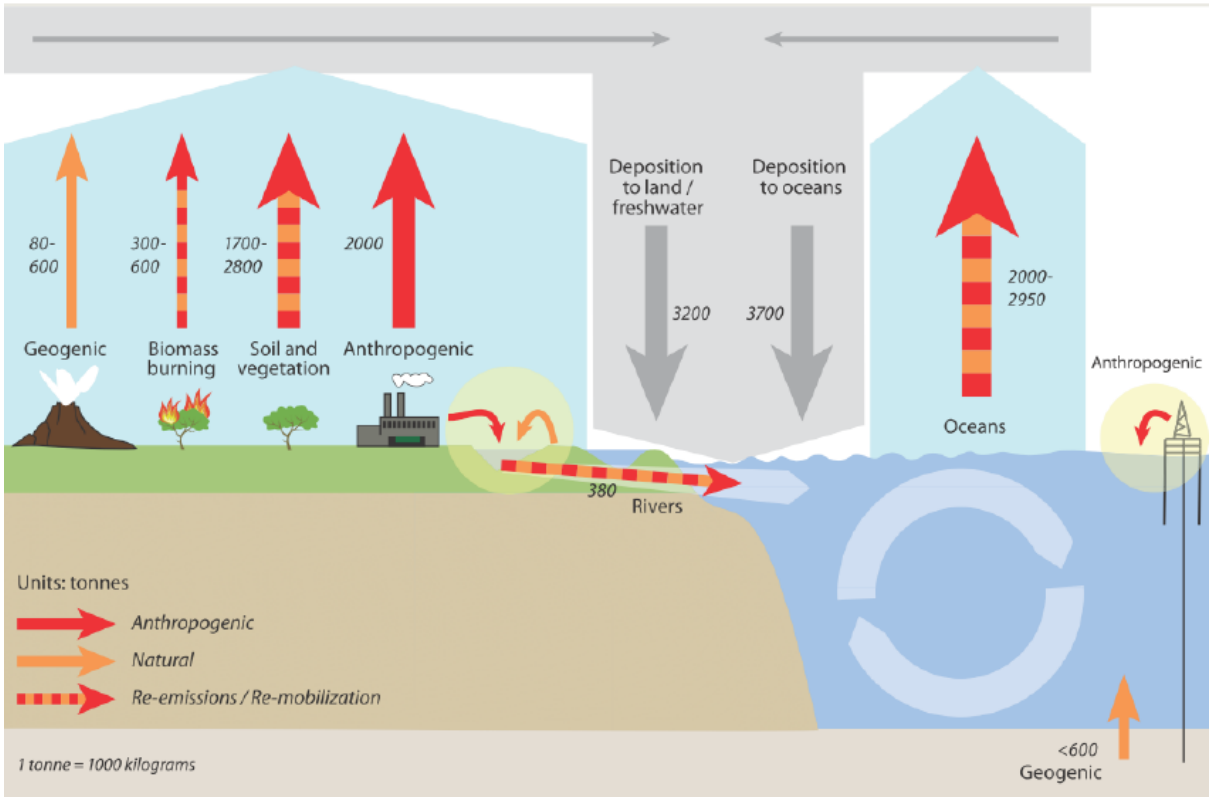

Figure 1: The Global Mercury Cycle (adapted from Mason et al., 2012)

Although most studies on mercury (Hg) are focused on its depositional and post-depositional processes, as well as environmental health impacts, recent studies on Hg variations in environmental archives highlight the role of climate in modulating Hg deposition and accumulation. Hg emissions from natural sources (mainly volcanic eruptions) are the largest source of Hg into the atmosphere and an essential component of the global Hg cycle (Gworek et al., 2016), with concentrations in natural archives varying over past climatic cycles (Jitaru

et al., 2009). Its dynamics in the environments are controlled by global and regional climatic factors such as productivity, sea ice cover, riverine discharge, sea-level changes, and precipitation patterns. For instance, evidences from certain studies (Bay et al., 2004; Baldini et al., 2015) suggest a direct relationship between the occurrence of millennial climate changes and volcanism, inferring that atmospheric Hg from volcanic sources is likely to increase during millennial scale events. Studies of sedimentary Hg profiles in environmental archives such as lake sediments, peats, glacial ice, and marine sediments have been used in paleoclimatic and paleoenvironmental reconstructions (Nriagu 1992; Engstrom and Swain 1997, Santos et al., 2001; Pérez-Rodríguez et al., 2015) in order to understand how natural processes affect Hg cycling in the environment. For example, Vandaal et al., (1993) and Jitaru et al., (2009) recorded higher Hg deposition during cold climates than in warm ones, thus highlighting the role of high atmospheric dust loads on Hg deposition during cold climates. In addition, studies have identified organic matter (OM) as the major driver of Hg accumulation in ocean sediments, which is supported by significant positive correlations between Total Organic Carbon (TOC) and Hg variations in the respective archives (Grasby et al. 2013; Kita et al., 2013; Kita et al., 2016). To determine the effect of the Intertropical Convergence Zone (ITCZ) on atmospheric Hg deposition, Kuss et al., (2011) and Soerensen et al., (2014), compared atmospheric and aquatic Hg concentrations across the latitudinal transect of the Atlantic Ocean (Kuss et al. 2011; Soerensen et al., 2014). Aquatic Hg concentrations were found to be higher in the surface water below the Intertropical Convergence Zone (ITCZ) compared to those of other latitudes, regardless of the low atmospheric Hg concentration near the ITCZ location. As such, the authors concluded that precipitation in the ITCZ favors Hg-wet deposition into the surface water below the ITCZ.

Upwelling zones are characteristically important in driving ocean biogeochemical processes because of their high primary productivity. Therefiore, Hg sequestration to marine sediments

is expected to increase in these high productivity zones. According to Rolfhus and Fitsgerault (1995), upwelling regions are noteworthy to the Hg biogeochemical cycle due to the usual high productivity and large organic matter deposition that occur in the regions. However, very limited studies address sedimentary Hg biogeochemistry in upwelling regions. In a study on Hg deposition in sediments from Cabo Frio, an upwelling region in Southeast Brazilian continental shelf (Figueiredo, et al, 2013), the high Hg flux recorded was attributed to the large organic matter deposition typical of the upwelling region. While a large number of published studies (e.g. Outridge et al., 2007; Stern et al., 2009, Grasby et al., 2013, Kita et al., 2013 and 2016) have established significant positive correlations between Hg and organic matter in environmental archives within and outside of upwelling regions, some authors (e.g. Roulet et al. 1998; Oliveira et al., 2001; Fadini and Jardim, 2001), have identified uncharacteristic trends in Hg post-depositional process in South American soils and sediments that links Hg variations to Iron (Fe) -oxyhydroxides rather than with organic matter (Roulet et al. 1998; Fadini and Jardim, 2001; Oliveira et al., 2001).

With regards to forest fires, they equally play an essential role in the understanding of global atmospheric Hg sources. Although their impacts are evident only in specific instances (Corella et al., 2017), they are important in the release of mercury (Hg) stored in vegetation and soils into the atmosphere. Thus, higher frequencies and intensities of forest fires will likely result in increased Hg emissions from soils (Amos et al., 2013). Mercury releases from volcanic activities and forest fires have been registered in mountain lakes from the Northern Patagonian Andes (Daga et al., 2016). In a study by Power et al., (2008), charcoal data suggested that the recorded rise in atmospheric Hg concentration is consequent to an increase in fire activity during the Last Glacial Maximum at the tropical latitudes of South America. Similarly, according to Cordeiro et al., (2011), warmer temperatures and the high rates of

forest fires of the late Holocene in the Brazilian Amazon are key factors which lead to increased mercury deposition.

Several studies (e.g, Martínez Cortizas, et al., 1999; Jitaru et al., 2009; Outridge et al., 2007 and Kirk et al., 2011), have established that Hg profiles are driven by climate-modulated processes, however, limited comparative analyses of the influence of climate process on Hg deposition in Western and Eastern South Atlantic Ocean exist. On the Western South Atlantic, Santos et al., (2001) showed that the threefold increase in Hg deposition of a sediment core from Lake Pata (northern Amazon) during the Holocene compared with the Last Glacial Maximum (LGM) was due to the high temperatures and the prevalence of forest fires during the Holocene. Other studies also show that Hg fluxes were significantly higher during wet climate episodes compared to dry ones (Lacerda et al. 1999; Barbosa et al., 2004). In a recent study from Caço Lake, NE Brazil (Lacerda et al., 2017), Hg fluxes for the last 22 ka were associated with global changes in atmospheric dust and climate, as well as global volcanism. On the Eastern South Atlantic however, literatures on Hg dynamic over varying climatic conditions are lacking. For this study, marine sediment cores GL-1248 from the continental slope off northeastern Brazil covering the last 128 ka and ODP 1077 from the Lower Congo Basin off West Africa extending to the last 130 ka were studied. In subsequent chapters, details of the research objectives, methodology, results and discussions are explained. In section 3, regional conditions of both study sites are separately discussed in subsections 3.1.1 and 3.1.2. Also, analyses which were carried out on only one marine sediment core are identified. All results of analyses from the two (2) studied cores are presented in section 4 under two broad subsections. In section 5, the discussion is presented in three (3) parts; the first two (2) parts sub-sections 5.1 and 5.2 discuss the climate mechanisms responsible for Hg dynamics in northeastern Brazil and Lower Congo Basin

respectively, while subsection 5.3 compares Hg responses in both locations over changing climate.

2. RESEARCH OBJECTIVES

General Objective

The main objective of this study is to understand the variations in mercury deposition over timescales covering the last Glacial-Interglacial cycle (~130 ka till recent) from marine sediments from the South American and African continental shelves. Using other proxies from the studied marine sediment cores, as well as regional and global climate proxies, the climate mechanisms responsible for mercury variations on either side of the South Atlantic are explored. Further to the general objective, this work pays special attention to explore the following specific objectives:

Specific Objectives

- ✓ Determine if the mercury deposition and accumulation in the South American and African margins are consequent to the same factors and synchronous;
- ✓ Determine the impacts of abrupt global climate change over the mercury deposition;
- ✓ Compare the climate impact over mercury deposition on both sides of the South Atlantic Ocean.

3. MATERIALS AND METHODS

3.1 Study sites

To accomplish the objectives of this research, two (2) marine sediment cores from the South American and African margins were studied. The two cores exhibit few similarities in that their locations are within the tropics (Figure 2), they both date back to the last interglacial (LIG), and are influenced by branches of the South Equatorial Current (SEC).

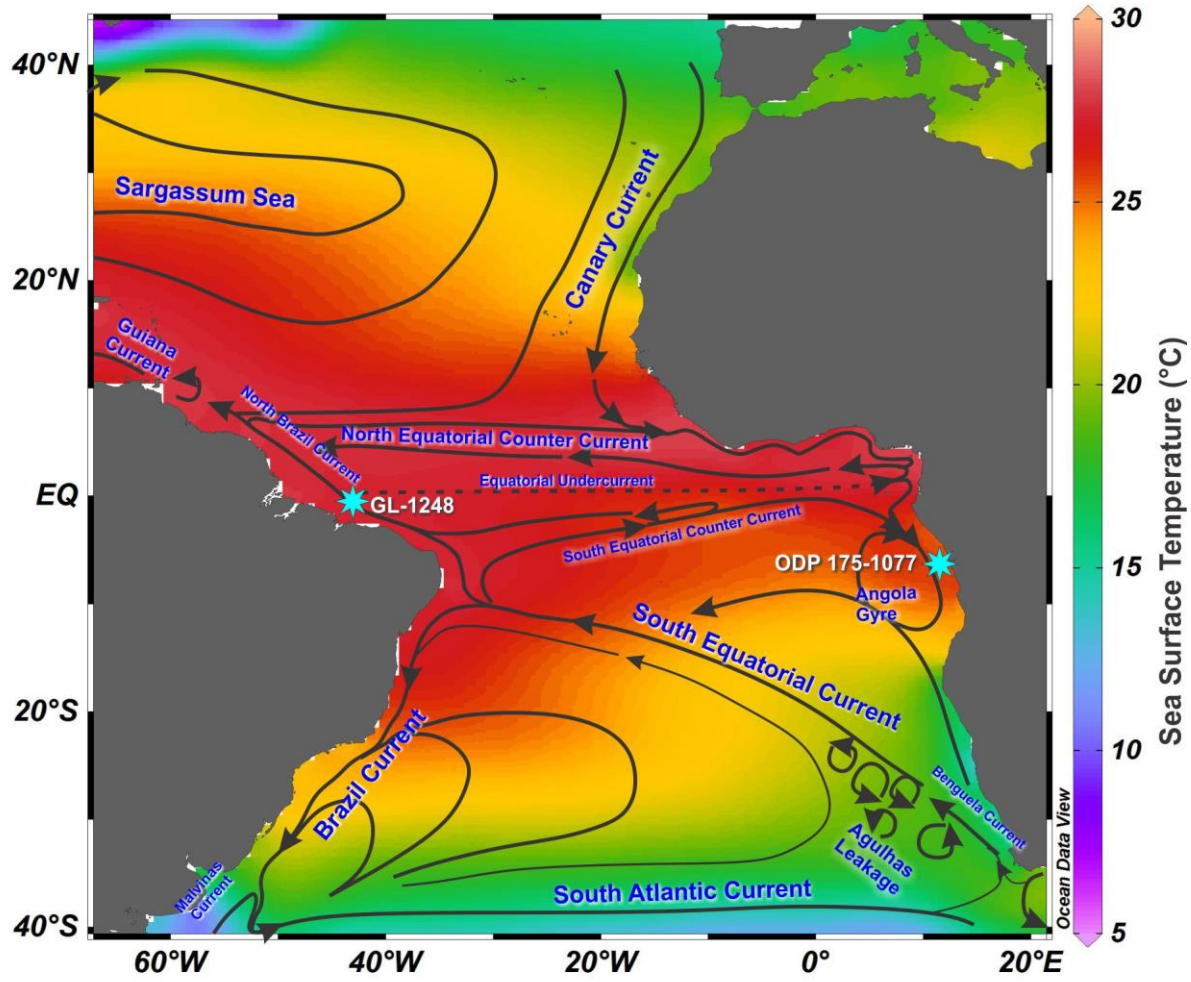

Figure 2: : Map showing the positions of the marine sediment cores GL-1248 (0°55.2'S, 43°24.1'W) and ODP 175-1077 (5°10.8´S, 10°26.2´E) used in this study. They are located on the continental slope of northeastern Brazil and the Congo deep-sea fan respectively. Also shown are surface currents including South Equatorial Current (SEC), North Brazilian Current (NBC), Brazilian Current (BC), South Equatorial Counter Current (SECC) and North Equatorial Counter Current (NECC).

3.1.1 Marine sediment core GL-1248

Marine sediment core GL-1248 (0°55.2'S, 43°24.1'W, 2264 m water depth, 19.29 m long) was collected by Petrobras from the continental slope off northeastern Brazil, a location under the influence of the North Brazil Current (NBC) and at a distance of about 280 km to the north of the mouth of the Parnaíba River (Figure 3). Located northwest to the core site at a distance of approximately 739 km is the mouth of Amazon River. The 6,400 km long Amazon River is the world's largest river in terms of discharge volume (209,000 m^3/s), and accounts for approximately a fifth of global freshwater discharge (Richey et al., 1990; Moura et al., 2016). Comparing the average distances of both rivers to the core site, the Parnaíba River is in closer proximity, therefore is more likely to be the source of fluvial waters and terrestrial sediments to our core site. The River´s main course has a length of approximately 1,400 km (Ramos et al., 2014), and the modern Parnaíba drainage basin area is approximately 344,000km^2 (Marques et al., 2004). The Parnaíba River serves as a transition zone between the Caatinga's semi-arid land in the east area of the basin, and the more humid climate of Cerrado, in the west (Rosa et al. 2003; Ramos, 2012). The Caatinga is a mixed biome comprising of shrubs with areas of periodically dry forest (Leal et al., 2005), while the Cerrado is characterised by varying vegetation structure ranging from dense grassland with sparse shrubs coverings and small trees, to densely covered woodlands (Ratter et al., 1997). Dominant soil types in the basin include latosols, plinthosols, podzols, lithic soils and quartz sands (Paula Filho et al., 2015). The dominant vegetation in the region are the Caatinga, the Cerrado, the semideciduous forest and the coastal vegetation. Two transitional areas namely the Caatinga/Cerrado and Cerrado/Semideciduous forest have also been identified (Farias Castro, 2003).

The climate in northeastern Brazil is tropical and semi-humid with a wet season between the months of March through May. The precipitation regime is mainly influenced by seasonal

Intertropical Convergence Zone (ITCZ) migrations (Hastenrath, 2012). In the boreal summer and fall when southeast (SE) trade winds are intense, the ITCZ is displaced northwards (Hastenrath and Merle, 1987). During boreal winter and spring when the northeast (NE) trade winds are intensified, the ITCZ attains its southernmost position, leading to enhanced precipitation in the Parnaíba River catchment (Hastenrath, 2012).

The upper water column circulation off northeast Brazil is mainly influenced by the NBC dynamics (Figure 3). The NBC originates from the northern branch of the bifurcation of the South Equatorial Current (SEC) at 10ºS (Stramma et al., 1995). The NBC transports warm and salty waters to the North Atlantic and the strength of its transport varies seasonally with the trade wind system. With an intensification of the SE trade wind during the boreal summer, the NBC flows north eastwards retroflecting at 6º-7ºN (Johns et al., 1998) and feeds the North Equatorial Counter Current (NECC), which transports surface waters eastwards (Richardson and Reverdin, 1987). Conversely, when the NE trade winds gain strength during boreal winter, NBC transport reduces (Stramma et al., 1995; Johns et al., 1998) leading to the weakening or total absence of NECC thereby aiding NBC north-westward flow along the South American continental margin (Hastenrath and Merle, 1987; Stramma et al., 1995).

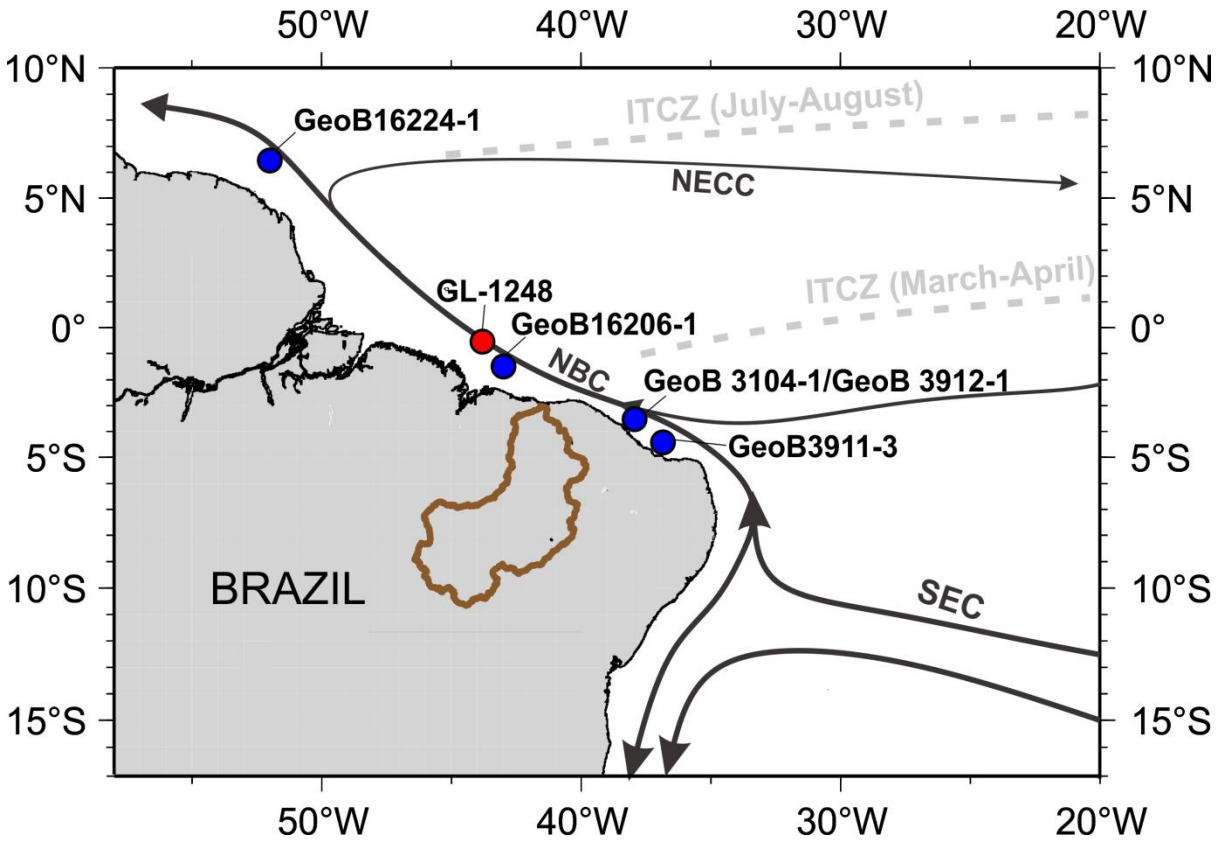

Figure 3: Map showing the Parnaíba basin, NE Brazil and the location of marine core GL-1248 (0°55.2'S, 43°24.1'W) in red dot. Blue dots represent other cores discussed in the text namely: GeoB 16206-1 (1◦34.75'S43◦ 01.42'W) / GeoB 16224-1 (6◦39.38'N52◦ 04.99'W) [Zhang et al., 2015] and GeoB 3104-1/GeoB 3912-1 (3◦40.0'S, 37◦43.0'W) / GeoB 3911-3 (4◦36.8'S, 36◦38.2'W) [Jennerjang et al., 2004]. The grey dotted lines show the seasonal positions of the Intertropical Convergence Zone (ITCZ) during boreal winter (July – August) and boreal summer (March – April) when it attains northernmost and southernmost positions respectively. Also shown are relevant surface currents namely the South Equatorial Current (SEC), the North Brazil Current (NBC) and North Equatorial Counter Current (NECC) in Black solid lines with arrows (adapted from Stramma and England, 1999). The boundary of the Parnaíba basin is marked in brown line.

3.1.2 Marine sediment ODP1077

Marine sediment ODP 1077(5°10.8´S, 10°26.2´E, 2,384m water depth), was collected in the Lower Congo Basin off West Africa during the Ocean Drilling Program (ODP) [Dupont et al., 2001; Jansen and Dupont, 2001]. The Congo deep-sea fan, located in the Eastern tropical Atlantic off the Western African margin, is one of the largest submarine depocenters of the world in the Cenozoic (Savoye et al., 2009). The core site is situated in the north (~273 km offshore) of the Congo River deep-sea fan (Figure 4) and is one of the three drilling sites

(1075, 1076, and 1077) along a transect on the northern rim of the Congo River plume (Shipboard Scientific Party, 1998a). The 4,700 km long Congo River is the second largest in the world in terms of discharge volume (41,800 m^3/sec) and mean annual flow (1,300 km^3), and it supplies freshwater, nutrients (and dissolved silica [Giresse et al., 1990]) and terrigenous particles to the Atlantic Ocean.

The Congo River is crescent shaped and it has a unique feature being the only large river in the world to cross the Equator twice (Molliex et al., 2019). The climate of the Congo Basin is predominantly tropical (hot and humid) around the equatorial region, and the Congo River discharge regime is linked with precipitation and monsoonal circulation (Eisma and van Bennekom, 1978; van Bennekom and Berger, 1984; Gasse, 2000). Owing to the fact that the basin crosses the north-south global climatic zone, seasonal movements of the ITCZ is the dominant factor controlling rainfall in the basin, which is predetermined by the seasonal variations of the trade winds regime (Eriksen and Katz, 1987). The basin experiences two wet seasons; the northern hemisphere wet season from April to September that maintains the outflow of the southerly flowing tributaries (e.g. the Oubangui River), and the northerly flowing tributaries of the southern catchment having high flows during the southern wet season, from October to May. A larger part of the north central and east central Congo Basin, north of the Equator has no dry season although the rest of the basin experiences two wet and dry seasons; maximum rainfall occurs over November - December with the rainy season being 7–12 months long (Nicholson 2000). Consequently, the Congo River has a double discharge peak flow regime, although there is a limited water level fluctuation in Malebo Pool at the Lower Congo River (Runge, 2008). The larger peak occurs during November–January, and a smaller, second peak occurs during April–June (Eisma and van Bennekom, 1978; Laraque et al. 2009). Modern freshwater outflow from the Congo River is observable by diminishing surface water salinities reaching a maximum extension of 800 km offshore

between February and March; meanwhile the river-plume attains its most westward to northwestward direction when the monsoonal circulation and precipitation reach their maximum seasonal intensities in August – October (van Bennekom and Berger 1984). The main direction of the plume is WNW close to the river mouth. Offshore the direction of the plume axis changes to SW or SSW in February and March, to W or WSW from April to August, while in October and November the plume spreads in a NW direction (van Bennekom and Berger, 1984).

The modern vegetation in the Congo catchment area is controlled by tropical rain forest whose productivity is determined by the West-African monsoon (Ning and Dupont, 1997). The late Quaternary insolation cycles strongly influenced African paleoclimate that varied between arid conditions during glacial and interglacial periods, to humid conditions characteristic of their warm periods. Previous observations using marine palynological records showed that an expansion of the savannah belts occurred on both sides of the equator during dry climatic conditions to replace the tropical rain forest being the dominant type of vegetation in the Congo catchment area (Frédoux, 1994; Jahns et al., 1998; Dupont et al., 2001).

The surface and subsurface ocean circulation in the Congo deep-sea fan is dominated by the Angola Current (AC) and the Benguela Current (BC) (Figure 4). The AC transports warm, saline, low nutrient water to the southeast between 5 and 14°S along the African coast, and is fed by the shallow subsurface warm South Equatorial Countercurrent (SECC) which flows eastward. The Benguela Coastal Current (BCC) transports cold and nutrient-rich waters northward across the Walvis Ridge (Uliana et al., 2002). Between 24 to 30°S, the BC splits into two branches, the Benguela Oceanic Current (BOC) that migrates to the Northwest before joining the South Equatorial Current (SEC), and the BCC that flows along the coast (Hatin et al., 2017). The AC and BCC converge between 14 and 17°S and form a strong

temperature and productivity gradient called the Angola-Benguela Front (ABF) [Figure 4]. The ABF separates low productivity waters to the north from high productivity waters to the south (Shannon et al., 1986). The position of the ABF varies with the intensity of the AC and BCC (Meeuwis and Lutjeharms, 1990), which are predetermined by changes in the seasonal atmospheric circulation (Shannon and Nelson, 1996). The complex interaction of AC, SECC and BC between 5 and 15°S leads to the formation of a gyre known as the Angola Dome (AD) (Meeuwis and Lutjeharms, 1990). The gyre pumps sub-surface waters upwards causing a seasonal oceanic upwelling with nutrient-rich waters into the photic zone. Two seasonal coastal upwelling cells have been detected south and north of the Congo River mouth at 5 and 7°S (Lutjeharms and Meeuwis, 1987). When nutrient-rich freshwater from the river is forced through the narrow estuary, river induced upwelling of subsurface oceanic waters occurs (Jahn et. al., 2005). Beyond this zone of high productivity, primary production in the region is solely dependent on oceanic mixing of nutrients from subsurface to surface waters (van Bennekom and Berger 1984). Consequently, the surface water in the region is characterised by very high primary productivity assumed to be caused by riverine input from the Congo River, upwelling of subsurface oceanic waters, and by open-ocean inputs (Uliana et al., 2002).

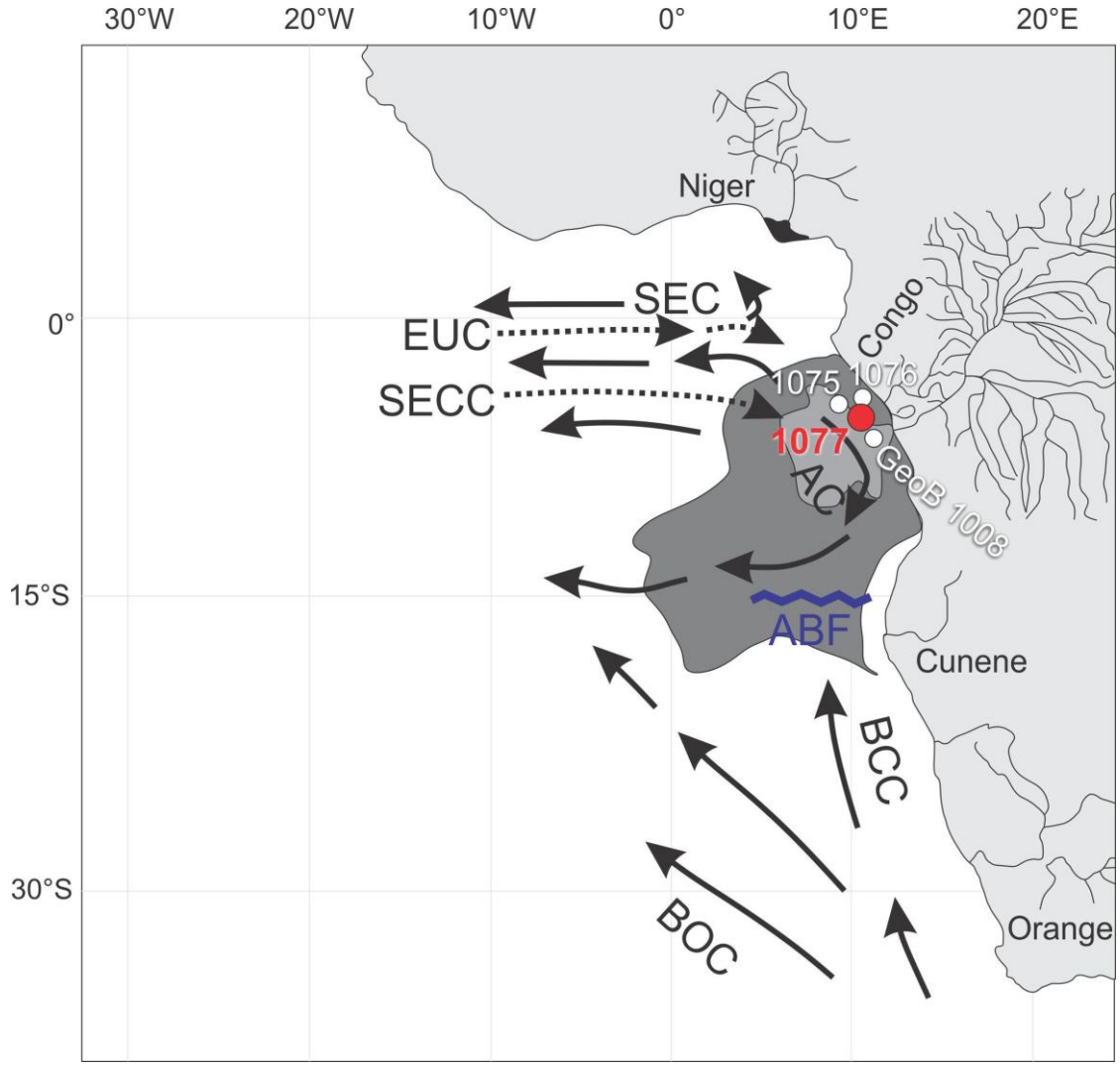

Figure 4: Location of marine sediment cores 0DP1075 (white circle), ODP1076 (white circle), ODP1077 [red circle] (this study), and GeoB1008 (Schneider et al., 1997). and main surface and subsurface currents and areas with high primary productivity in the Eastern Angola Basin.). Cold surface currents namely Benguela Oceanic (BOC) Current and Benguela Coastal Current (BCC), as well as the warm surface currents, Angola Current (AC) and South Equatorial Current (SEC) are shown in black solid lines. Undercurrents, Equatorial Undercurrent (EUC) and South Equatorial Countercurrent (SECC) are shown in dotted black lines. Angola-Benguela Front (ABF) is shown in blue, and regions of river plume and oceanic upwelling are identified in light and dark grey colours respectively. The map is modified from Schneider et al. (1994).

3.2 Analytical Methods

3.2.1 Sediment core chronology

Chronology of core GL-1248 was fully described by Venancio et al., (2018). The age model is based on 12 Accelerator Mass Spectrometry (AMS) radiocarbon ages on 400-500 planktonic foraminifera (*Globigerinoides ruber* and *Trilobatus sacculifer*) tests, which were handpicked from the fraction larger than 150 µm for the upper 6.30 m of the core. The radiocarbon dating reached 43.674 ka at 6.30 m depth. The chronology of the lower part of the core (6.30 - to 16.66 m core depth; ≈ 44 –129 ka), was obtained by aligning the Ti/Ca record of core GL-1248 to the ice $\delta^{18}O$ record of the North Greenland Ice Core Project (NGRIP) (NGRIP Members, 2004) using the extended Greenland Ice Core Chronology (GICC05modelext). According to Venancio et al., (2018), the alignment is based on the assumption that Greenland stadials are associated with increased precipitation over northeastern Brazil and increased delivery of terrigenous material to the Western equatorial Atlantic, as supported by speleothem and marine records of the last glacial period (Jaeschke et al., 2007; Wang et al., 2004; Zhang et al., 2017). The main Ti/Ca fluctuations of core GL-1248 were matched with corresponding major changes in $\delta^{18}O$ from the NGRIP record, with tie points being mostly located at the midpoint of abrupt excursions on both records. Also, the start of the Last Interglacial was defined by aligning the Ti/Ca record of core GL-1248 with the Antarctic methane record from EPICA Dome C (Loulergue et al., 2008) at approximately 129 ka on the AICC2012 timescale (Veres et al., 2013), similar to previous studies (Govin et al., 2015). The basis for this tuning is that abrupt Greenland warming events occurred simultaneously with methane increases during millennial-scale events of the last glacial period and the last deglaciation (Baumgartner et al., 2014; Chappellaz et al., 1993; Huber et al., 2006). Radiocarbon ages and tie points defined for GL-1248 with their respective 2σ errors are summarized in Supplementary Table 1.

The age model of ODP1077 was previously presented by Uliana et al. (2001, 2002). The ages were assigned through the alignment of the $\delta^{18}O$ record of *Globigerinoides ruber* (pink) from ODP1077 to the record from site 677 (Panama basin) (Shackleton et al., 1990). Magnetic susceptibility of ODP1077 was eventually used in intervals of low carbonate content (e.g., between 60 and 95 m) (Uliana et al., 2001). As more suitable age model strategies are presently available, the ODP1077 age model between 0 and 28.30 m was rebuilt (Figure 8). For the first 21.99 m the ODP1077 $\delta^{18}O$ record was aligned to the regional intermediate South Atlantic stack of Lisiecki and Stern (2016). These recent stacks are based on radiocarbon data from 0 to 40 ka, correlation to a layer counted Greenland ice-core from 40 to 56 ka and correlation to radiometrically dated speleothems from 56 to 150 ka (Lisiecki and Stern, 2016). The LR04 stack (Lisiecki and Raymo, 2005) was used between 21.99 and 28.30 m. The ages were interpolated with the software Bacon v 2.2, which uses Bayesian statistics to reconstruct Bayesian accumulation histories for sedimentary deposits (Blaauw and Christeny, 2011). Error estimations of $\delta^{18}O$ tie-points take into account the mean resolution of the ODP1077 planktonic $\delta^{18}O$ record around the tie-point depth, the mean resolution of the reference curve around the tie-point age and the absolute age error of the time-scale used for the reference record.

3.2.2 Geochemical analysis

Bulk analyses

Core GL-1248 was sampled every 5 cm (n = 323 samples) while ODP-1077 (n = 264) was sampled every 7 cm (n = 263 samples) for bulk analyses. Samples were decarbonated before total organic carbon (TOC), and stable isotopes ($\delta^{13}C$ and $\delta^{15}N$) analyses. Each sample was encapsulated in tin (Sn) foil after carbonate removal by acidification with 1 M HCl, 60 mg of dried and pulverized sediment. The bulk analysis was performed using a PDZ Europa

ANCA-GSL elemental analyzer at the Stable Isotope Facility of the University of California, Davis (USA) within an analytical precision of ±0.09 %.

Major Element Composition

Elemental intensities of core GL-1248 were obtained by scanning the split core surfaces of the archive halves with X-ray fluorescence (XRF) Core-Scanner II (AVAATECH Serial No. 2) at the MARUM, University of Bremen (Germany). The XRF data were measured downcore every 0.5cm in the core by irradiating a surface of about 10 mm × 12 mm for 20 s at 10 kV (Venancio et al., 2018).

To determine major elemental intensities of marine sediment ODP1077 (n = 264), a Niton XL3t handheld X-ray fluorescence (XRF) unit (Thermo Fisher Scientific) at the Laboratory of Observational Oceanography and Paleoceanography (LOOP) from Department of Geochemistry, Fluminense Federal University, Niteroi, Brazil was used on smoothly pulverised samples. The instrument was set up on a stand and was calibrated empirically using 4 soil standard reference materials with certified elemental concentrations. For the analysis, finely homogenised dry samples (~ 10g) were placed on a Mylar® thin- film (gauge 3.6µm, diameter 63.5mm) in a 2 cm diameter sample cup, with necessary precautions to avoid airspaces in the sample. Each sample was aligned with the centre of the analyser window on the handheld XRF stand. Samples were analysed for a fixed period of 180 s and in triplicates.

Mercury Concentration

For the determination of total Hg concentrations, 2g of sediment were freeze-dried and lyophilized using TERRONE® lyophillizer for 24 hours. Following the homogenization of lyophilized sediments, about 30mg of each sample was analysed using Zeeman Mercury Spectrometer RA-915M coupled to the two-chamber pyrolyzer PYRO-915+ according to the

procedure described by Sholupov et al., (2004). The PYRO-915 + accessory coupled to the RA915 + permits sample analysis for Hg contents without pre-treatments. This is because all mercury species are completely decomposed and the generated vapours are transported from the atomizer to the detection chamber. Following the homogenization of lyophilized sediments, about 30mg of each sample was inserted into the first chamber with a temperature range of 680-740°C. The mercury compounds are evaporated and part of them decomposes to form elemental Hg. All generated products, including mercury vapour, are transported to a second atomization chamber where there is complete degradation of the mercury compounds. The air flow from the atomizer passes through the cell and the generated signal is converted into concentration values. The analytical method was validated through the analysis of the certified reference material (PACS-2) purchased from the National Research Council Canada (NRCC). A total of 10 replicates were analysed, having a recovery of 100% for elemental mercury. The detection limit was 0.5ng/g for 10 – 400mg of sediment. Total Hg analysis was carried out in the same resolution as with bulk analyses and in triplicates for quality control, with Relative Standard Deviation (RSD) of ≤5% as the acceptable level of precision. Analysis for total Hg concentrations in both marine sediment cores were executed at the Department of Geochemistry, Fluminense Federal University, Niteroi, Brazil.

Mineralogical Analysis and Iron (Fe) oxy-hydroxides measurements

Further analyses were required for only marine sediment core GL-1248. Mineralogical characterization was carried out on pulverized samples. Representative samples were selected from two (2) depths within each marine oxygen isotope stage (MIS), and analysed using a Bruker D8 Advance X-ray powder diffractometer (XRD) with Cu Kα radiation at the Institute of Physics, Fluminense Federal University, Niteroi, Brazil. Diffractograms were collected using 2θ between 3º to 70º with a step-size of 0.02° and 1.0s scanning time. For mineral identification, generated patterns were compared with tables from Brindley and

Brown (1980) and data from the Mineralogy Database (http://webmineral.com/), similar to the methodology adopted by Silveira et al. (2016).

Iron (Fe) oxy-hydroxides were extracted using the citrate-dithionate-bicarbonate (cdb) buffer method as described by Lucotte and d'Anglejan, (1985), then analysed by Inductively Coupled Plasma Atomic Emission Spectroscopy (ICP-AES) on a Shimadzu, model ICPE-9000. Quality control was assessed by analysis of blank reagents and using six (6) samples prepared in duplicate and analysed at random positions within a batch and the analytical precision of these measurements is better than ± 8%.

3.3 Time Series Analysis

In order to verify the presence of periodicities, a spectral analysis was performed on GL-1248 Hg results using the REDFIT algorithm (Schulz and Mudelsee, 2002) of the PAST software package (Hammer et al., 2001) was performed. For this analysis, a setting of two segments tapered with a Welch spectral window was selected, the oversampling factor was set to 4. Subsequently, the primary data set of Hg, in addition to other indicators such as TOC (discrete samples) and Fe/Ca ratio (XRF), and secondary data from other sources were analysed using cross wavelet-spectral and cross-coherence techniques (Grinsted et al, 2004). Wavelets are two-dimensional transformations that present information about the distribution of events with relative energy to the whole time series, isolating the scale (frequency) of individual events (Grinsted et al., 2004; Salmond, 2005). The cross-wavelet is a bivariate version of the spectral analysis for comparing two sets of data (eg, Davis 2002). Torrence and Webster (1999), and Grinsted et al. (2004) provide detailed explanations of the cross-wavelet, in particular the coherence and the cross-phase angle using the Morlet wavelet based on a continuous wavelet transform. In this technique, Monte Carlo simulations are used to provide a distribution of frequency-specific probability (global spectrum of wavelets) that can be

tested by wavelet coefficients. Although discrete Hg data of GL-1248 and other paleo-proxies are not regularly spaced in time (along the core), Prokoph and El Bilali (2008) have shown that uncertainty in geological time scales due to stratigraphic error which adds non-stationary to paleoclimatic records can be minimized with a good interpolation process. The GL-1248 data of Hg, TOC, Fe/Ca and other paleo-proxies were interpolated with a resolution of 50 yr, using the nearest neighbours' interpolation technique, which preserves all the original features of discrete data.

The cross-wavelet transform (Figure 5), shows the standard analysis between two series of a graphical output, as applied in this study. The upward pointing arrows indicate the dominance of the cycle of variable 1 over 2, while the arrows pointing down show the dominance between variable 2 over 1. The left-facing arrows are out of phase and the right facing arrows are in-phase.

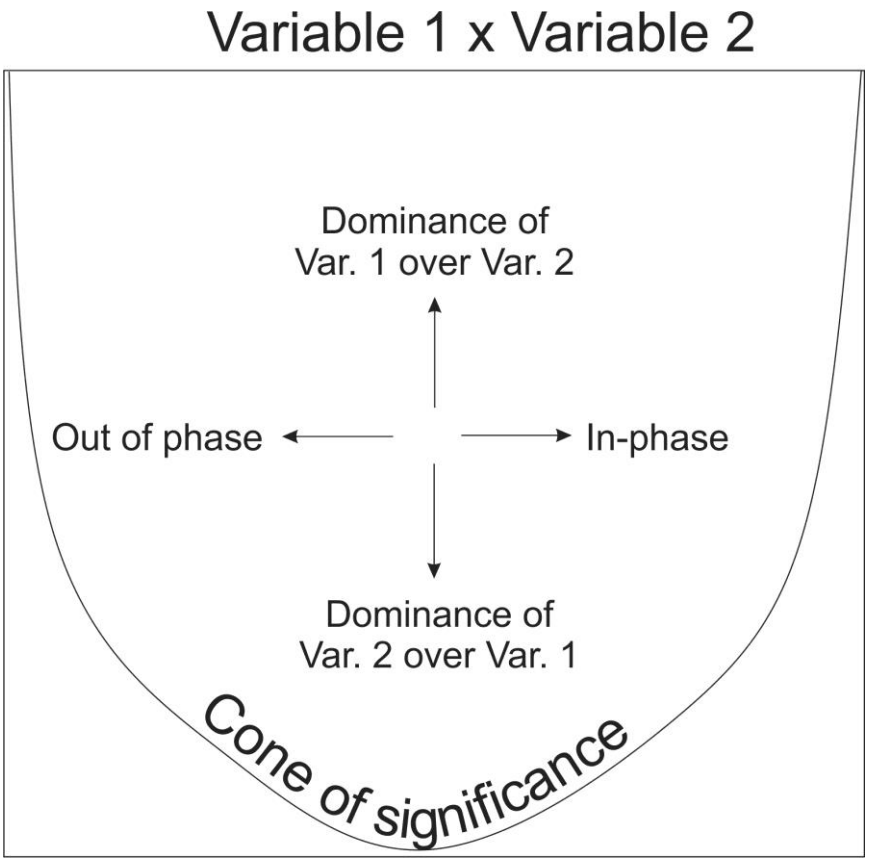

Figure 5: Cross-wavelet transform legend

4 RESULTS

4.1 GL-1248 Results

4.1.1 Age model and sedimentation rates

The age model for the upper 6.3 m core depth of GL-1248 based on 12 AMS radiocarbon ages terminated at about 44.0 ± 0.7 ka. The alignment of Ti/Ca ratio from the XRF data of the lower part of the core (6.3-16.65 m) with $\delta^{18}O$ record from NGRIP extended till 128.3 ka (Figure 6). As described by Venancio et al. (2018), sedimentation rates from core GL-1248 exhibit large fluctuations. Within Marine Oxygen Isotope Stage (MIS) 5 (5a, 5b, 5c and 5d), sedimentation rates vary significantly having the highest average sedimentation rates occurring in MIS5a (25.7 cm/ka). Although the glacial period started with low sedimentation rates in MIS 4 (mean = 13 cm/ka), it increased significantly in MIS 3 to an average value of 32.1cm/ka. For the interglacial periods, sedimentation rates in MIS 5e are fairly constant with an average of 6.93 cm/ka, whereas MIS 1 values are irregular and have a higher average of 16.28 cm/ka. At the interval 2.18 m – 1.7 m core depth, unusually low sedimentation rates (3 cm/ka) for the region and period (see Zhang et al., 2015) were recorded. An implication of this is the possibility of the presence of a hiatus. Although no significant lithological changes were observed, sedimentation rates and other data are not reported for this interval (MIS 2; 1.7 m –2.18 m core depth; ≈ 14 – 29 ka).

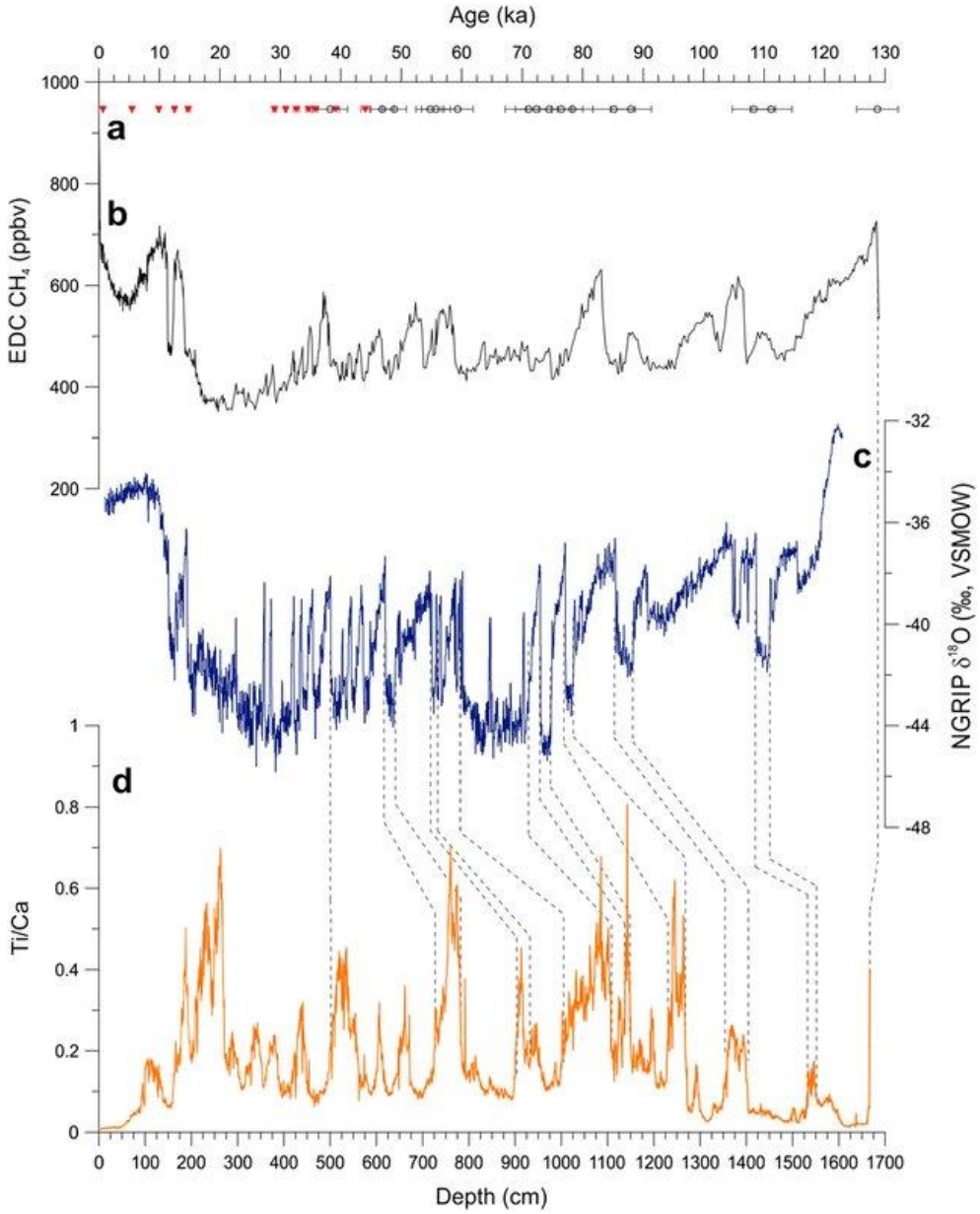

Figure 6: Reference curves and age-depth model of core GL-1248. (a) Calibrated radiocarbon dates (red symbols) and tiepoints (open circles) with their respective 2σ errors. (b) EPICA dome C (EDC) methane record (Loulergue et al., 2008) on the AICC2012 timescale (Veres et al., 2013) (black line). (c) δ 18 O ice from NGRIP on the GICC05modelext time scale (NGRIP members, 2004; Wolff et al., 2010; blue line). (d) Ti/ca record from GL-1248 versus core depth (orange line). The black dotted lines represent the tie-point alignment. SOURCE: Venancio et al. 2018.

4.1.2 Total Organic Carbon (TOC), Carbon/Nitrogen ratio (C: N), Organic Matter $\delta^{13}C$ and $\delta^{15}N$

The result obtained from the bulk analyses shows the variation of TOC, C/N, $\delta^{13}C$, and $\delta^{15}N$ in GL-1248 since the Last Interglacial period (Figure 7). Two major periods can be identified

from the TOC concentrations which ranged from 0.42 % to 1.22 %. Elevated concentrations occurred in the glacial periods (as well as cold sub-stages of MIS 5), while lower concentrations were recorded in the interglacial periods (and warm sub-stages of MIS 5) respectively. C/N ratios follow the same glacial-interglacial pattern shown by TOC concentrations, displaying values between 4.5 and 12.75. $\delta^{13}C_{org}$ fluctuated throughout the studied periods between –24.21 per mil (‰) and –19.16 per mil (‰) although fairly constant within MIS 3 around –21.74 ‰. $\delta^{15}N_{org}$ followed a similar pattern ranging between 4.48 per mil (‰) and 7.52 per mil (‰) with an average of 5.91 per mil (‰).

4.1.3 Major element composition and Fe-oxyhydroxide (Fe_{cdb}) profile

The Fe/Ca ratios of core GL-1248 (Figure 7d) show a clear trend of high values with frequent peaks in the glacial period and low values in the interglacial periods. A remarkable observation is the interruption of the baseline trend of Fe/Ca in MIS 5 by peaks, which occurred in MIS 5d and 5b. Peaks in the Fe/Ca ratios during MIS 4 and MIS 3 are coincident with Millennial-scale events

Fe_{cdb} concentrations in our sediment core ranged from 0.01 – 0.45% and follow the Hg profile of higher concentrations in the cold periods of MIS 4 and 3 than in the interglacial periods (Figure 12a). Also, higher Fe_{cdb} percentages occurred in the cold substages of MIS 5 (5d and 5b) along with Hg concentrations.

4.1.4 Total Hg concentrations

Mercury (Hg) concentrations in the sediment core ranged from 14.29 ng/g to 69.43 ng/g (average = 42.67 ng/g) having the highest concentration occurring at 6.4 ka within the current interglacial period (Figure 6f). Sedimentary Hg concentrations were particularly high in glacial phases (MIS 4 and MIS 3), as well as in MIS 5d and 5b (MIS 5 cold sub-stages). In comparison, low concentrations were recorded in interglacial sediments and MIS 5 warm stages (MIS 5c and 5a).

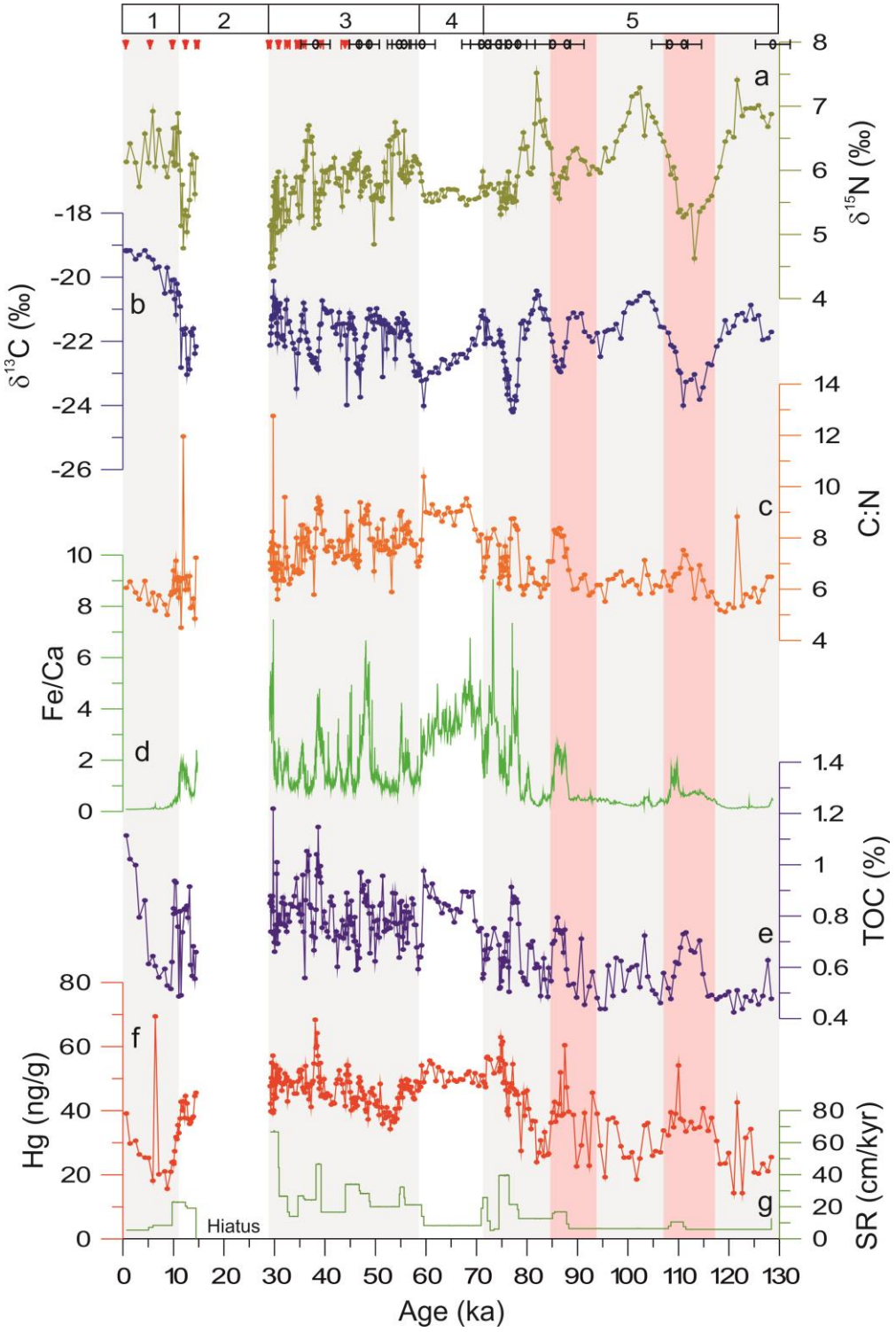

Figure 7: Hg variation and paleoenvironmental proxies of the core GL-1248. (a) $\delta^{15}N_{org}$ in ‰ (olive green line) (b) $\delta^{13}C_{org}$ of core given in ‰ (navy blue line) (c) Carbon-Nitrogen ratio (orange line) (d) Fe/Ca ratios (green line) (e) Total Organic Carbon (TOC) in % (blue line) (f) Total Hg (red line) reported in ng/g. MIS boundaries in the studied time interval are numbered from 1 to 5. Vertical error bars denote 2σ confidence interval of the calibrated ages (red) and tie points (black).

4.1.5 Mineralogy

The mineralogical spectrum of all representative samples (*n=16*) of core GL-1248 revealed a moderately varied array of minerals during the last 128 ka. The identified minerals in the marine sediment include kaolinite, goethite, feldspars, calcite, aragonite, quartz and halite (Figure 8). From the powder x-ray diffraction mineral identification of all samples, an alteration between continent and marine sourced minerals during glacial period (and cold substages) and interglacial periods (and warm substages) respectively was observed. (Table 1).

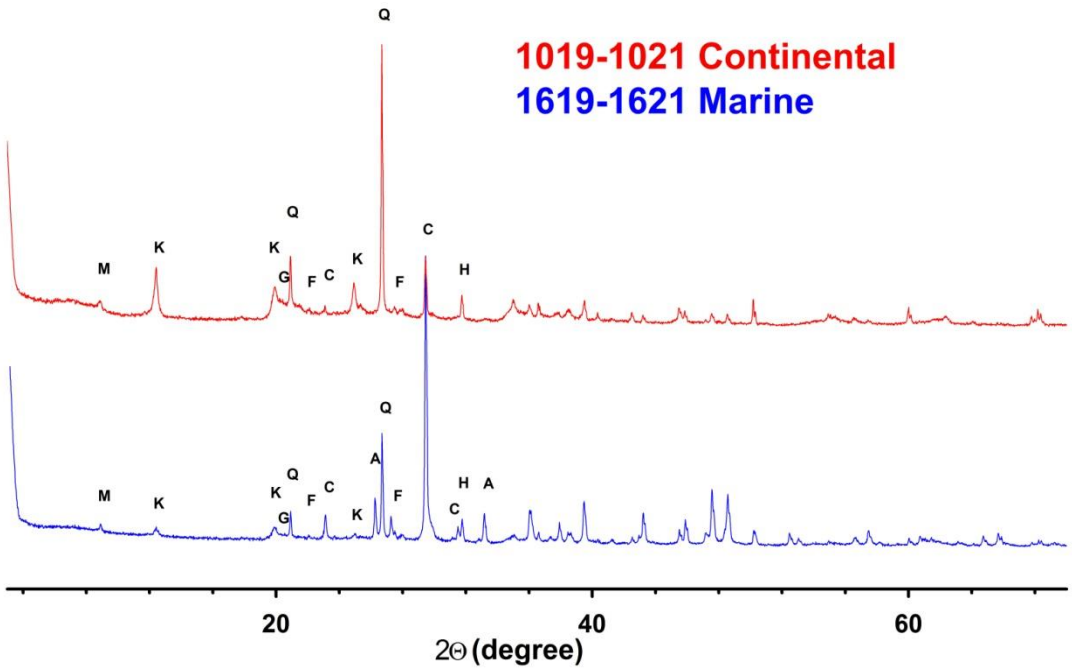

Figure 8: Identified x-ray diffactogram of GL-1248 samples 1019-1021 and 1619-1621 representing continental and marine sources of minerals respectively. Identified minerals are: M = mica, K = Kaolinite, G = Goethite, F = Feldspars, C= Calcite, A= Aragonite, Q = Quartz, H= Halite.

Table 1: Mineral array in selected samples of marine sediment GL-1248 with corresponding Ages (ka), Marine Oxygen Isotope Stage (MIS) and main mineral source. Minerals are differentiated into main minerals, other minerals and trace minerals by red, blue and black text colours respectively.

Sample ID/Depth	Age (ka)	Marine Oxygen Isotope Stage (MIS)	Minerals	Main source
0-2	0.679	1	Calcite, Aragonite, Mg Calcite, Mica, Kaolinite, Quartz, Goethite, Feldspar, Halite	Marine
103-105	29-78.139	3 - 4	Kaolinite, Quartz, Mica, Calcite, Goethite, Halite, Feldspar	Continental
633-635 863-865			Kaolinite, Quartz, Feldspar, Calcite, Goethite, Mica Halite, Aragonite, Magnesium Calcite	
1019-1021			Kaolinite, Feldspar, Quartz, Calcite, Goethite, Mica, Halite	
1159-1161 1163-1165			Kaolinite, Feldspar, Quartz, Calcite, Goethite, Mica, Halite	
1204-1206			Kaolinite, Feldspar, Quartz, Calcite, Goethite, Mica, Halite, Aragonite, Magnesium Calcite	
1248-1250 1264-1266			Kaolinite, Feldspar, Quartz, Goethite, Calcite, Mica, Halite	
1313-1315	81.917	5a	Calcite, Kaolinite, Quartz, Feldspar, Aragonite, Mica, Goethite, Halite, Magnesium Calcite	Marine
1393-1395	87.482	5b	Kaolinite, Feldspar, Quartz, Calcite, Mica, Halite, Goethite, Mg Calcite	Continental
1449-1451 1523-1525	95-107	5c	Calcite, Kaolinite, Quartz, Feldspars, Goethite, Aragonite, Mica, Halite, Magnesium Calcite	Marine
1539-1541	109	5d	Kaolinite, Feldspar, Quartz, Calcite, Goethite, Mica, Halite, Aragonite, Magnesium Calcite	Continental
1619-1621	120	5e	Calcite, Kaolinite, Quartz, Aragonite, Goethite, Halite, Mica	Marine

.

4.1.6 Time Series Analysis

When the discrete wavelet analysis is applied to the time series of Hg and TOC (Figure 9), the millennial-scale signals can be identified throughout the series with greater intensity (5% significance level against red noise), especially during MIS 3 and MIS 5. Although with a lower significance, signals with longer periods in orbital scale (> 23k) presented strong spectral energy throughout the series time span.

Spectral analysis on the Hg concentrations from core GL-1248 revealed two significant periodicities (Figure 10). The first one is centred at 56 ka, and the second one at 900 yr. Both are significant over a 99% confidence level.

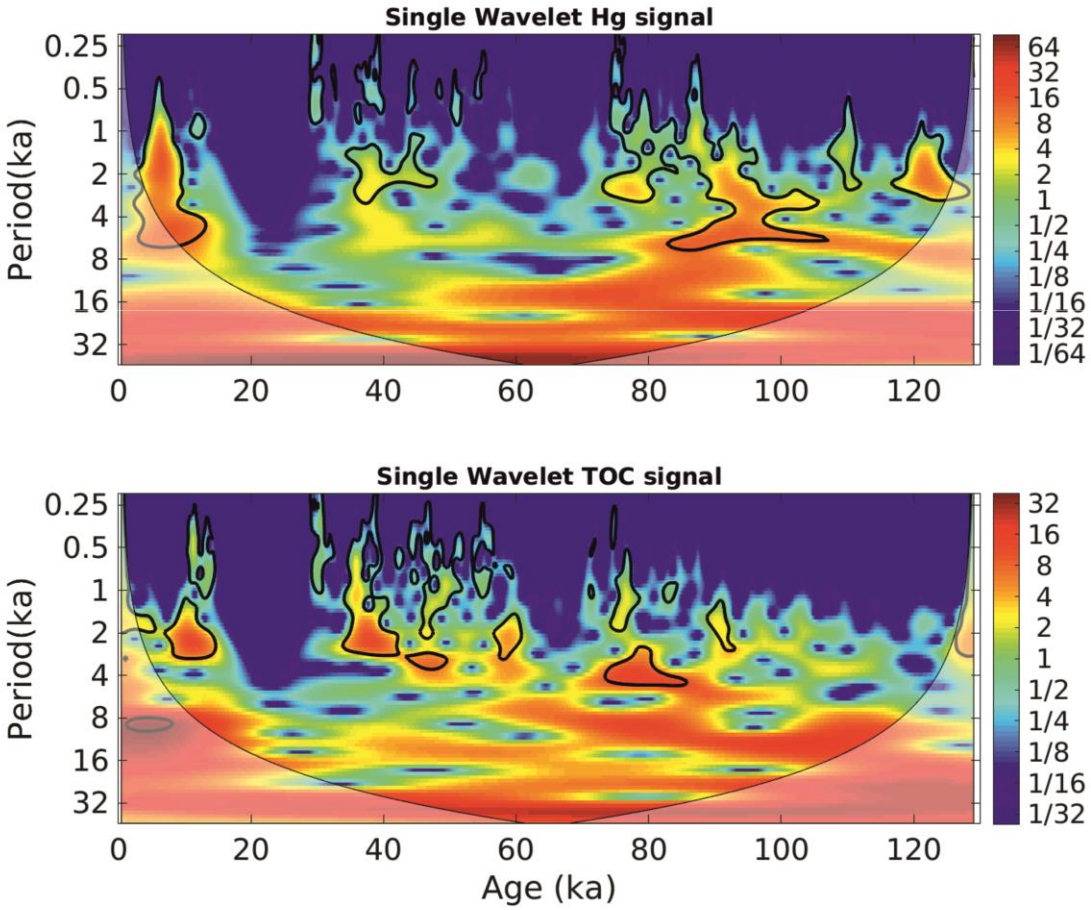

Figure 9: The continuous wavelet power spectrum of Hg signal (top) and TOC (bottom). The thick black contour designates the 5% significance level against red noise and the Cone of Influence (COI) where edge effects might distort the picture is shown as a lighter shade.

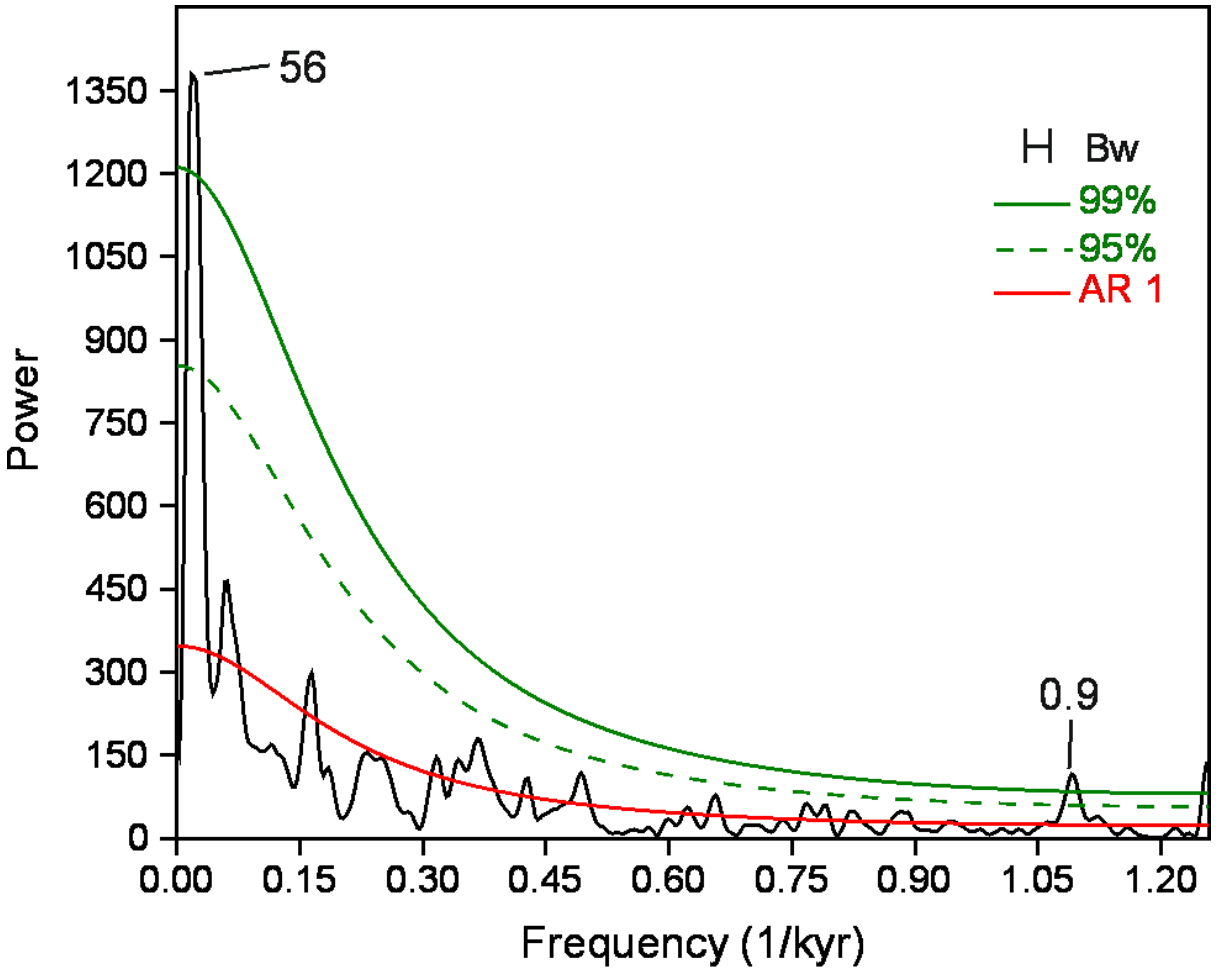

Figure 10: Time series analysis performed with REDFIT (Schulz and Mudelsee, 2002) on GL-1248 Hg concentrations. The two periodicities that exceed the 95 % (dashed green line) or 99 % (solid green line) are labeled. The AR (1) red noise model (solid red line) and the bandwidth (black line; upper right corner) are displayed.

4.2 ODP 1077 Results

4.2.1 Age model and sedimentation rates

For the purpose of this study, our analyses are limited to the last 130 ka. According to the revised age model, the upper 24.49 m cover the last 130 ka. Mean 95 % ages probability distribution ranged 6.8 ka. In Uliana et al. (2001, 2002) age model, the $\delta^{18}O$ Holocene peak at 1.25 m was tied at 7 ka, while in our revised age model, this $\delta^{18}O$ Holocene peak occurred at 6.1 ka (Figure 11).

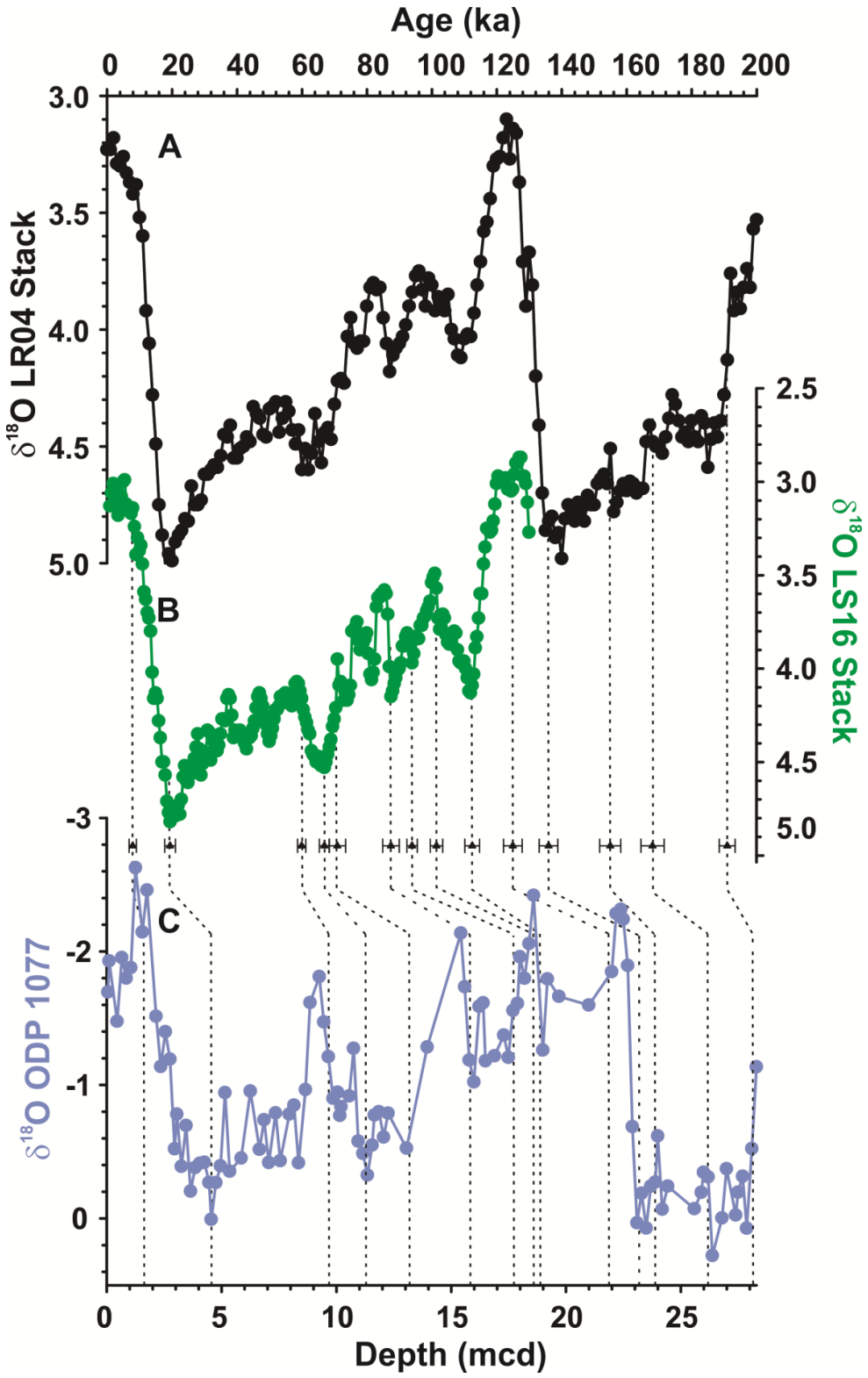

Figure 11: Reference curves and age-depth model of core ODP1077 with black dotted lines representing the tie points alignment and their respective 2σ errors. (a) $\delta^{18}O$ ice from LR04 stack (Lisiecki and Raymo, 2005) (black line). (b) $\delta^{18}O$ ice from LS16 (Liscieki and Stern, 2016) (green line). (c) $\delta^{18}O$ record from ODP 1077 (Uliana et al., 2001, 2002) (purple line).

This close correspondence suggests that the sedimentation rate was not drastically changed by the update process. Sedimentation rate varied between ~ 4 and 29 cm/ka (Figure 11). Minimum sedimentation rates were found between ~ 19 and 18 m, as well as between ~ 10 and 4.7 m. Maximum sedimentation rates occurred between ~ 22 and 19 m and ~ 18 – 15.6 m within MIS 5, as well as from 5 m towards the top of ODP1077 (Figure 11). Marine sediment samples were unavailable for the interval 14.5– 10.8 m core depth corresponding to ≈ 79.4 – 64.4 ka. As such, sedimentation rates and other data are not reported for the periods MIS 5a and 4.

4.2.2 Total Organic Carbon (TOC) and Organic Matter $\delta^{13}C$

TOC and $\delta^{13}C_{org}$ results in the marine sediment are presented in Figure 12 d and e. TOC ranged from 1.58% to 3.98% with an average of 2.74%. Mean TOC concentrations were comparably lower in MIS 5 (2.38%) compared to MIS 3 and 2 (3.27%), although elevated concentrations occurred within MIS 5e and MIS 5c. During MIS 5, the lowest TOC concentration was recorded at the 124 – 122 ka interval. Starting at the MIS 2/1 transition and ending at midway in MIS 1 (at ~6 ka), an abrupt decrease by ~ 1.5% was noted. Overall, highest TOC values coincide with cold climates (MIS 3 and 2), while minimum values occurred during MIS 1 and 5.

$\delta^{13}C_{org}$ in the marine sediment range between -23.41 per mil (‰) and -20.35 per mil (‰), and exhibited a plot pattern similar to the TOC concentrations. The lowest $\delta^{13}C_{org}$ measurements, that is, more negative values, were registered during MIS 1, MIS 5c and MIS 5e.

4.2.3 Fe/Ca ratio

In the Fe/Ca ratios (Figure 12c), two distinct intervals can be identified in the studied period; the first occurring between 20 and 0 ka, and the second, between 130 and 20 ka. Rapid variations in Fe/Ca ratios occurred between 130 and 80 ka, although the highest ratios was

recorded between 123 and 120 ka, as well as at the MIS 5c/5d transition, before the descent to the least ratio in MIS 5b. Likewise between 64 and 20 ka, the Fe/Ca ratios varied significantly from the start of MIS 3 by alternating between high and low ratios in two short cycles, before finally descending to a short-term period of near baseline ratios commencing at 20 ka and ending at about 5 ka, when a rise in the ratio is observed. The relative variations and amplitudes of these records are better displayed by their running averages.

4.2.4 Total mercury (Hg) concentrations

Sedimentary mercury concentrations ranged from 23.12 ng/g to 256 ng/g (average = 77.61 ng/g), and showed two trends distinguished by approximately a ten-fold increase in the average concentrations (Figure 12b). The lowest values (23.12 – 116.3 ng/g) occurred during the interval 130 – 20 ka with minor occasional increases within MIS 5 and 3. Hg concentrations in the interval 20 – 0 ka were anomalously high having concentrations in the range of 84.5 – 256 ng/g.

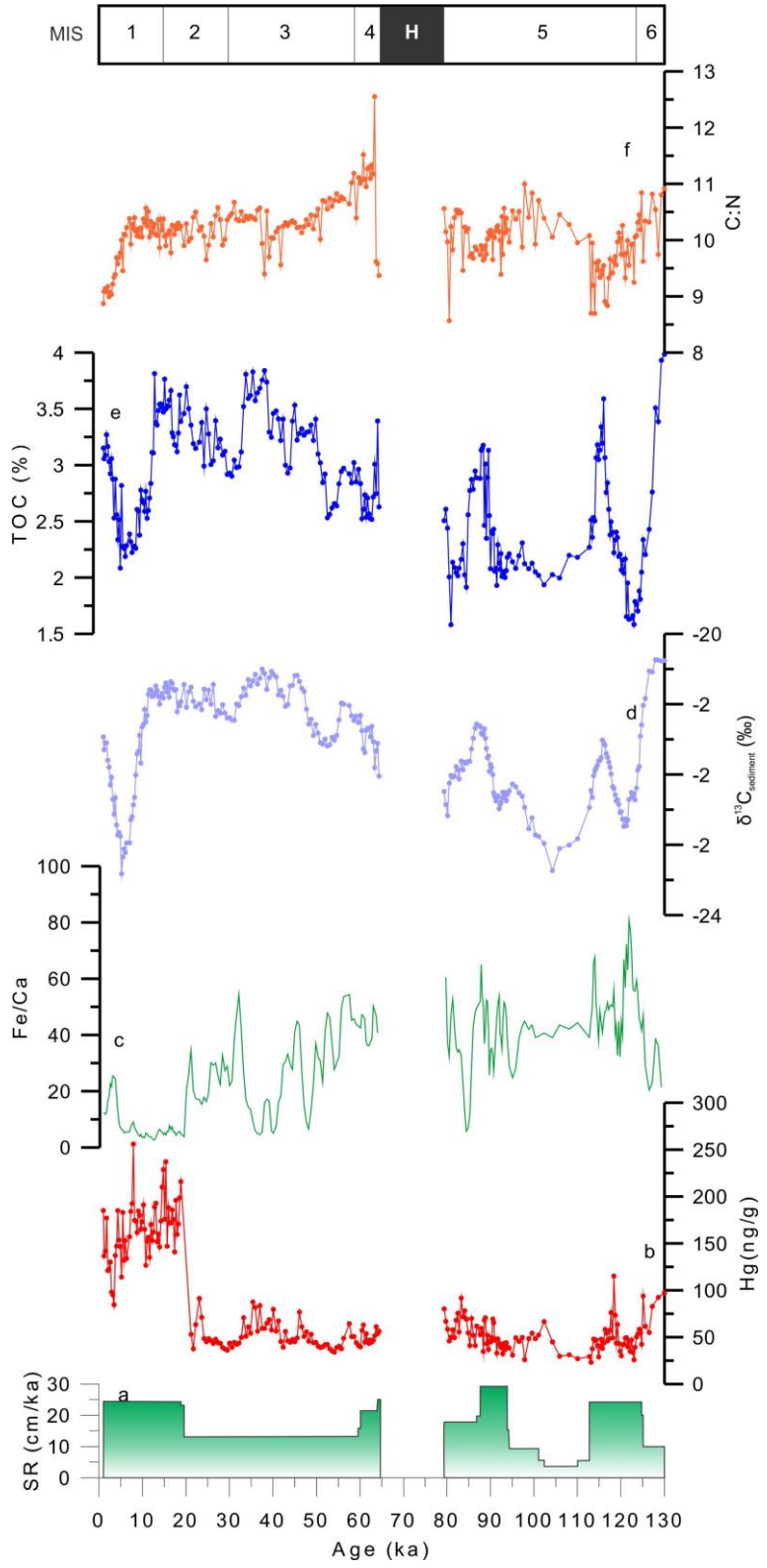

Figure 12: Hg variation and paleoenvironmental proxies of the core ODP1077. (a) Sedimentation Rates, sedimentation rates in cm/ka (olive green line) (b) Total Hg (red line) reported in ng/g (c) Fe/Ca ratios (green line) (d) $\delta^{13}C_{org}$ of core given in ‰ (purple line) (e) Total Organic Carbon (TOC) in % (blue line) (f) bars Carbon-Nitrogen ratio (orange line. MIS 1 – 5e intervals are identified by numbers, as well as grey and white bars.

5. DISCUSSION

Paleoclimatic controls on sedimentary Hg variations in marine sediments from the continental margins of tropical South American and African continents are discussed separately in sub-sections 5.1 and 5.2 as well as comparatively in 5.3.

5.1 Paleoclimatic Controls on Mercury Deposition in Northeast Brazil since the Last Interglacial

5.1.1 Primary source of sedimentary mercury in marine sediment core GL-1248

Sedimentation rates of marine sediment core GL-1248 vary significantly over the studied period with sedimentation rates reaching 67.42 cm/ka during MIS 3, and lower sedimentation rates with averages of 16.28 cm/ka and 14.87 cm/ka during MIS 1 and MIS 5 respectively. Considering the proximity of our core to the adjoining continent and its location offshore Parnaíba River mouth (Figure 3), marine sediments arriving and accumulating at the site are likely predominantly controlled by continental input from the Parnaíba Basin which are conveyed to the study site by fluvial transport. This conjecture is supported by the findings from a study by Lacerda et al., (2013) which showed that the distribution of metals (Al, Ba, Cu, Fe, Mn, Ni and Zn) in outer shelf sediments in NE Brazil at the Potiguar Basin are controlled by continental inputs from the proximal continent. In another study on the source of terrigenous materials to the NE South American continental margin, Zhang et al., (2015) showed, using neodymium (Nd) isotopic compositions of marine sediment cores GeoB16224-1 and GeoB16206-1, that terrigenous sediments deposited off NE Brazil, nearby our core location (Figure 3), are not affected by Amazonian source. This latter finding is crucial to this study as it eliminates the Amazon as a potential source of Hg to GL-1248 since it has been established that the Amazon soils are a major link in the global Hg biogeochemical cycle due to their capacity to trap approximately 21% of global atmospheric Hg (Fostier et al., 2015). As such, Hg in marine sediment core GL-1248 originates from the

input of fluvial sediments transported by the Parnaíba River from the Parnaíba Basin offshore.

Mercury concentrations recorded in marine sediment GL-1248 (range = 14.29 – 69.43 ng/g; average 42.67 ng/g) over the last 128 ka are relatively lower than pre-industrial concentrations from Madeira River, southwest Amazonia (50-280 ng/g) [Lacerda et al., 1987], Tapajos River, one of the major tributaries of the Amazon (10-140 ng/g) [Padberg, 1990], and Itacaiunas River, South Pará (40-3370 ng/g) [Bidone, 1991]. In the southeastern part of Brazil, the Paraiba do Sul River, Pfeiffer et al., (1989) presented values between 300-550 ng/g. Although the reported Hg concentrations are quite dissimilar across respective locations, they are comparable considering that the concentrations were recorded where no Hg-bearing geology exists (Wasserman et al., 2003; Lacerda et al., 2017), and date back to prehistoric times, therefore suggestive of the atmosphere as a major source of the recorded Hg variations. Aula et al. (1994) measured Hg concentrations reaching 100 ng/g in the Tucuruí reservoir region, northern Brazil and concluded that the enrichment is a result of atmospheric Hg deposition. Similarly, Lacerda et al. (1999) using a record covering the last 30 ka from remote Amazonian lakes, which have no local Hg sources, attributed the Hg accumulation recorded to atmospheric inputs. In general, changes in Hg concentrations are linked to variations in atmospheric Hg sources or atmospheric conditions (Lacerda et al., 1999; Santos et al., 2001; Barbosa et al., 2004). These findings broadly support the outcome of a recent study from Caço Lake, NE Brazil (Lacerda et al., 2017), where the authors concluded that the atmosphere is the dominant source of Hg to the lake sediment. On account of the conclusion in these studies stating that the atmosphere is the major source of Hg to the South American continent, and the finding by Zhang et al. (2015) that Parnaíba Basin is the origin of terrigenous sediments deposited off NE Brazil, it is important to

summarize the main post-depositional process related to Hg, as well as the mineralogy of soils in Parnaíba Basin

The Tropical soils of northeastern Brazil are notable for their high content of iron oxides mainly goethite and ferrihydrite; an amorphous Fe-oxyhydroxide precursor of hematite formation (Bigham et al., 2002). From the XRD result (Table 1), goethite is present in all samples and it is assumed that other iron oxides (and oxyhydroxides) are also present but in uncrystallised amorphous state thus unidentifiable by the XRD. Iron-oxyhydroxides are important cementing agents and because of that, they play a pivotal role in metal adsorption processes in tropical soils (Selim, 2013). A positive correlation between deposited atmospheric Hg and Fe-oxyhydroxide (Fe_{cdb}) has been reported in tropical soil profiles (Roulet et al. 1998; Oliveira et al., 2001). This geochemical association of Hg with Fe_{cdb} in soils is supported by evidences of strong correlations between Fe_{cdb} and Hg profiles reported in soils and sediments originating from French Guiana (Roulet and Lucotte, 1995), Tapajos River (Roulet et al. 1996) and Rio Negro Basin (Fadini and Jardim, 2001). Other studies have also identified Fe-oxyhydroxides as an effective Hg-carrier phase (Laurier et al., 2003; Grimaldi et al., 2015) either by complexation with goethite (Forbes et al., 1974) or adsorption (Kinnibrgh and Jackson, 1978; Schuster et al., 1991). In Figure 13b, the profile of Fe counts covary with Hg concentrations in core GL-1248 and have a correlation coefficient of 0.74 ($p < 0.01$) thereby suggesting that the Fe minerals in the sediment are significantly important in the accumulation of Hg in marine sediment GL-1248. Furthermore, the similar variations of Hg and its carrier-phase, Fe_{cdb}, (Figure 13a) suggest that iron oxyhydroxides are the principal factor controlling Hg profile in GL-1248. The cross wavelet transform (Figure 14) show that Fe and Hg are in phase throughout the record. In general, the described Hg-Fe (and Fe_{cdb}) relationships suggest that Hg in GL-1248 is transported alongside fluvial terrigenous sediments from NE Brazil continent to the core site. The Hg-bearing Fe_{cdb} particles are

eroded from the Parnaíba Basin and transported by Parnaíba River until they are immobilized in the continental slope. The strong positive correlation between Hg and Fe-oxyhydroxides corroborates the outcome of aforementioned studies (Roulet and Lucotte, 1995; Roulet et al. 1996; Fadini and Jardim, 2001) that link Hg variations with Fe_{cdb} profiles in tropical soils. A similar significant finding is that the peak of Hg concentration occurred concomitantly with Fe signal during the Mid-Holocene (Figure 15). This observed peak may be linked to the findings of Cruz et al., (2009), who reported using $\delta^{18}O$ ratios in cave speleothems from NE Brazil that significantly wetter conditions persisted during the Mid-Holocene. As such, the synchronous Hg-Fe peaks could be attributed to abrupt terrigenous material delivery, and it further confirms the association between Hg and Fe profiles in tropical soils, as well as the continental source of Hg records in GL-1248 sediments. However, the possible influence of fires on Hg concentration during the Holocene cannot be ruled out. Although the link between high Hg deposition and high frequency of forest fires in the Holocene has been raised by Santos et al., (2001), other authors have described the fire regime of the Holocene as unstable (Carcaillet et al. 2002; Corderiro et al. 2008). In the study by Cordeiro et al. (2008), the authors recorded highest accumulation rates of charcoal particles, an indicator of paleo-fires, during the driest period of the Holocene, i.e., early and Mid - Holocene. Owing to the divergence in the findings of Cordeiro et al. (2008) from Eastern Amazon and Cruz et al. (2009) from NE Brazil, both suggesting dry and wet conditions respectively in the Mid-Holocene, the influence of forest fires on our Holocene Hg concentration needs to be interpreted with caution. However, it could be argued that the discrepancy is due to the site locations. Also, unlike other studies which explicitly discuss forest fires using high-resolution Holocene records, this study presents a lower resolution for the Holocene that is relatively fragmentary to allow definite conclusions.

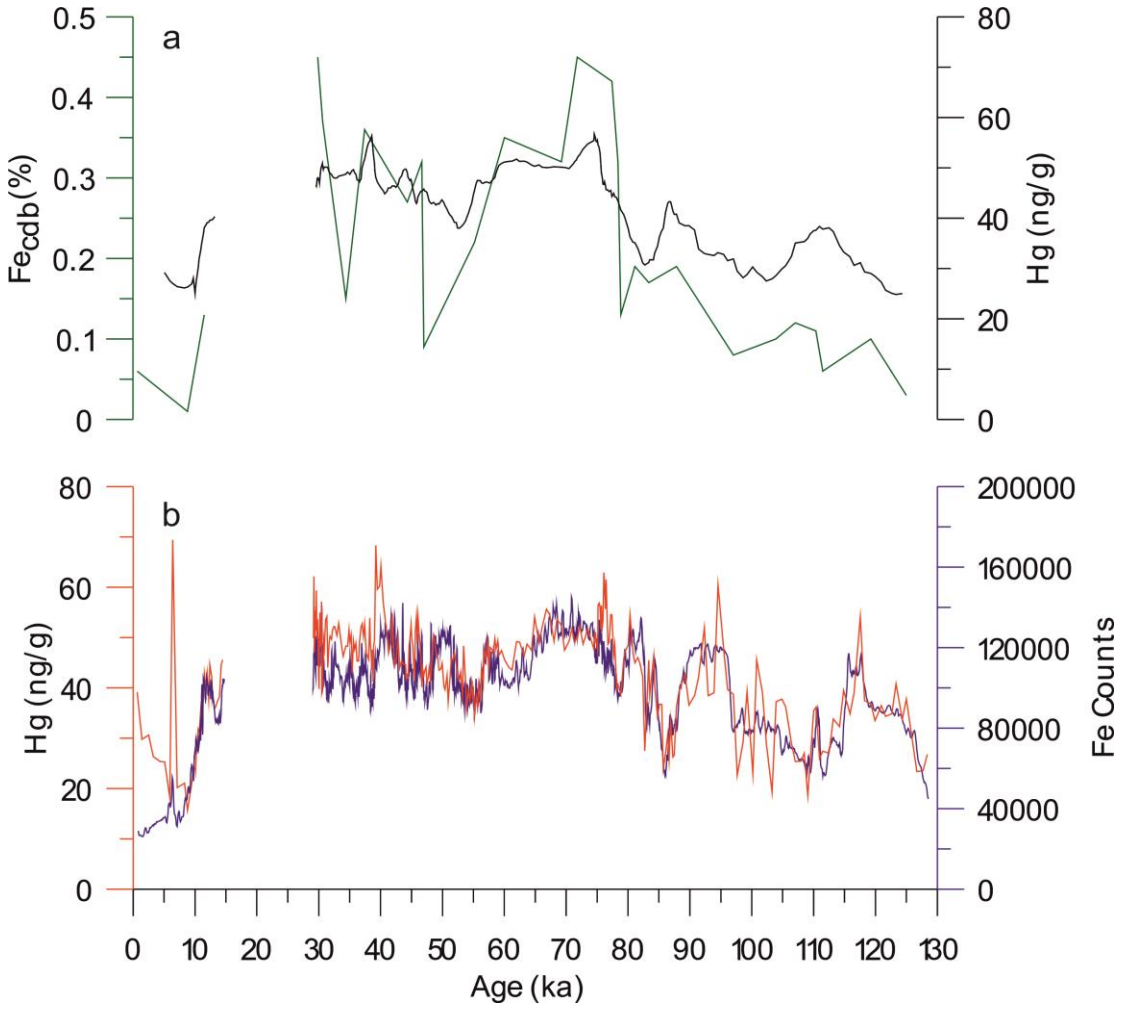

Figure 13: Fe-Hg relationship across the studied period shown by: (a) Profile of Hg concentration (running averages shown in black line) and Fe_{cdb} in GL-1248 (green line). (b) Plot of Hg concentration in ng/g (red line) and Fe counts (in running average) (blue line).

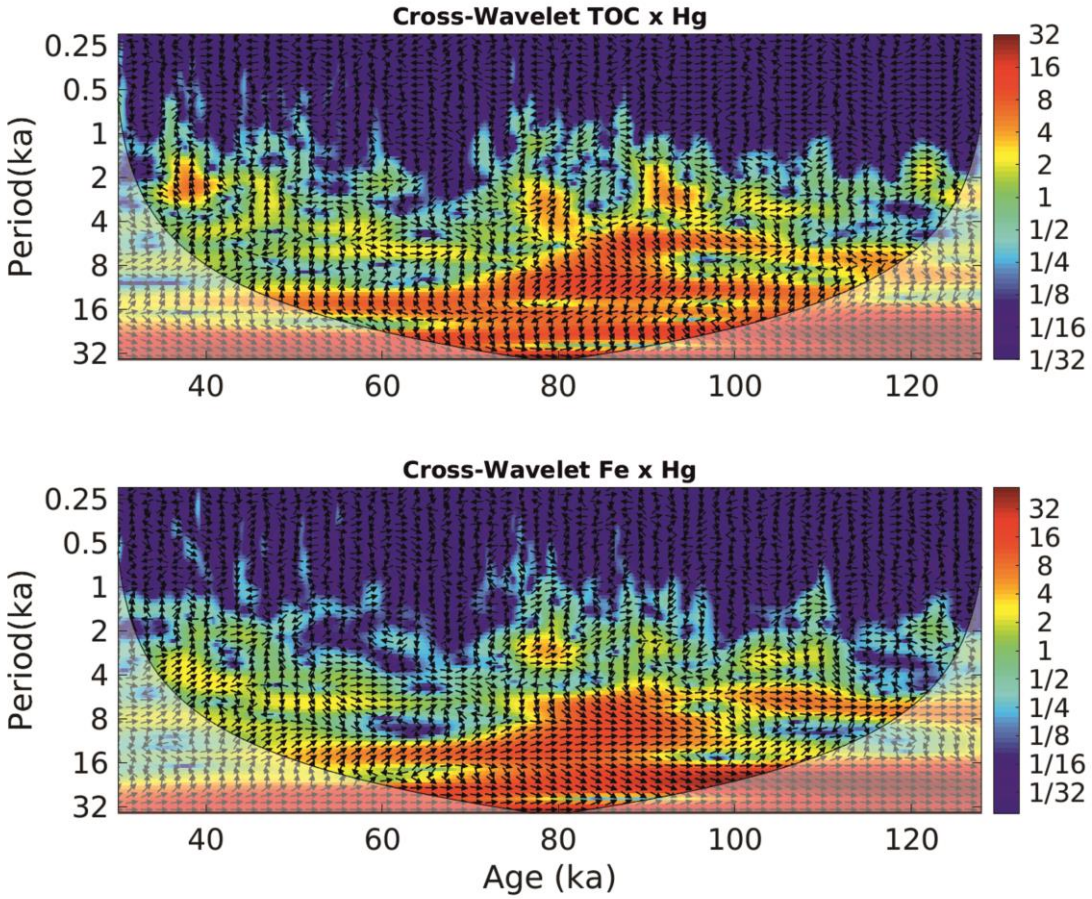

Figure 14: Cross wavelet transform of TOC and Hg time series (top) and Fe and Hg timeseries (bottom). The relative phase relationship is shown as arrows, with in-phase pointing right, anti-phase pointing left, and TOC leading Hg by 90◦ pointing straight down (top) and Fe leading Hg by 90◦ pointing straight down (bottom).

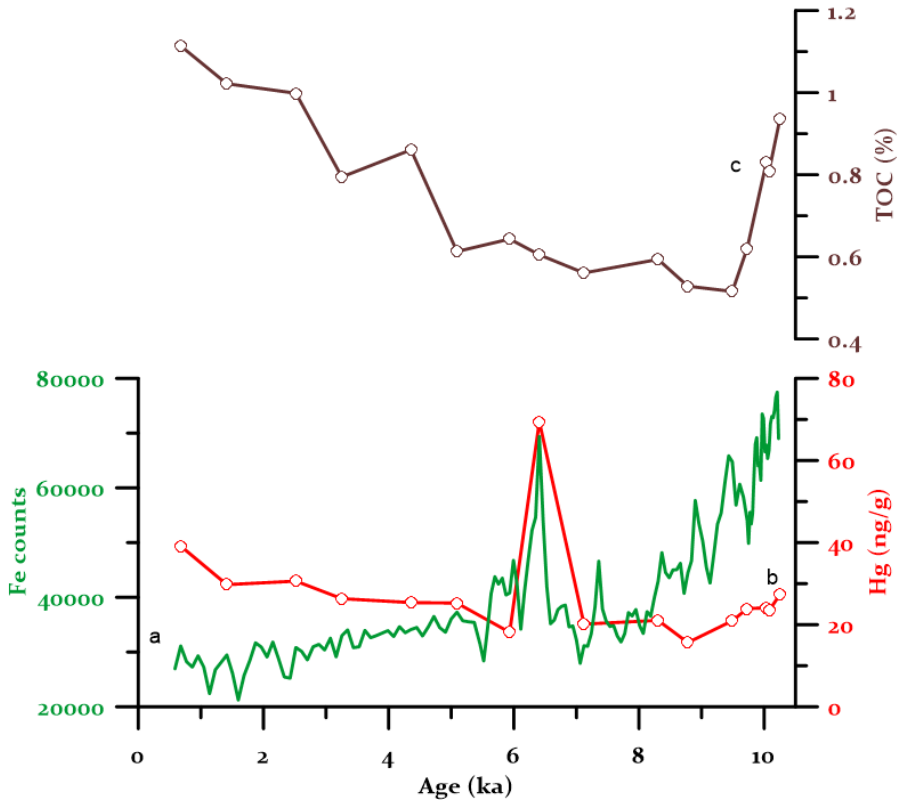

Figure 15: (a) XRF-Fe counts (green line) (b) Hg concentration in ng/g (red line) (c) TOC in % (brown line). Figure shows Mid-Holocene Hg peak coincident with Fe peak at 6.4 ka.

5.1.2 Glacial-Interglacial controls on Hg concentrations

As shown in Figure 16, high Hg concentrations during glacial periods are coincident with elevated dust deposition recorded in both Greenland (Ruth et al., 2007) and Antarctica (Lambert et al., 2008) ice cores. The similarity in dust plots from the two extreme locations supports the notion that high atmospheric dust loads are characteristic of glacial periods. Elevated Hg concentrations in the cold substages of MIS 5 (i.e. MIS 5d and 5b) are also concurrent with minor increases in dust concentrations above their minimum concentrations in the same substages. Another possible dust source that can impact Hg deposition in glacial-interglacial timescales at our site is the Saharan dust (Kumar et al. 2014; Williams et al.,

2016). We compared the Hg record from core GL-1248 with dust fluxes from core MD03-2705 located on the coast of Africa (Skonieczny et al., 2019) and observed a good match between both datasets (Figure 17). Saharan dust fluxes increase during MIS4 and cold substages of MIS5, similar to our Hg concentrations from the Western equatorial Atlantic. This further supports to influence of atmospheric dust concentrations on Hg deposition at our site. On a global scale, cold and dry climatic stages have been identified as periods with high dust levels that enhance rapid Hg sequestration from the atmosphere (Cordeiro et al., 2011). Jitaru et al., (2009) showed that Hg deposition in surface snows over the last 670 ka was notably higher during cold climates, as a consequence of high atmospheric dust loads. However, in a study by Vandaal et al., (1993), the three-fold increase in Hg concentration in Dome C core from Antarctica between 27 and 17 ka, compared to both older and younger periods in the same record, was attributed to increased oceanic productivity. Comparing the findings of Vandaal et al., (1993) with the core GL-1248, although both Hg and TOC concentration plots in this study exhibit similar variations by of elevated concentrations occurring during the glacial periods compared to the interglacial periods (Figure 18 b and c), it is important to note that the TOC include incursions of terrestrial OM to the study site. Although the latter is mainly of marine origin, the influx of terrestrial organic matter has the capacity to dilute marine organic matter (Machado et al., 2016). As a result, Hg and TOC concentrations are poorly normalized (Figure 18a), and have a correlation coefficient, R^2 of 0.18 ($p < 0.001$), thus implying that TOC is unlikely a major driver of Hg records in GL-1248 marine sediments. This finding is contrary to previous studies that have suggested a strong positive relationship between Hg and organic matter in sediments (Vandaal et al., 1993; Outridge et al., 2007; Stern et al., 2009, Grasby et al., 2013, Kita et al., 2013 and 2016), due to the fact that OM scavenges Hg within the water column through sorption, and is subsequently deposits it in marine sediments (Hermann et al., 2012). The outcome is however

consistent with results on Hg-OM relationships from sites located in South America, where authors observed better correlations between Hg and iron (Fe) minerals rather than with organic matter (Roulet and Lucotte, 1995; Marins et al., 1998; Roulet et al., 1998; Wasserman et al., 2003; Selim, 2013). Therefore, it can be conceivably hypothesized that increasing (and decreasing) trends in Hg concentrations over glacial (and interglacial) periods in GL-1248 are in response to the changes in atmospheric Hg deposition onto the NE Brazil continent, which is controlled by the global variation in atmospheric dust loads. Also, the non-correlation between Hg and TOC in the marine sediments, and the existence of strong correlation and parallel trends of Hg and Fe concentration plots (Figure 13), confirm the geochemical association reported by several authors which suggest that Fe- minerals act as the carrier-phase of atmospheric Hg deposited onto tropical soils.

In previous studies of marine sediment cores collected in the coast of NE Brazil, Fe/Ca ratios was used as a proxy for terrigenous vs. marine input (Arz et al., 1998; Jaeschke et al., 2007; Govin et al., 2012). Higher Fe/Ca ratios are recorded during periods of increased terrigenous sediment influx relative to the carbonate fraction. In these studies, elevated Fe/Ca values were reported within glacial periods due to low sea-level and/or to increases in precipitation (wet phases). The occurrence of wet phases in NE Brazil during the glacial periods MIS 4 and MIS 3, when the mean SST reached 23.89 ± 0.79°C, has been associated with Henrich Stadials (Jennerjahn et al., 2004; Nace et al., 2014; Zhang et al., 2015). Further to the increase in terrigenous sediment delivery ensuing from enhanced precipitation, the latter also favours atmospheric Hg 'wet' deposition. Additionally, SST data from prior studies suggest that the glacial periods experienced the most SST reduction (Bard et al., 2000; Martrat et al., 2007), Notable SST reductions in the North Atlantic during the cold sub-stages MIS 5b and 5d are coincident with the extension of the Scandinavian ice sheets (Svendsen et al., 2004). During these periods of low SST and ice sheets enlargement, the relative sea-level is

characteristically low. Therefore, the river mouth is nearer to the core site, and the erosion of shelf sediments, as well as enhanced deposition onto the continental slope (Lacerda et al., 2013; Nace et al., 2014) enhances the delivery of terrigenous materials to the core site. As shown in Figure 16, during MIS 4 and MIS 3 when the RSL was significantly low with averages reaching -71.51 m and -69.03 m respectively, we observe high Fe/Ca values suggesting increased incursion of terrigenous materials offshore via Parnaíba River. This accords the findings of previous studies, which showed enhanced delivery of terrigenous materials onto the continental slope of Western South Atlantic during the glacial periods. Contrarily, the near baseline Fe/Ca ratios recorded in the interglacial periods signify lower terrestrial material delivery. Although both MIS 1 and 5e are interglacial periods, previous studies have suggested that the MIS 5e (SST = 28.9°C) interglacial experienced higher temperatures than MIS 1 (SST = 28.3°C) (Rama-Corredor et al., 2015). This difference in SST between both interglacial periods has been attributed to precessional modulation (Martrat et al., 2014). As a result of the higher SSTduring MIS 5e, ice sheet reduction ensued and the global sea-level rose by up to 5m than the modern sea-level (Hodgson et al., 2006; Rohling et al., 2007). The seal-level rise presumably positioned the core site farthest from the river mouth, thus reducing the amount of continental material and Hg delivery. Accordingly, it is significant to mention that the least average Hg concentration in this study was recorded in MIS 5e.

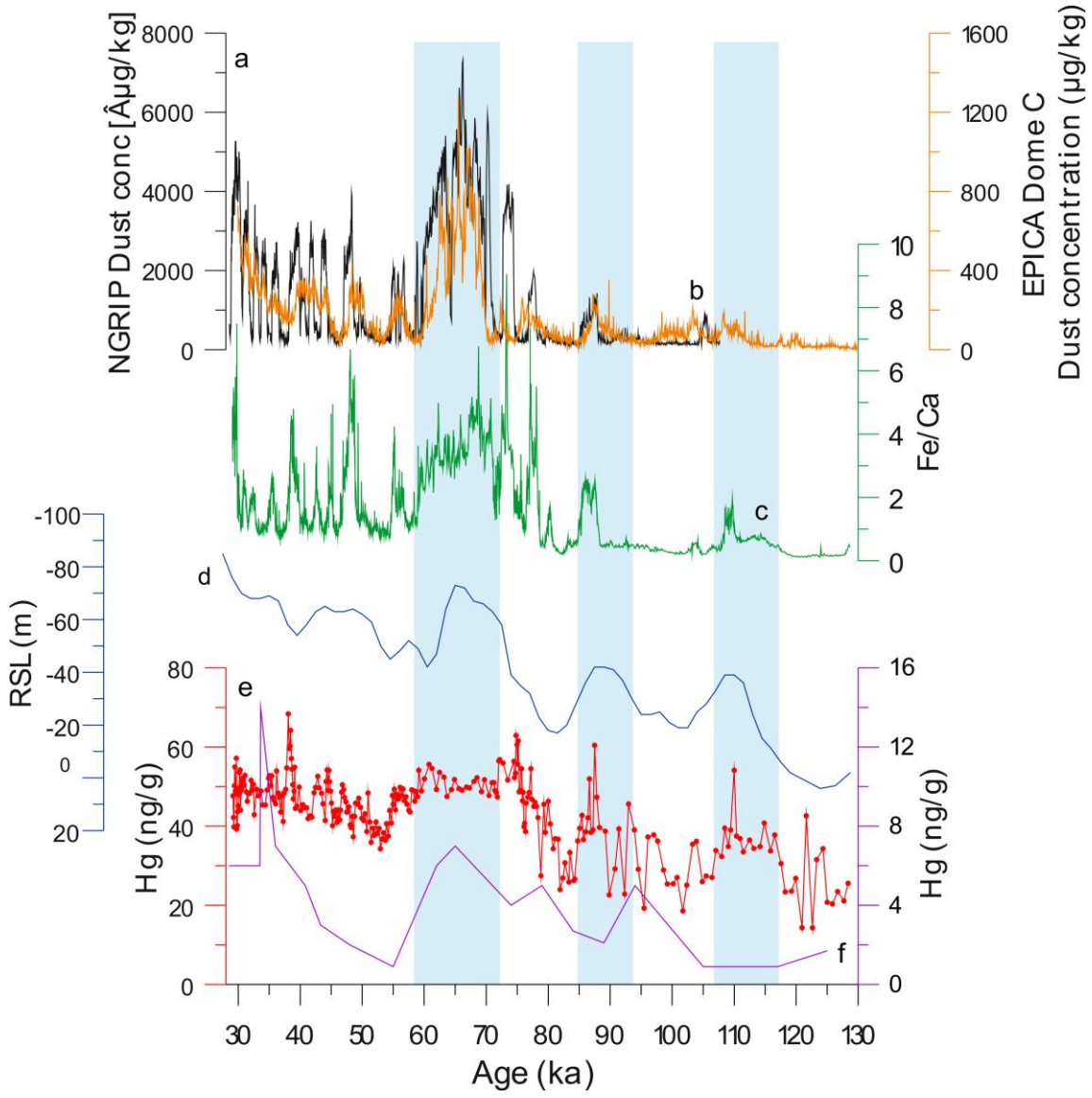

Figure 16: (a) NGRIP ice core record of atmospheric dust deposition (Ruth et al., 2007) [brown line] (b) EPICA Dome C ice core record of atmospheric dust deposition (Lambert et al., 2008) [red line] (c) Fe/Ca ratio from GL-1248 indicating periods of high and low terrigenous sediment delivery to the study site [green line] (d) Relative sea-levelsea-level (m) from Waelbroeck et al. (2002) [blue line]. (e) Hg concentration in GL-1248 [orange line]. (f) Hg data from Antarctica (Jitaru et al. 2009) [purple line]. High dust concentrations, low sea-levelsea-levels and high amount of terrestrial load delivery to the core site are coincident with elevated Hg records in MIS 4 and 3 as well as in the cold substages of MIS 5 (5d and 5b). These cold periods are highlighted in blue bars.

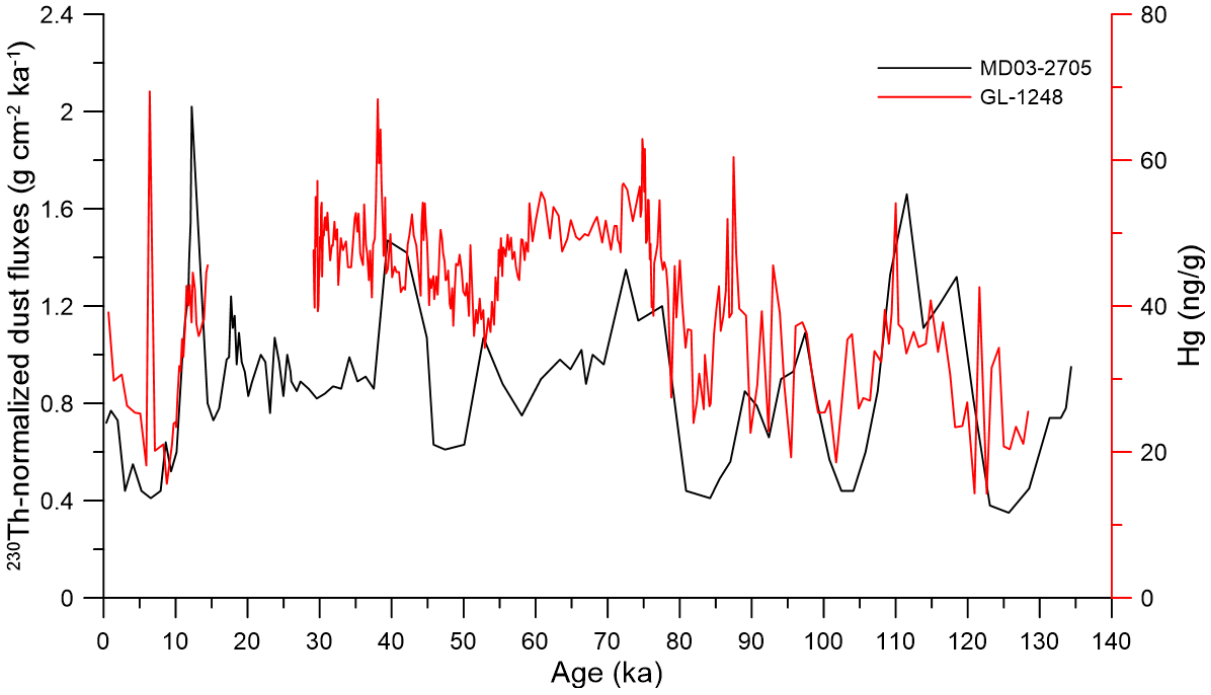

Figure 17: Hg concentrations from core GL-1248 (red line) and 230Th-normalized dust fluxes from core MD03-2705 (black line) (Skonieczny et al., 2019) for the last 130 ka. The Younger Dryas (YD) and the Heinrich stadial 4 (HS4) are highlighted in each record.

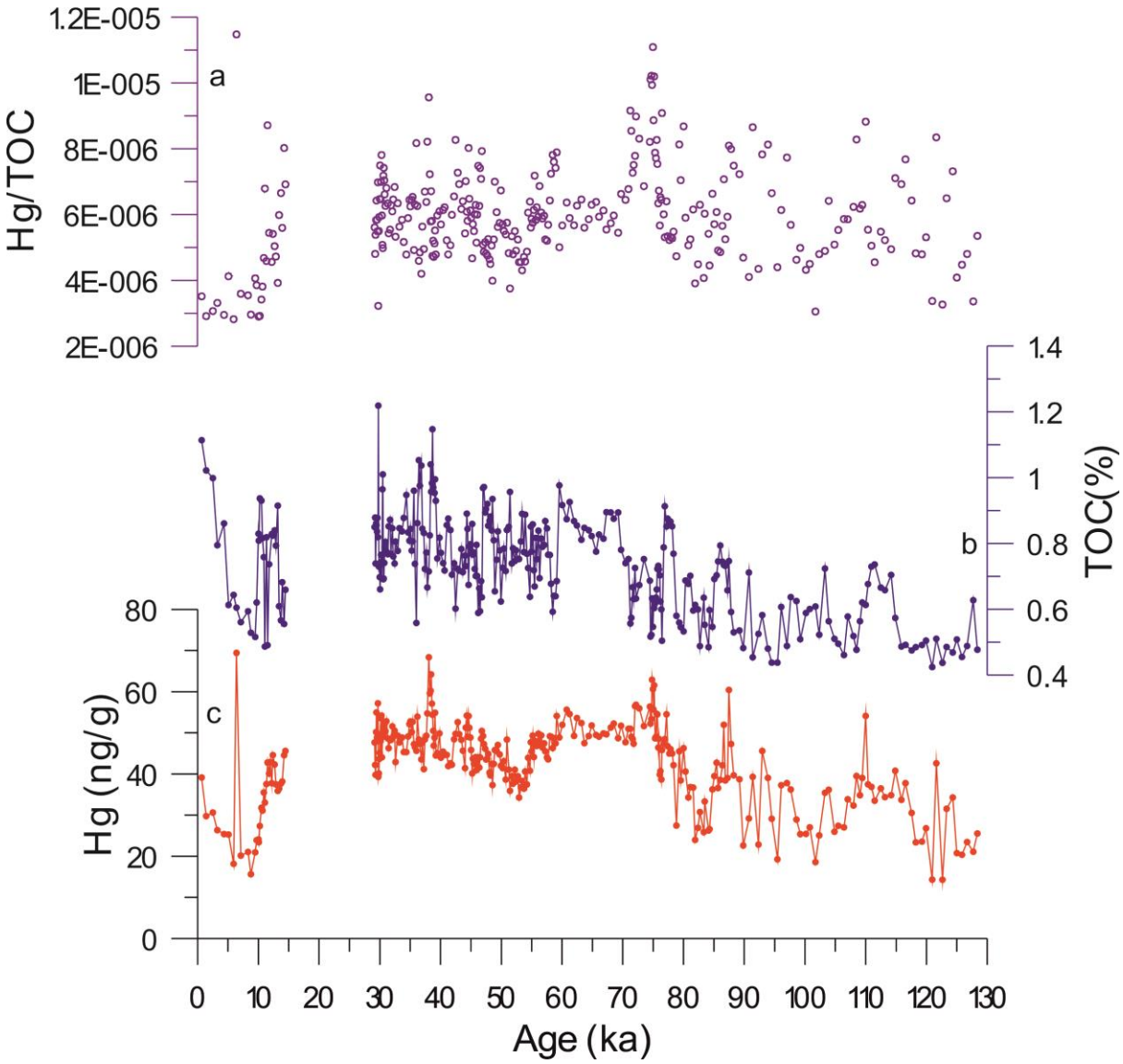

Figure 18: Hg-TOC relationship as shown by (a) Hg/TOC normalization plot (b) TOC in % (blue line) (c) Concentration plots of Hg in ng/g (orange line).

Carbon and nitrogen isotopic ratios ($\delta^{13}C$ and $\delta^{15}N$) of organic matter are proxies whose variability helps to understand the source and quality of organic matter in sediments. $\delta^{13}C_{org}$ distinguishes between marine and continental sedimentary organic matter, while $\delta^{15}N_{org}$ variations signify the changes in OM source and quality, with high values denoting high degrees of OM degradation during times of normal sedimentation

Meyers, 1994; Jennerjhan et al., 2004). The high variability of $\delta^{13}C_{org}$ values (fluctuating between -20‰ and -24‰) recorded in the glacial period (Figure 7b) depicts changes in the origin of organic matter between marine and terrestrial sources. Jennerjhan et al., (2004) studied sedimentary cores from the continental margin of NE Brazil and observed decreases in $\delta^{13}C_{org}$ from -20‰ to values between -23‰ and -24‰. The authors attributed the 3‰ reduction to a contribution of terrestrial OMto the study site. Seeing that the $\delta^{13}C_{org}$ values vary similarly with theirs, and considering the proximity of the sediments cores in their study to this present study (Figure 3), it is possible to infer that the $\delta^{13}C$ variation indicates the influx (as a result of low sea-level as explained in the previous paragraph) of terrestrial organic matter mainly produced by C_3 land plants. Supporting the findings of Jennerjhan et al., (2004) in the same study where the authors ascribed minimum (maximum) $\delta^{15}N_{org}$ values to low (high) sedimentation rates in NE Brazil continental shelf, Zhang et al, (2015) have showed that in the glacial periods when the sea-level was low, most of the NE Brazilian shelf was exposed and rapid sedimentation of river-transported terrestrial material on the continental slope occurred. The findings suggest that the minimum $\delta^{15}N_{org}$ values (average 5.8‰) recorded in the glacial periods can be attributed to high sedimentation rates ensuing from increased continental runoff, whereas the maximum $\delta^{15}N_{org}$ values recorded during the interglacial periods (average 6.05‰) depicts average sedimentation conditions. Altogether, the $\delta^{13}C_{org}$ and $\delta^{15}N_{org}$ variations in GL-1248 support the earlier hypothesis that higher amounts of continent-derived materials were deposited on the continental slope of NE Brazil in the glacial periods as opposed to interglacial periods. These results are consistent with the XRD mineralogy results which follow the same glacial-interglacial alteration in the origin of marine sediment GL-1248 between a continental source during glacial periods and cold substages, to a marine source during interglacial periods and warm substages (Table 1).

In general, Hg concentration in core GL-1248 varied in response to glacial-interglacial changes. To further support this, time series analysis of Hg concentration (Figure 10) show a peak centred in 56 ka (half eccentricity) indicating glacial- interglacial variability. The high Hg values recorded in glacial periods are favored by a combination of global (high atmospheric dust loads) and regional (augmented wet deposition, precipitation, enhanced erosion, and material transport and low sea-level) climatic factors. In contrast to glacial periods, the interglacial periods (MIS 1 and MIS 5e) and the warm sub stages of MIS 5 (MIS 5c and MIS 5a) witnessed opposing climatic conditions. Since interglacial periods present less atmospheric dust deposition (Jitaru et al., 2009) and high sea-level, as well as low regional precipitation and nominal erosion, the outcome of this contrasting climatic trend in the warm periods is the lower Hg values recorded in the core (Figure 27 a and b). However, inconsistent with the depleted Hg concentrations noted during interglacial periods and warm substage MIS 5c, Hg peaks occurred at the end of MIS 5a. These peaks are coincident with Fe/Ca peaks and they correlate with Dansgaard-Oeschger (DO) stadials.

5.1.3 Millennial-scale events recorded by Hg concentrations

Several marine sediment cores collected offshore northeastern Brazil show Fe/Ca and Ti/Ca peaks during Heinrich Stadials (HS) (Arz et al., 1998; Jaeschke et al., 2007; Nace et al., 2014). Wang et al. (2004) also observed speleothem growth phases, correlating with HS1, HS5, and HS6, as a result of increased precipitation, at 10°S in northeastern Brazil. Large pulses of terrigenous sediment supply offshore NE Brazil occurred during the Younger Dryas (YD) (Jaeschke et al., 2007; Deplazes et al., 2013; Nace et al., 2014; Zhang et al., 2015). In addition to the evidences on HS and YD signals in the tropics, Dansgaard-Oeschger (DO) variability has been recorded in sediments of the Cariaco Basin (Deplazes et al., 2013) and NE Brazil (Venancio et al., 2018). Enhanced precipitation over northeastern Brazil during

DO stadials coincide with dry periods in Cariaco Basin (Jaeschke et al., 2007), thus signifying an anti-phase response in precipitation patterns between both locations. These tropical signals of millennial-scale events indicate that intensified precipitation in NE Brazil possibly due to higher Sea Surface Temperature (SST) and the accompanying southward ITCZ migration which resulted in increased continental runoff in NE Brazil during the cold North Atlantic events. Several studies (Broccoli et al., 2006; Stouffer et al., 2006; Mulitza et al., 2017) have attributed these occurrences to the reductions in AMOC strength. Consistent with these studies, abrupt increases in the Fe/Ca ratios from core GL-1248 (Figure 18d) are observed during certain millennial-scale events. In addition, certain Hg peaks occur within these periods and coincide with these Fe/Ca peaks of millennial-scale events. Specifically, distinct rises in Hg concentrations which are synchronous with Fe/Ca peaks are observed in Heinrich Stadials 5a, HS5, HS4 and the Younger Dryas, as well as DO-12, 11 and 8 (Figure 18). These observation of high Hg concentrations during millennial-scale events is consistent with findings from numerous studies which show that millennial climate change are strongly correlated with active Quaternary volcanism (Bay et al., 2004; Baldini et al., 2015), as it is anticipated that the atmosphere is burdened with more Hg from volcanic eruptions during these millennial-scale events. In like manner, the possible influence of Sahara dust on GL-1248 sediment, and by extension its Hg concentrations, cannot be ruled out owing to the fact that Prospero et al., (1981) showed that high quantities of dusts are transported from the Sahara Desert to mainly South America. Combining the findings of Moreno et al. (2002) which showed that Saharan wind intensity increased during D-O and the Heinrich Stadials with the observation of high Hg concentrations during HS4 and the YD in core GL-1248 that are synchronous to increases in Saharan dust flux (Supplementary Figure 2), it is possible that Saharan dust may play a role in Hg deposition at our site during millennial-scale events.

Correspondingly, Hg fluctuates with periods of 900 yr (Figure 9) thus reinforcing the evidence of millennial-scale variability in the Hg records.

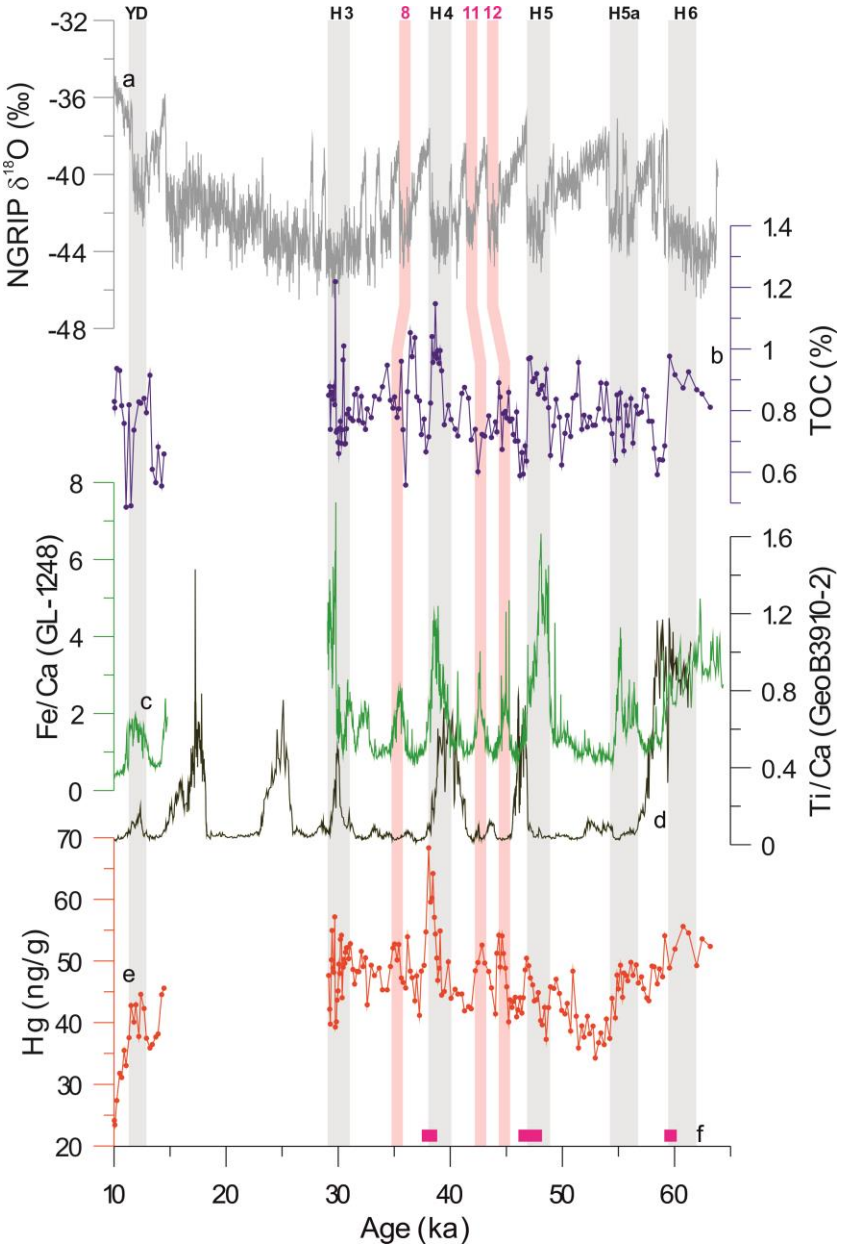

Figure 19: Millennial-scale (MS) variability as shown by the comparison of Hg and Fe/Ca ratio from GL-1248 with NGRIP data and other proxies from NE Brazil. (a) speleothem growth phases (red rectangles) consequent to increased precipitation in NE Brazil (Wang et al., 2004). (b) Hg record (brown line) from core GL-1248. (c) Fe/Ca (blue line) from core GL-1248 (d) Ti/Ca record from core GeoB3910-2 (black line) collected off northeastern Brazil (Jaeschke et al., 2007) (e). TOC from GL-1248 (green line). (f) $\delta^{18}O_{ice}$ from NGRIP on the GICC05 modelext time scale (orange line). Heinrich Stadials (HS 6-3) and Younger Dryas (YD) are marked in gray bars. The pink coloured bars mark the Dansgaard-Oeschgerstadials 8, 11 and 12 respectively.

However, differently from glacial-interglacial variations where sea-level change was a major determinant of Hg variations, changes in Hg concentration during stadials were not influenced by sea-level fluctuations since sea-level changes are not significant in the millennial timescale. Figure 19 shows a comparison of original Hg concentrations with the same Hg data but extracting the effect of sea-level variation. It is observed that although millennial frequencies are present in both graphs, their statistical power increases after filtering the sea-level change. This confirms the masking effect of sea-level fluctuations by the millennial-scale variability in the record.

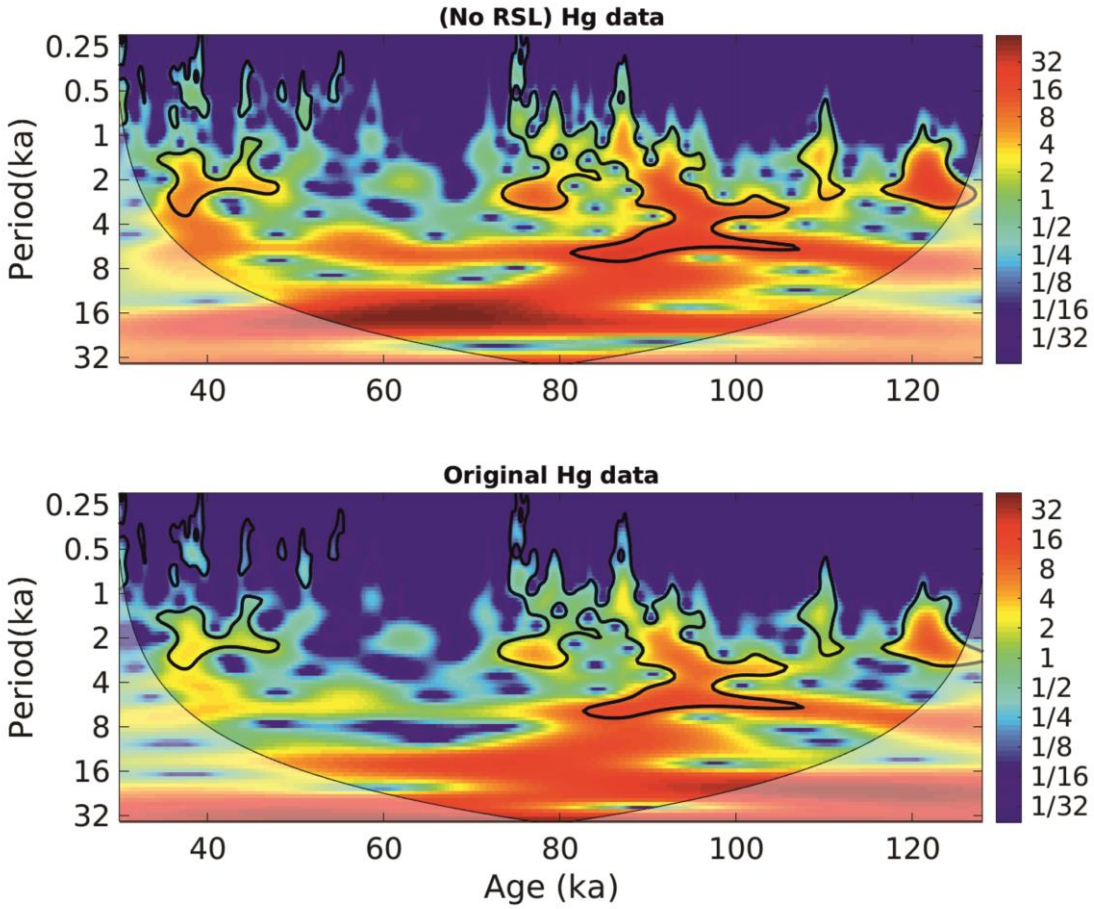

Figure 20: The continuous wavelet power spectrum of Hg signal without RSL influence (top) and original Hg signal (bottom). The thick black contour designates the 5% significance level against red noise and the cone of influence (COI) where edge effects might distort the picture is shown as lighter shade.

The observed rise in the Hg concentrations during millennial climate variability could be explained by a sequence of climate mechanisms which ensue from the southward positioning of the ITCZ during the stadials (Broccoli et al., 2006; Stouffer et al., 2006). Noting that high frequency of volcanism in this period will increase the background levels of atmospheric Hg, increased precipitation during millennial-scale events will boost atmospheric Hg deposition on the continent (wet deposition). Furthermore, influx of fluvial sediments by the Parnaíba River created by intensified fluvial erosion on the Parnaíba Basin will contribute to the increased transportation and deposition of terrigenous materials at the continental slope of NE Brazil during these millennial-scale events (Figure 18c). While it could be argued that direct atmospheric Hg deposition over the ocean is equally a noteworthy contribution to the sedimentary Hg records, the observed Fe-Hg correlation described in previous sections suggests that Hg in GL-1248 is essentially from a continental (secondary) origin. It is important to note that despite the evidences of millennial-scale variability in Hg records of GL-1248 sediment core, discrepancies in the magnitudes of both Hg and Fe/Ca peaks evident during these events (Figure 18 d and f). For example, the Fe/Ca peaks are well-defined in HS5a to HS3 (Figure 18d), whereas only HS4 is distinct in Hg records (Figure 18f). Following the idea that Hg is transported alongside eroded continental material from NE Brazil via the Parnaíba River to the core site, in the absence of other mechanisms controlling Hg variation in sediments, the amount of Hg delivered at the study site should be consistent with continental material delivery as indicated by the Fe/Ca ratios. Thus, both records should present a similar trend in the magnitude of their peaks. Due to the lack of this expected comparable trend, it could be argued that the observed millennial-scale events in the Hg variations are unlikely to be solely related to precipitation and erosion intensification, due to ITCZ southward displacement. Surprisingly, enhanced organic matter deposition shown by elevated TOC values occurred during millennial-scale events with their amplitudes varying

similarly with those of Hg (Figure 18b). in the cross wavelet transform of TOC and Hg time series (Figure 8), an in-phase relationship between the two parameters is evident by the right-pointing arrows that occur occasionally between 90 ka and 60 ka in the 6 ka band. Furthermore, arrows between periods 30 ka and 75 ka point upwards and indicate a dominance of TOC over Hg. The implication of this is that both total organic carbon and Hg show some correlation at the mentioned interval. This observed changes in TOC concentrations during millennial-scale events are in line with earlier findings (Jennerjhan et al., 2004; Sach and Anderson 2005; Menviel et al., 2007). Since variations in total organic carbon influence Hg sequestration into marine sediments, it is possible that the sedimentary Hg records during these periods are somewhat inclusive of the sequestration of "free" Hg (unbound to Fe- compounds) by TOC within the water column, followed by immobilization in marine sediment, a finding that is supported by various studies (Outridge et al., 2007; Stern et al., 2009, Grasby et al., 2013, Kita et al., 2013 and 2016). Hence, it can be hypothesized that, although TOC is not a major driver of sedimentary Hg variations throughout the studied period in marine sediment GL-1248, the likelihood of its influence in certain periods cannot be dismissed. This is further supported by the fact that the correlation coefficient (R^2) generated from the linear regression between TOC and Hg is not 0 (i.e. $R^2 \neq 0$), rather they are poorly correlated ($R^2 = 0.18$). These findings suggest that Hg variations in GL-1248 during millennial-scale events are modulated mainly by changes in fluvial transport and marginally influenced by total organic carbon.

5.2 Hg Profiles in Sediments of the Congo Basin over the Past 130 ka

5.2.1 Factors controlling sediment material arriving at ODP1077

The Congo River delivers both water and sediment to the Atlantic Ocean, and it is directly, as well as permanently connected to an active deep-sea fan through the 1,135 km-long deeply incised submarine Congo Canyon and channels (Babonneau et al., 2002). This hydrographic network remained relatively stable throughout the Quaternary despite sea-level and climatic changes (Flügel et al., 2015; Guillocheau et al., 2015). As a result, marine sediments in ODP1077 contain a mixed record of sediment supply by the Congo River, intercalated with the oceanic record (Berger et al, 1998), and could therefore be a useful proxy in understanding both marine and terrestrial ecosystems. In a study by Gingele et al. (1998), the authors reported that no less than 95% of sediment deposited in the deep-sea fan is directly provided by the Congo River, and aeolian contribution is limited. This propounds that Hg records in ODP1077 majorly originate from the continent. Despite being the world's second largest river in terms of both drainage area (3,700,106 km^2) and water discharge (41,000 m^3/s) (Laraque et al., 2013), the Congo basin has experienced much less scientific attention in basin hydrology and sediment supply than other large tropical catchments (Alsdorf et al., 2016), factors which are essential to understanding variations in Hg delivery to the study site.

In a recent study by Molliex et al., (2019), water and sediment discharge leaving the Congo Basin were reported to be both controlled by climatic (precipitation and river discharge) and environmental (oceanic upwelling and forest cover) factors. Surprisingly however, both water and sediment discharges were 'negatively' correlated (Figure 20). The observed discrepancy could be explained by the opposing effects which both climatic and environmental factors can have on sediment production within the same period. For instance, in periods of low precipitation rates during cold climate conditions, water discharge is reduced, leading to minimal sediment erosion. Also in the same period, the regression of forest cover that is

characteristic of cold climates will boost soil erosion, thereby leading to increased sediment production. On the assumption that sediments at the study site mainly originate from the Congo basin, Hg recorded in ODP1077 are mainly sourced from the adjoining continent. Therefore, recorded Hg variations are affected by the same factors that control sediment delivery at the marine sediment site, that is, both environmental and climatic factors.

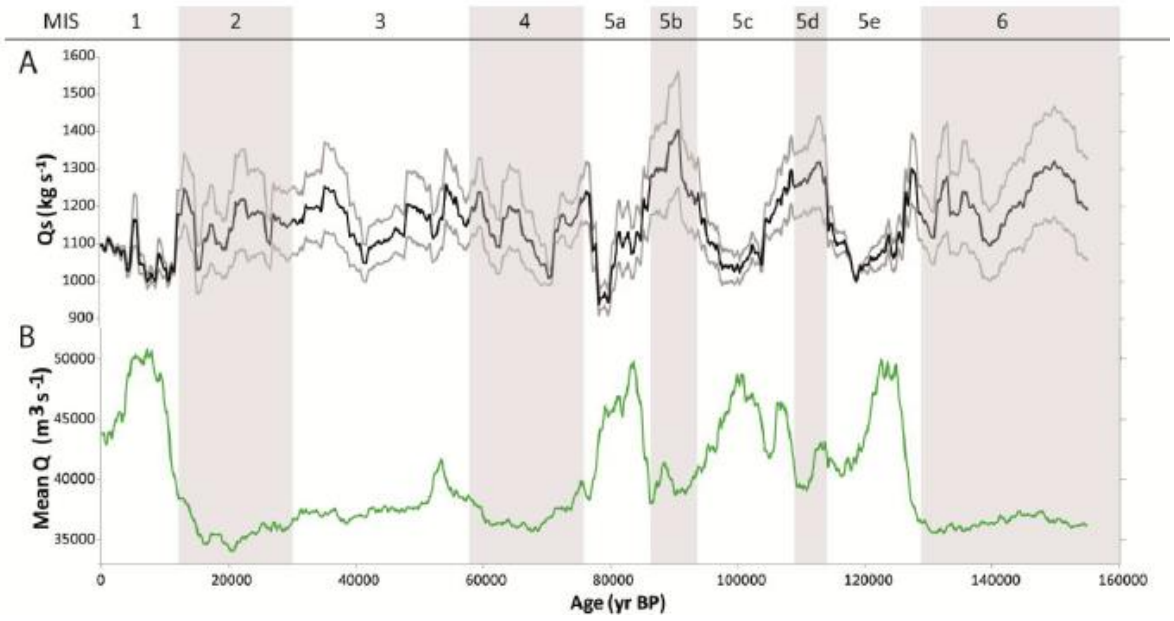

Figure 21: HydroTrend simulations of sediment load and water discharge over the last 155 ka. A) Simulated suspended sediment load evolution (Qs). The black curve corresponds to the mean sediment load grey curves are the minimum and maximum with respect to vegetation index. B) Simulated water discharge (Molliex et al., 2019).

Precipitation is a key determinant of sediment discharge, thus, elevated precipitation rates will inevitably yield increases in sediment export (Xianxio et al., 2013). The latitudinal migration of the mean ITCZ position across the Congo basin from its southerly position creates monsoonal conditions over the basin, which accordingly leads to high precipitation and accompanying increased terrigenous discharge from the basin (Marret et al., 2001). During periods of high precipitation, large pulses of eroded sediments from the Congo Basin are transported offshore. Fe/Ca ratio, is a proxy used to determine the variations of

terrigenous inputs to the ocean with higher (lower) ratios indicates stronger (lesser) discharge of terrigenous sediments (Adegbie et al., 2003; Govin et al., 2012). The semi-quantitative XRF Fe/Ca ratios (Figure 21) varied significantly within all periods of the last 130 ka in ODP1077, with the exception of the near baseline ratios recorded between 20 ka and 5 ka, and relatively constant ratios within MIS 5c. A possible explanation for the high Fe/Ca variability during the intervals 130 – 110ka, 98 – 80 ka and 60 – 20 ka could be that climatic and/or environmental factors changed vastly over these periods, which lead to drastic changes in the intensities river runoff and coastal erosion, as well as variations in sediment production and discharge. According to Zabel et al., (2001), moisture carrying SW monsoonal wind causes precipitation over the Congo basin, thus leading to the weathering and erosion of sediments and rock materials into the Eastern South Atlantic Ocean. Although precipitation is a major determinant of sediment yield and discharge, forest cover is also a remarkable factor to be considered in terms of sediment discharge. Forest cover protects soils from the impact of raindrops by intercepting them to reduce their kinetic energy (Morgan, 2005). They also control the rates of infiltration, soil water transpiration, and reduce surface runoff (Castillo et al., 1997; Gyssels et al., 2005; Xin et al., 2010; Roller et al., 2012; El Kateb et al., 2013). As expected, the regression of forest cover enhances soil erosion thereby leading to increased sediment production, meanwhile the expansion of forests reduces sediment production and export. Likewise, the low extension of the tropical rainforest in cold climates will favour the supply of terrigenous sediments to the Congo deep-sea fan area. Therefore, it is likely that the variations in ODP1077 Fe/Ca ratio indicate changes in both the environmental and climatic factors which control sediment production and transportation to the ODP1077 core site. In the study by Molliex et al., (2019), although lower water discharge occurred during the cold periods, sediment yield at the time was higher. The sediment yield was therefore attributed to the less dense vegetation cover which is characteristic of the cold periods, especially the Last

Glacial Maximum (LGM) where tropical rainforests decreased by about 70-80% for the Congo catchment (Jolly et al., 1998; Rommerkuirchen et al., 2006).

For most part of the studied period, Fe/Ca ratios followed the expected pattern of high sediment production coinciding with the periods of reduced forest cover, and vice versa (Figure 21). For instance, at the 20 – 5 ka interval, sediment export reduction coincided with increasing forest cover. However, exceptions to this general trend are evident between 40 – 35 ka and at around 47 ka and 85 ka where drastic reductions in terrigenous sediment supply coincided with forest cover reduction. also at the interval 62 – 55 ka, increases in forest cover occurred alongside elevated terrigenous sediment delivery. As shown by Caley et al., (2011), the Monsoon Index (Figure 21b) is low during MIS 3 and 2, which suggests that precipitation rates ought to be low, therefore low sediment runoff is anticipated. Contradictorily however, occasional elevated Fe/Ca ratios were recorded during both stages. however, decreasing tend in Monsoon Index starting at ~ 20 ka and terminating at ~ 5 ka coincides with low values of Fe/Ca ratio during the same interval. Owing to these unsatisfactory evidences of both consistencies and non-conformities of Fe/Ca ratios with climatic and environmental proxies, the marine sediments of ODP1077 and by extension its Hg variations could be speculated to be influenced by both climatic and environmental factors, which could have occurred synchronously or asynchronously. Notwithstanding, both climatic and environmental proxies are insufficient to explain the Hg variations in ODP1077.

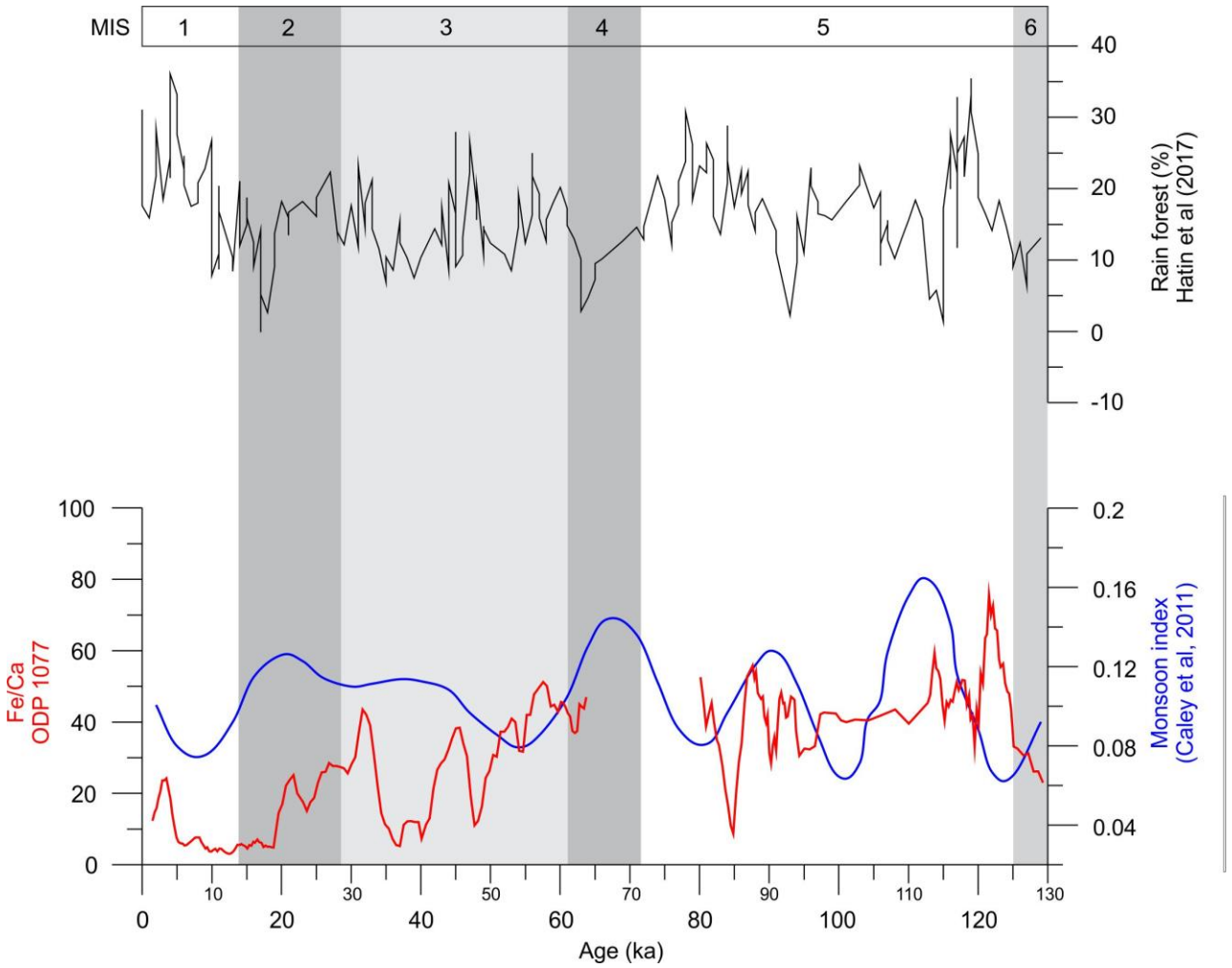

Figure 22: Fe/Ca variations of the marine sediment core ODP1077 with climate and environmental proxies. (a) Fe/Ca ratios (green line) (b) Monsoon Index (black line (Caley et al., 2011) (c) Rain Forest percentage (orange line) (Hatin et al., 2017).

5.2.2 Sources of organic carbon in the Congo deep-sea fan area over the last 130 ka

ODP1077 was retrieved from a high primary productivity region of the Eastern South Atlantic (Figure 4). The characteristic high primary productivity of the marine sediment core location is as a result of the complex interactions of oceanic/river induced upwelling, as well as nutrient supply by the Congo River (Schneider et al., 1997; Hopkins et al., 2013). Variations in the total organic carbon recorded are similar to those from the nearby site ODP1075 reported by Schneider et al., (1997) and Jahn et al., (2005). Comparable to the findings of these studies, highest total organic carbon of marine sediment core ODP1077 of the last 130 ka coincided with glacial phases and cold substages (MIS 3 and 2, MIS 5d and

b), while minimum values occurred during the interglacial periods (MIS 5e and 1) and warm substage (MIS 5c) [Figure 23 c and d]. Owing to the aforementioned regional conditions which control paleopeoductivity in the Congo deep-sea fan area, the total organic carbon is a combination of autochthonous (marine) and allochthonous (terrigenous) organic carbon. Interestingly, Schneider et al. (1997) distinguished between continental and marine sources of organic carbon in the same region over the last 200 ka by calculating the continental and marine portions from $\delta^{13}C_{org}$ using a simple mixing equation. The authors showed that variations of total organic carbon in the Congo Fan core GeoB1008 (Figure 4) over glacial/interglacial periods are mainly the result of changes in marine organic carbon MOC, and that the contributions of terrigenous organic carbon to the sediment was minimal and not responsible for the observed changes in the TOC.

$\delta^{13}C_{org}$ in ODP1077 marine sediment show a mixture of organic carbon from both terrestrial and aquatic sources. Similar to the TOC trends, $\delta^{13}C_{org}$ values are highest in MIS 3 and 2 (Figure 23e) maintaining values between -21.59‰ and -20.50‰. Elevated values are also registered within cold substages of MIS 5 (5d and 5b). According to Meyers et al., (1994), marine organic carbon from marine algae has $\delta^{13}C_{org}$ values between -22‰ and -20‰, thereby suggesting that organic carbon records during cold periods are dominantly of marine origin. In contrast, notable decreases in $\delta^{13}C$ values to values lower than -22‰ are observed during MIS 5e and 1, as well as the warm substage of MIS 5 (5c). These variations in $\delta^{13}C_{org}$ values are comparable to those reported by Jennerjahn et al., (2004), and are consistent with those of Jahn et al. (2005) in latter's study of the same marine sediment core where the authors indicated that enhanced supply of allochthonous organic carbon during periods of increased terrigenous supply. Therefore, both total organic carbon and $\delta^{13}C_{org}$ variations suggest that the organic carbon was mainly of terrestrial origin during warm climate

conditions, and was influenced mainly by increased river discharge (Schneider et al. 1997), whereas, marine biological production prevailed during the cold climate conditions.

The elevated total organic carbon dominantly of marine origin during MIS 3 and 2 (Figure 23) likely ensued from a combination of oceanic and atmospheric conditions. According to Dupont et al., (1999), MIS 3 was characterised by strong oceanic circulation that occurred under the influence of weak atmospheric conditions. This supposedly resulted in BC intensification and subsequent upwelling conditions (Jansen et al., 1996). Supporting the purported upwelling conditions of MIS 3, Dupont et al. (1999), showed, using pollen records, that oceanic productivity increased during MIS 3. The period also experienced low extension of tropical rain forest, as is expected of the cold and dry climate condition that is typical of glacial stages (Dalibard et al., 2014). In addition to the enhanced sediment production which will ensue from the rain forest reduction, the close proximity of the river mouth to the core site, a consequence of the low sea-level stand during glacial periods (Figure 23g), will favour the erosion of shelf sediments and subsequent deposition of the eroded materials (Lacerda et al., 2013; Nace et al., 2014) to the continental margin. The MIS 2 glacial period also experienced a similar condition although with weaker African monsoon than MIS 3 (Figure 22b), and higher precipitation (Schneider et al., 1994; Caley et al., 2011; Dalibard et al., 2014).

The interglacial period, MIS 5e on the other hand witnessed opposing oceanic and atmospheric conditions with reports of strong Africa monsoon, increased precipitation and intensified Congo River discharge (Figure 21 a and b) (Gasse et al., 1989; Uliana et al., 2002; Caley et al., 2011). According to Schneider et al., (1994), the weak trade winds during African monsoon maximum hindered the occurrence of coastal upwelling. These atmospheric conditions favoured the influx of terrigenous materials to the Congo deep-sea fan area. Contrary to the expectation that the high relative sea-level in MIS 5e (Figure 23g) should

have diminished the Fe/Ca ratio, elevated Fe/Ca ratio is observed during the period. This finding suggests that the noted high terrigenous material delivery during MIS 5e that ensued from the prevailing atmospheric conditions attenuated the effect of the distant river mouth to the core site which should have diminished terrigenous material delivery (Figure 23 b and g). A different condition occurred in MIS 1, where Fe/Ca rose from background ratios at the MIS 2/1 transition to moderately elevated ratios at the middle of MIS 1, despite the sea-level being equally as high as during MIS 5e. Therefore, the Fe/Ca ratios recorded in MIS 5e are higher than those recorded in MIS 1. A similar difference between the two interglacial periods was also reported by Dupont et al. (1999), who reported higher Al/K ratios during MIS 5e than in MIS 1.

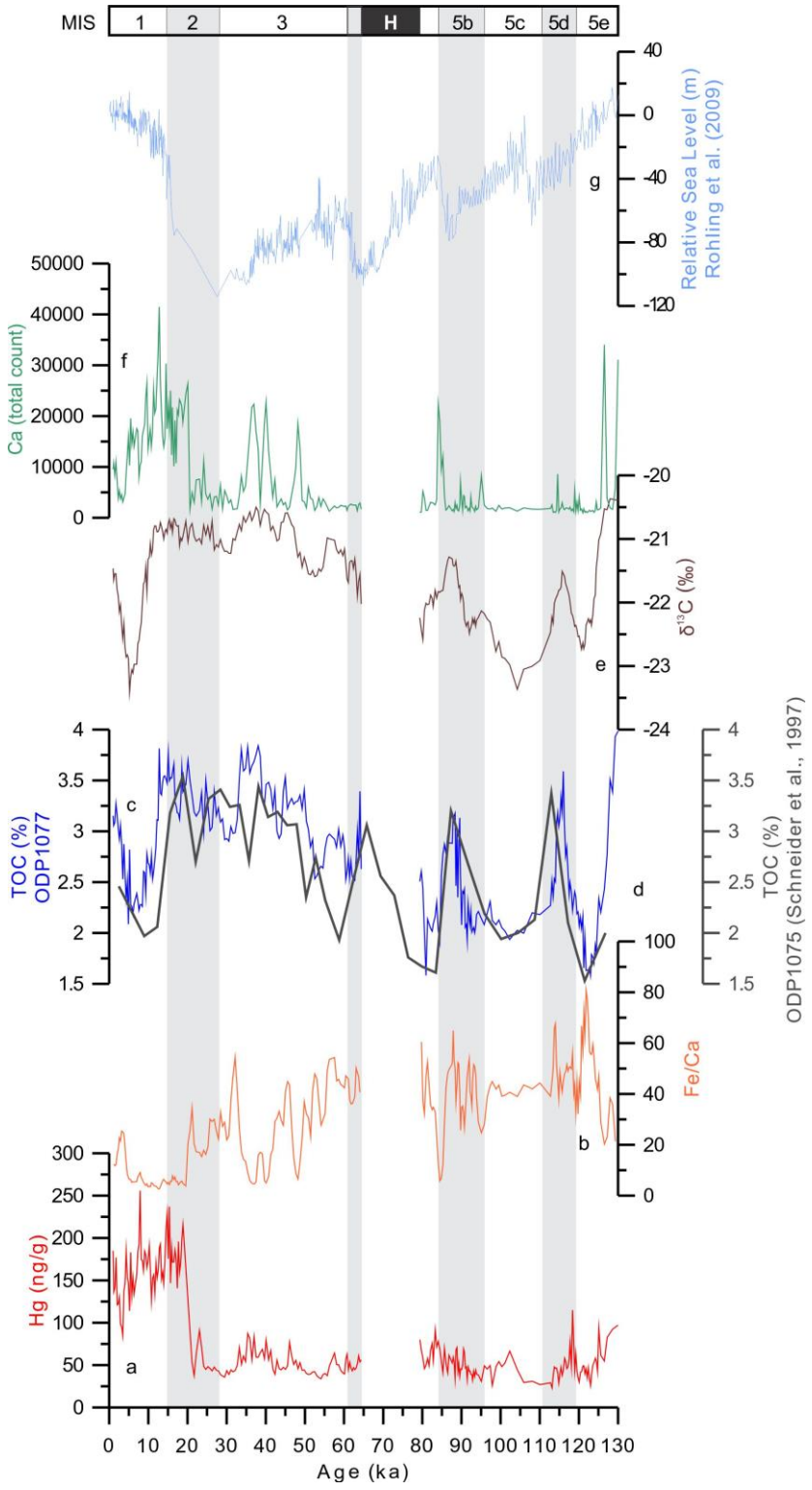

Figure 23: (a) Hg concentration in ODP1077 (red line), (b) Fe/Ca ratios (orange line), (c) TOC in ODP1077 (blue line), (d) TOC in ODP1075 from Schneider et al., 1997 (grey line), (e) $\delta^{13}C_{org}$ of core given in ‰ (brown line), (f) Ca counts (green line), (g) Relative sea-level, m, from Rohling et al., (2009).

Understanding the conditions governing TOC variations has important implications on Hg accumulation in ODP1077 sediments. Mercury concentration plot shows no similarity with both total organic carbon and $\delta^{13}C$ variations (Figure 23), also, both parameters are poorly correlated with Hg having correlation coefficients, $R^2 = 0.06$ ($p < 0.001$) and 0.02 ($p < 0.001$) respectively. Sedimentary Hg concentrations are up to 3 orders of magnitude higher between 20 – 0 ka than the rest of the studied period (Figure 23), whereas no such changes are observed within TOC and $\delta^{13}C$ values. From this observation, it is likely that contrary to findings of several studies which shows strong correlation between total organic carbon and Hg concentrations (Grasby et al. 2013; Kita et al., 2013; Hermanns et al., 2013; Kita et al., 2016), the TOC in ODP1077 are insufficient to interpret Hg accumulation over the studied period in the Congo deep-sea fan area. Perhaps a possible explanation is two different sources of organic carbon in the marine sediment. In the plot of XRF-Ca, $\delta^{13}C$, TOC, and Fe/Ca ratio as functions of age (Figure 23), maximum TOC values coincided with periods of high $\delta^{13}C$, and Ca intensities. Assuming that the Ca intensities were predominantly from marine carbonates, the similarity in the trends of Ca, TOC and $\delta^{13}C$ plots (Figure 23 c, e and f), shown by higher records in the cold stages than the warm stages accords with the findings of Schneider et al. (1997), which reported that marine organic carbon controls total organic carbon variations in the Congo Fan area. This finding, alongside the variable Fe/Ca ratios that indicate terrigenous sediment contributions from the Congo Basin are consistent with the findings of Adegbie et al. (2003), which showed that total accumulation rates are higher for both marine and terrigenous organic carbon during glacial periods, due to the higher absolute supply of both terrigenous and calcareous materials. The reason for this high accumulation rates could be attributed to the combined effects of the close vicinity of the core site to the river mouth under glacial low sea-level conditions and to high productivity in the surface ocean.

5.2.3 Role of marine and continental signals on Hg variations

Following previous discussions (5.2.1 and 5.2.2), sediment accumulation in ODP1077 marine sediment site are resultant effects of climatic and environmental factors, and Hg accumulation in the sediment core over time is conceivably influenced by both terrigenous supply and organic carbon fluxes. In the absence of definite associations between Hg and well-studied environmental proxies, further attempt to verify the major controlling factor(s) relevant to Hg delivery in the marine sediment and how the changes occurred over time is imperative.

The consistent anti-phase relationship (Figure 23) in the plots of Fe/Ca ratio and Hg suggest two distinct periods of low terrigenous material influx that occurs concurrently with high Hg delivery between 20 – 5 ka,, and the period of higher terrigenous material delivery by the Congo River that coincides with low Hg accumulation between the 130 ka and 20 ka interval. Isolating the longer time interval, the opposing trends, that is, the increasing (decreasing) Hg concentrations synchronizing with decreasing (increasing) Fe/Ca ratios is further conspicuous (Figure 24). Specifically, the abrupt transition of the trends of both Hg concentration and Fe/Ca ratio at 20 ka (Figure 23 a and b), and apparent inverse relationships at 120 ka, 85 ka, 45 ka, and 35 ka (Figure 23 b and c) are noteworthy. Although the association between the two variables are best described as inverse, the consistency in the trends suggests that Hg concentrations in ODP1077 seems to be largely determined by terrigenous sediment supply by the Congo River. This may be explained by the fact that the marine sediment core is directly under the influence of the Congo River discharge (Figure 4), is situated outside the turbidite fan area (van Weering and van Iperen, 1984; van Iperen et al., 1987; Pufahl et al., 1998), and experiences minor aeolian contribution to its sediments (Uliana et al., 2001). Given that the Fe/Ca ratios vary significantly between 130 – 20 ka, an interval that crosses glacial/interglacial boundaries over periods that are characterised by opposing atmospheric,

oceanic and environmental conditions, an interplay of several factors are likely responsible for the abrupt changes in terrigenous material delivery as shown by the Fe/Ca ratios. Such factors will include changes in the intensity of Congo River discharge which is consequent to variation in precipitation patterns (Gasse et al. 1989; Uliana et al., 2002), as determined by the intensity of African monsoon (Schneider et al., 1997; Gingele, 1998).

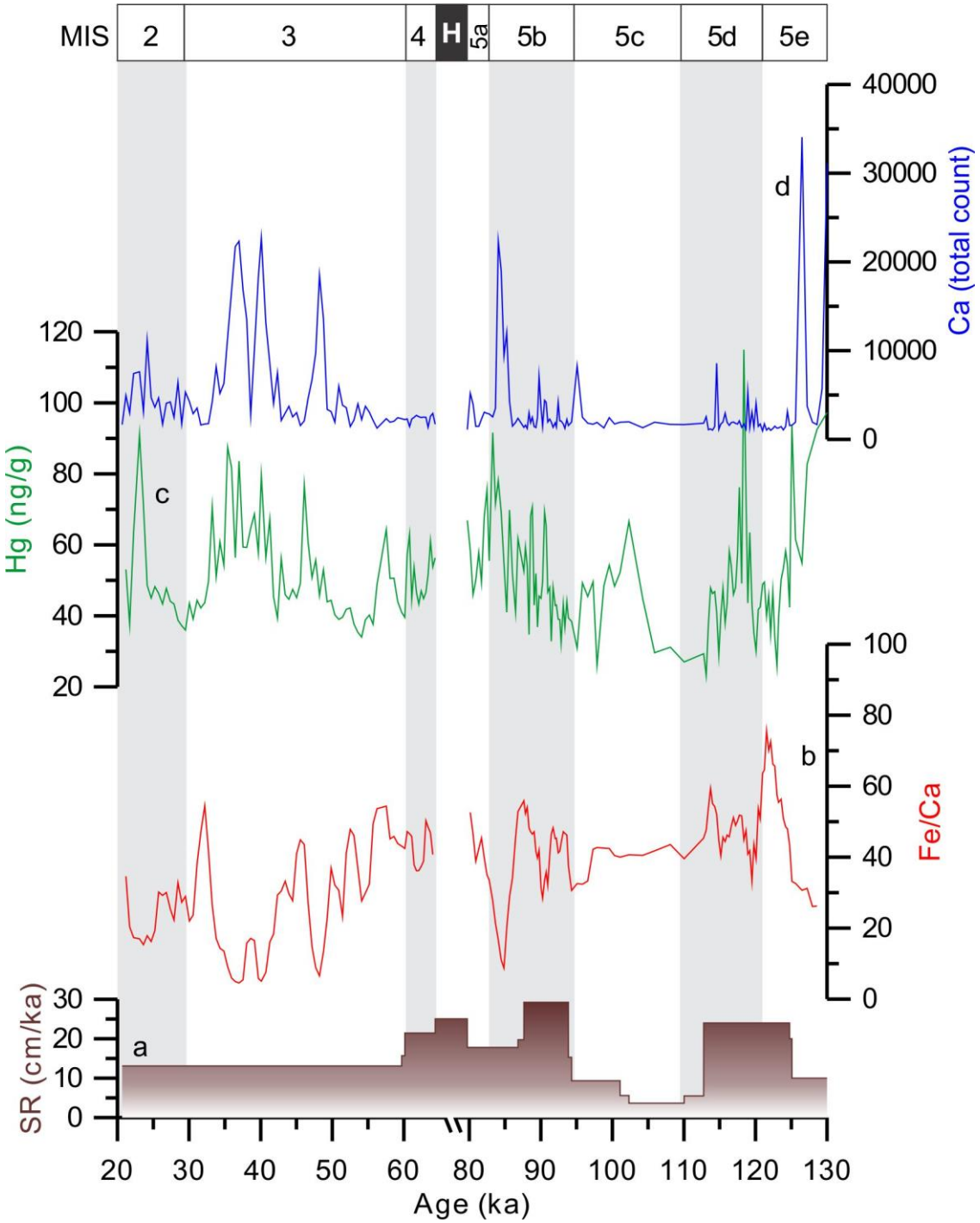

Figure 24: Hg concentration and paleoenviromental proxies of the core ODP1077 between the time interval 130 – 20 ka. (a) Sedimentation Rates, SR in cm/ka (brown line), (b) Fe/Ca ratios (red line), (c) Hg concentrations in ng/g (green line), (d) Ca counts (blue line). MIS 3, MIS 5b and 5d are marked in light blue bars.

However, the anti-phase relationship between Fe/Ca ratios and Hg concentrations is insufficient to explain Hg accumulation in ODP1077. Considering that the marine sediment

core was recovered from a high primary productivity region, and because Hg accumulation in marine sediments is largely controlled by primary productivity, the probability that organic matter had a role to play in the delivery of Hg to the marine sediments should not be overlooked. Using the XRF-Ca counts as a proxy for marine organic carbon production (Adegbie et al., 2003), Ca intensities during the 20 – 5 ka interval vary similarly with the Hg variations in the same interval (Figure 23), as well as all through the longer time interval (Figure 24). In the absence of other determinant factors of Hg accumulation in ODP1077 marine sediment, the evident similar trends in the variation plots of Ca counts and Hg concentration during the studied time interval, as well as the strong correlation coefficient of both variables, $R^2 = 0.50$ ($p < 0.001$), suggests that Hg sequestration into the marine sediments of ODP1077 is primarily controlled by marine organic carbon.

Taken together, the observed correlation between Ca intensities and Hg concentrations, as well as the anti-phase tends in the plots of Fe/Ca ratios and Hg concentrations may be explained thus; during intervals of high terrigenous material delivery shown by elevated Fe/Ca ratios, marine organic carbon in ODP1077 sediments are diluted by the influx of terrigenous sediments to the Eastern South Atlantic Ocean. The dilution of marine organic carbon by terrestrial organic carbon is relevant in this instance because some studies have reported the importance of the origin/source of organic carbon in the accumulation of Hg in marine sediments established that Hg sequestration into marine sediments is preferentially executed by marine organic carbon. Therefore, an influx of terrigenous sediments will invariably lead to a reduction in the amounts Hg delivered to marine sediments. In a study on Hg distribution in Vembanad Lake, Chakraborty et al. (2015), the authors noted that maximum Hg concentrations in marine sediments originated from the northern part of the lake where marine organic carbon was the dominant source of total organic carbon. In the southern part of the lake where total organic carbon was mainly of terrestrial origin, lower Hg

concentrations were recorded. The authors therefore concluded that marine organic carbon has a higher affinity for mercury than terrestrial organic carbon. Also, Bravo et al., (2017) acknowledged the essential role of autochthonous organic carbon in determining Hg concentrations in lake sediments. Similarly, Machado et al. (2016) in their study of a sediment core from SE Brazil explained that the observed negative correlation between Hg and organic carbon was due to dilution effect by the predominant allochthonous organic carbon.

Overall, the dynamics controlling Hg accumulation in ODP1077 can be hypothesised to imply that during the intervals of high terrigenous material delivery (shown by high Fe/Ca ratio), the influx of allochthonous (terrigenous) organic carbon is high, and given that Hg is preferentially sequestered by autochthonous (marine) organic carbon, low amount of Hg is delivered into the marine sediment (Figure 25a). In contrast, during periods of low terrigenous material influx (shown by low or near baseline Fe/Ca ratio), autochthonous (marine) organic carbon is higher, and on account of the fact that Hg is preferentially sequestered by marine organic carbon, Hg accumulation in the sediment is high (Figure 25b).

5.3 Hg variations over the last glacial-interglacial cycle: Western and Eastern South Atlantic

Several studies have addressed Hg dynamics in the environment. These studies detail mercury sources, its variations over different climates, as well as interactions within various compartments in the environment. In particular, a large and growing body of literature exists on the Hg dynamics in Latin America. This is probably due to the concern about Hg contamination as a consequence of the gold mining activities, particularly in Brazil. Moreover, the Amazon basin (mainly situated in Brazil) has received much attention in regards to Hg studies due to the role it plays in the global Hg biogeochemical cycle by acting as a sink to approximately 21% of total atmospheric Hg (Fostier et al., 2015). The basin also

housed numerous gold mining areas (Lodenius and Malm, 1998), and is therefore highly susceptible to Hg contamination following the Brazilian gold rush period. The Congo basin however, has not been privy to such attention in terms of published studies describing Hg variations over long timescales. Most studies of Hg dynamics in Africa as a whole (Biney et al., 1994; Ikingura et al., 1997; Ramlal et al., 2003) are focused on understanding Hg pollution trends from urban and industrialised areas, as well as gold mining activities, and as a result, they date back to a few centuries. For example, in a study of three (3) equatorial sediment cores from Uganda to evaluate the impacts of industrial activities on environmental Hg concentrations by Yang et al., (2010), , a 3-fold increase was recorded in Hg deposition since the start of the industrial period. Notwithstanding the scarcity of research information on long-term mercury distribution in sediments within and originating from the African continent, the climatic mechanisms that impact mercury variations in the marine sediment cores originating from the Western and Eastern South Atlanticare compared.

Paleoclimatic Hg variations from the Western South Atlantic showed evidences of glacial/interglacial variations and millennial-scale events. The glacial low sea-level conditions and the southward migration of ITCZ that ensue from intensified NE tradewinds, favour high terrigenous sediment influx to the continental slope off NE Brazil. These climatic dynamics are the dominant factors controlling the Hg variations in GL-1248 marine sediments, and they corroborate the recorded Hg patterns by showing higher concentrations in the glacial periods (and during MS events) than in the interglacial periods. Accordingly, Hg variations synchronize with terrigenous material delivery from the bordering continent.

On the Eastern South Atlantic however, no evidence glacial/interglacial variations were recorded. However, during the interglacial periods (MIS 1 and 5e) when the high sea-level stand and subsequent distant positioning of the river mouth to the core site ought to deter terrigenous material delivery to the continental margin of the Congo basin, the prevailing

climatic conditions favoured the discharge of terrigenous materials. Also, unlike the GL-1248 marine sediment core where unambiguous associations exist between climate dynamics, material export and Hg concentrations, similar associations in ODP1077 are vague. Other contrasts in both study sites and by extension, marine sediment cores include:

Sediment origin: Marine sediments in GL-1248 and ODP1077 originate from the Parnaíba and Congo basins respectively. In terms of drainage area and discharge volume, the Parnaíba Basin with an area of 344, 000 km^2 and 4,400 km river length yields 1,272m^3/s (Marques et al. 2004) discharge volume, while the Congo River has a basin area of 4, 014, 500 km^2, river length of approximately 4,700 km and discharge volume of 41,200m^3/s. Consequently, the amounts of terrigenous material arriving at ODP1077 are several orders higher than sediments being deposited at GL-1248.

Mercury source and concentration: Several studies have established that the atmosphere is the primary source of mercury in the South American continent. Although pre-industrial records on Hg studies in Africa are lacking, it is likely that the pre-industrial Hg records in ODP1077 are as a result of atmospheric deposition on the continent before re-mobilization to the Congo deep-sea fan area. The mean Hg concentration from northeastern Brazil was 42.67ng/g while the highest concentration recorded was 69.43ng/g. From the Eastern South Atlantic however, average Hg concentration was 77.61ng/g with the maximum concentration of 256ng/g. While Hg levels in GL-1248 did not vary significantly, a considerable 10-fold increase occurred within the studied period in ODP1077. Comparing Hg levels in both cores, it is cautiously deduced that although the elevated Hg concentrations in the Congo core are anticipated, higher concentrations than those recorded were expected considering that its basin size, river length and discharge volume are several orders higher than its counterpart on the Western South Atlantic.

Key influence of Hg accumulation over time: Hg records in both marine sediment cores show distinct evidences of the influence of terrigenous supply from their respective adjoining continents. While Hg concentrations in GL-1248 mainly increased (decreased) with increasing (decreasing) terrestrial material delivery, Hg concentration in ODP1077 increased (decreased) with decreasing (increasing) terrigenous material influx. Also, iron minerals in the soils of northeasern Brazil played a major role in Hg post-depositional processes by acting as the carrier phase of Hg through transportation and immobilization at the GL-1248 core location. On the other hand, sequestration of Hg into marine core sediment ODP1077 was chiefly executed by the marine organic carbon.

6. CONCLUSION

Mercury accumulation in marine sediment cores originating from the Western and Eastern South Atlantic Ocean varied over the last glacial-interglacial cycle, thus providing useful information in understanding the factors controlling Hg accumulation within the tropics. Due to the element's dynamic nature in the environment however, it responded differently to the same factors in both locations. Changes in global atmospheric dust concentrations and climate over the studied timescale contributed significantly to atmospheric Hg deposition in Parnaíba basin. Mercury variations show that atmospheric Hg deposition was higher in the glacial periods than during the interglacial periods (Figure 25 a and b). Regional factors such as precipitation pattern, runoff events and sea-level changes control Hg remobilization from the continent to its secondary location, the study site. Peaks of Hg correlated with peaks of Fe/Ca ratios from NE Brazil confirming that Hg delivered at GL-1248 was transported with fluvial materials during continental runoff events corresponding to millennial-scale variability (Figure 9c). Iron-oxyhydroxides, a major component of tropical Brazil soils, was the major carrier-phase of Hg in the soils, during transportation until immobilization at GL-1248 core site, although TOC might have aided Hg sedimentation during millennial-scale events. This study shows that (1) the atmosphere is the primary source of GL-1248 sedimentary Hg records and various climate mechanisms influence its deposition as well as transportation, and (2) due to Hg post-depositional processes and remobilization, Parnaíba Basin served as the secondary source of Hg reaching the marine sediment core location. Therefore, it can be suggested that Hg delivered at the continental slope off northeastern Brazil is in response to both global and regional climate phenomena, the latter being millennial-scale variability and superimposed by the former (glacial-interglacial variations).

Mercury concentrations in ODP1077 varied inversely with Fe/Ca ratios, recording an abrupt shift in measured sedimentary Hg accumulation from low to elevated concentrations

occurring at 20 ka. Contrary to expectations, Hg concentration and total organic carbon showed no similarity and were poorly correlated. Previous studies have reported that total organic carbon at the Congo deep-sea fan area contain a mixture of terrigenous organic carbon and marine organic carbon. Hg concentrations in ODP1077 correlates positively with marine organic carbon, that is, XRF-Ca. It can therefore be suggested that atmospheric and oceanic conditions that enhance (reduce) marine organic carbon production leads to reduced (elevated) Hg accumulation in the marine sediment core ODP1077. Likewise, considering that Hg is preferentially sequestered into marine sediments by autochthonous (marine) organic carbon, periods of high Hg accumulation in the marine sediments are recorded when marine organic carbon portion of the TOC is high, (Figure 26a), whereas low Hg concentrations were recorded during periods of increased terrestrial material delivery, when the influx of terrestrial organic carbon dilutes the total organic carbon (Figure 26b).

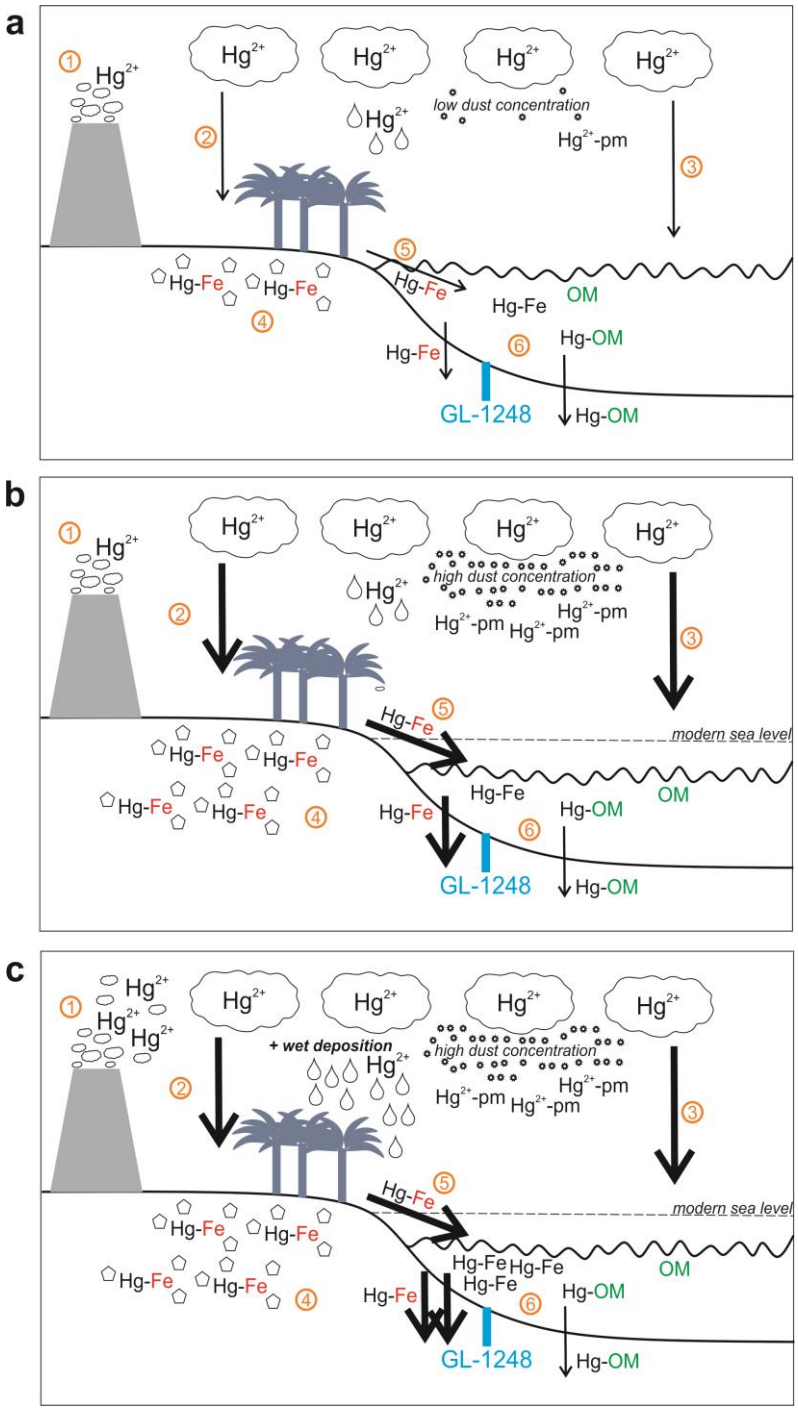

Figure25: Conceptual model showing the processes controlling mercury deposition and sedimentation in GL-1248.

①Volcanic emission ②Deposition (continent) ③Deposition (ocean)

④ Complexation with Fe-minerals ⑤ Runoff/erosion ⑥Immobilization/sedimentation

(a) Modern condition. In the interglacial period when atmospheric dust load concentration is low, minimal atmospheric Hg is deposited onto the NE Brazil continent

(b) Glacial condition. The glacial period is characterized by high atmospheric dust loads, thus, high amounts of Hg is deposited onto the NE Brazil continent. Consequent to the variations in amounts of Hg being deposited from the atmosphere to the continent in 8a and 8b, more Hg-bearing terrigenous materials were immobilized in the continental slope in the glacial period compared to the interglacial period

(c) Millennial-scale stadial conditions. Intensified precipitation during millennial-scale events complemented atmospheric Hg deposition by wet deposition. Enhanced erosion in the NE Brazil continent during these events contributed to the increased transport and deposition of terrigenous materials to the continental slope.

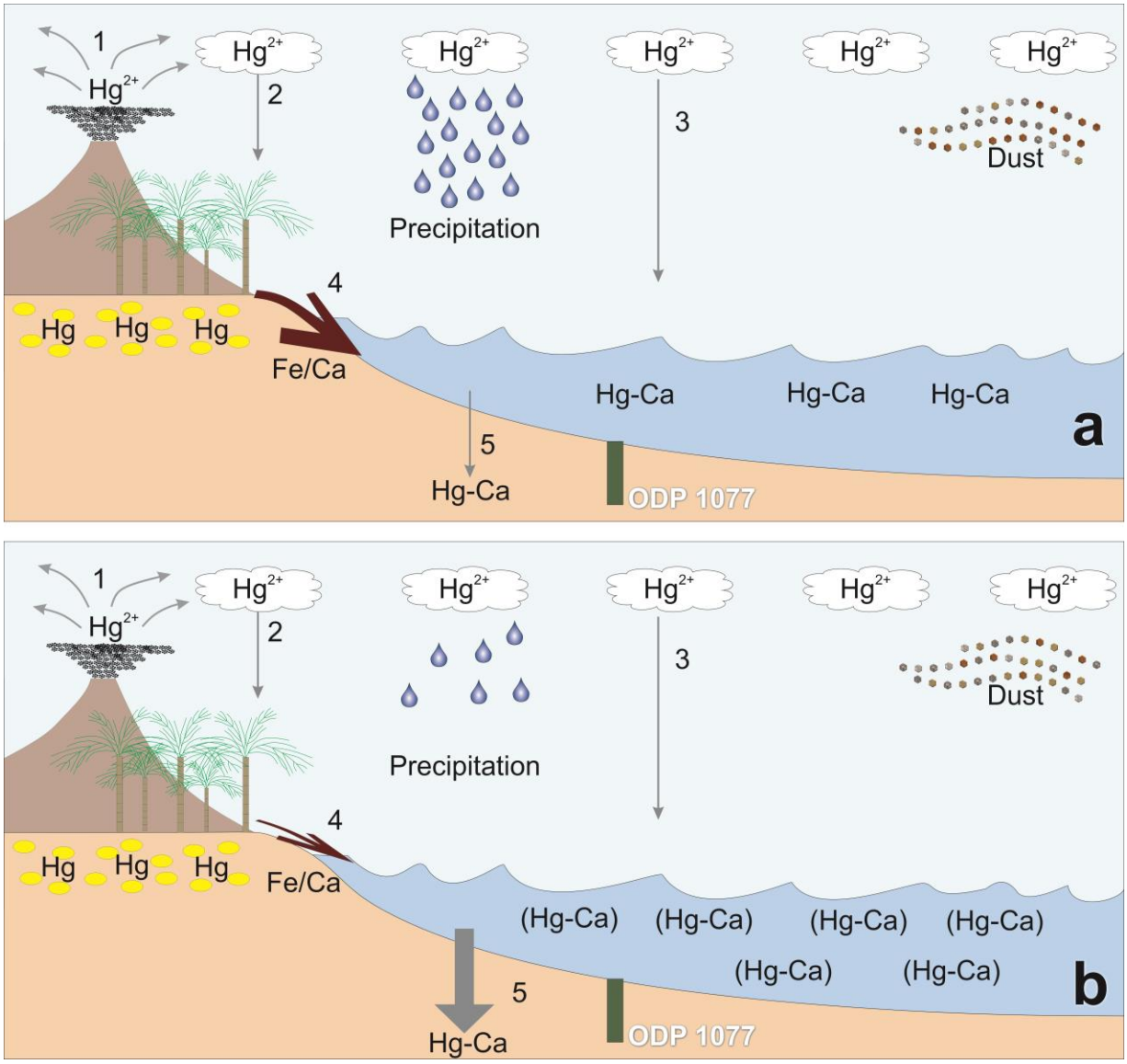

Figure 26: Conceptual model showing the processes controlling mercury deposition and sedimentation in ODP1077.

①Volcanic emission ②Deposition (continent) ③Deposition (ocean)

④ Runoff/erosion ⑤Immobilization/sedimentation

(a) Periods of intensified precipitation and enhanced erosion. With the high influx of terrigenous sediments to the Congo deep-sea fan area, the dilution of the total organic carbon by the terrestrial organic carbon diminishes mercury accumulation in marine sediments.

(b) Periods of reduced precipitation and minimal erosion. The high portion of marine organic carbon during these periods enhances mercury accumulation in marine sediment core ODP1077.

In conclusion, although the marine sediment cores are directly under the influence of terrigenous material delivery from the rivers originating from their respective adjoining continents, the effects of terrigenous export signal on Hg accumulation in sediments are dissimilar. Likewise, the role of organic matter in Hg sequestration in both cores is different (Figure 27). Also, the regional climate phenomena at GL-1248 can be said to be inadequate to completely mask global climate dynamics, whereas the global climatic conditions at the ODP1077 are completely obscured by the respective regional climate and its resultant effects.

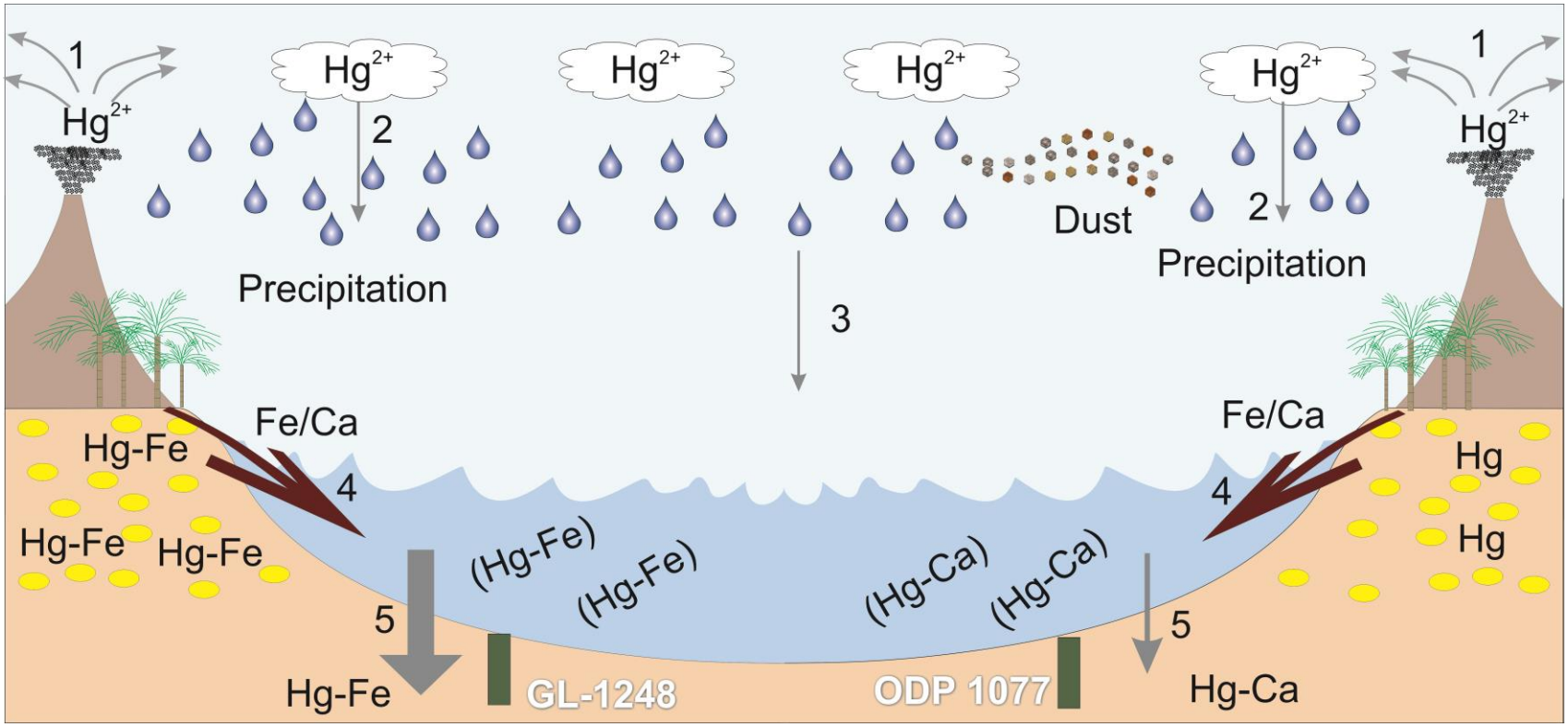

Figure 27: Conceptual figure showing the difference in post-depositional dynamics that control mercury remobilization from the Western and Eastern South Atlantic Ocean and its fixation into the marine sediments. This also depicts two different means by which mercury is incorporated in the mercury cycle within the tropics.

①Volcanic emission ②Deposition (continent) ③Deposition (ocean)

④Runoff/erosion ⑤Immobilization/sedimentation

This thesis has investigated Hg deposition in marine sediment cores originating from the Western and Eastern South Atlantic Ocean. The study aimed to determine and compare the climate mechanisms responsible for the Hg variations recorded in the studied marine sediment cores. An obvious finding to emerge from this study is that Hg variations in the studied marine sediment cores reveal paleoclimatic conditions from their respective locations, as well as reveal regional geochemical conditions in their post-depositional processes. The study has also shown that although Hg is a globally distributed metal whose atmospheric deposition varies over different climates, its records in environmental archives (e.g. marine sediments) are mainly subject to local climatic and environmental factors. Furthermore, the study makes noteworthy contribution to existing data on Hg variation over long timescales on the Western and Eastern South Atlantic Ocean, and it enhances the understanding of Hg dynamics on the global and regional climates over the last glacial/interglacial cycle. Finally, the evidence from this study identified two different pathways by which mercury is incorporated into marine sediments for prolonged storage and inclusion in the global mercury cycle. A limitation to this study is the absence of prior research studies on pre-industrial Hg variations from the African continent. It is recommended that further research on Hg variations across global and regional climates periods be undertaken and such studies should include projections on the likely impacts of climate change on Hg dynamics in the environment. This is particularly important for developing relevant mitigation techniques to minimize the potential environmental hazards that could be caused by this deleterious metal at a period such as the current interglacial stage, where the planet is experiencing drastic climatic changes, and with predictions of more climate change underway.

7. REFERENCES

Adegbie, A.T., Schneider, R.R., Röhl, U., Wefer, G., 2003. Glacial millennial-scale Adegbie, A.T., Schneider, R.R., Röhl, U., Wefer, G., 2003. Glacial millennial-scale fluctuations in central African precipitation recorded in terrigenous sediment supply and freshwater signals offshore Cameroon. *Palaeogeography, Palaeoclimatology, Palaeoecology*. 197(3–4), 323–333. http://doi.10.1016/S0031-0182(03)00474-7

Alsdorf, D., Beighley, E., Laraque, A., Lee, H., Tshimanga, R., O'Loughlin, F., Mahé, G., Dinga, B., Moukandi G., Spencer, R.G.M., 2016. Opportunities for hydrologic research in the Congo Basin. *Reviews of Geophysics*. 54. http://doi.10.1002/2016RG000517

Amos, H. M., D. J. Jacob, D. G., Streets, and M. Sunderland, 2013. Legacy impacts of all-time anthropogenic emissions on the global mercury cycle. *Global. Biogeochemical Cycles*. 27, 410–421. https://doi.org/10.1002/gbc.20040

Arz, H. W., Pätzold, J., and Wefer, G., 1998. Correlated millennial-scale changes in surface hydrography and terrigenous sediment yield inferred from Last-Glacial marine deposits off northeastern Brazil. *Quaternary Research*. 50(2), 157–166. http://doi.org/10.1006/qres.1998.1992

Aula, I., Braunschweiler, H., Leino, T., Malin, I., Porvari, P., Hatanaka, T., Lodenius, M. and Juras, A., 1994. Levels of mercury in the Tucuruí Reservoir and its surrounding area in Pará, Brazil. In: Mercury Pollution: Integration and Synthesis, Watras, C.J. and Huckabee, J.W. (eds), Lewis Publishers, Boca Raton, pp. 21–40.

Babonneau, N., Savoye, B., Cremer, M., Klein, B., 2002. Morphology and architecture of the present canyon and channel system of the Zaire deep-sea fan. *Marine and Petroleum Geology*. 19, 445–467. https://doi.org/10.1016/S0264-8172(02)00009-0

Bagniewski, W., Meissner, K.J. and Menviel, L., 2017. Exploring the oxygen isotope fingerprint of Dansgaard-Oeschger variability and Heinrich events. *Quaternary Science Reviews*. 159, 1-14. http://doi.org/10.1016/j.quascirev.2017.01.007

Baldini, J. U. L., Brown, R. J. and McElwaine, J. N., 2015. Was millennial-scale climate change during the Last Glacial triggered by explosive volcanism? *Scientific Reports.* 5,17442. https://doi.org/10.1038/srep17442

Barbosa, J.A., Cordeiro, R.C., Silva, E.V., Turcq, B., Gomes, P.R.S., Santos, G.M., Sifeddine, A., Albuquerque, A.L.S., Lacerda, L.D., Hausladen, P.A., Tims, S.G., Levchenco, V.A. and Fifield, L.K., 2004. 14C-MAS as a tool for the investigation of mercury deposition at a remote Amazon location. *Nuclear Instruments and Methods in Physics Research B*. 223/224, 528-534.

Barbosa, Roberto Cesar de Mendonça, Nogueira, Afonso César Rodrigues, and Domingos, Fábio Henrique Garcia., 2015. A glaciação fameniana na porção leste da Bacia do Parnaíba: evidências do avanço e recuo de geleira na Formação Cabeças. *Brazilian Journal of Geology*. 45(Suppl. 1), 13-27. https://dx.doi.org/10.1590/2317-4889201530147

Bay, R.C., Bramall, N. and Price, P.B., 2004. Bipolar correlation of volcanism with millennial climate change. *Proceedings of the National Academy of Sciences U. S. A.* 101(17), 6341– 6345. https://doi.org/10.1073/pnas.0400323101

Berger, W. H., Wefer, G., Richter, C., Lange, C. B., Giraudeau, J., Hermelin, O., and Party, Shipboard Scientific. 1998. The Angola-Benguela upwelling system: Paleoceanographic synthesis of shipboard results from Leg 175. In G. Wefer, W. H.

Berger, C. Richter, et al. (Eds.), Proceedings Of The Ocean Drilling Program, Initial Reports. 175, 505–531. College Station: Ocean Drilling Program.

Berger, W.H., Lange, C.B., Wefer, G., 2002. Upwelling history of the Benguela-Namibia system: a synthesis of Leg 175 results. In: Wefer, G; Berger, WH; Richter, C (eds.) Proceedings of the Ocean Drilling Program, Scientific Results, College Station, TX (Ocean Drilling Program), 175, 1-103, https://doi.org/10.2973/odp.proc.sr.175.235.2002

Berger, W.H., Wefer, G., Richter, C. and Shipboard Scientific Party. 1998. Color cycles in Quaternary sediments from the Congo Fan region (Site 1075): A statistical analysis, In: Wefer, G., Berger, W.H. and Richter, C. (eds) Proceedings of the Ocean Drilling Program, Initial Reports, 175.

Bigham, J. M., Fitzpatrick, R. W. and Schulze, D. 2002. Iron oxides. In: Dixon, J. B. and Schulze, D. G. Soil mineralogy with environmental applications. Madison: Soil Science Society of America Book Series. 323-366

Biney C., Amuzu. A.T., Calamari D., Kaba N. Mbome I.I,., Naeve H.. Ochumba P.B.O., Osibanjo O., Radegonde V. and Saad M.A.M. 1994. Review of heavy metals in the African aquatic environment. *Ecotoxlcology and Environment Safety.* 28. 134-159. https://doi.org/10.1006/eesa.1994.1041

Blaauw, M., Christen, J.A., 2011. Flexible paleoclimate age-depth models using an autoregressive gamma process. *Bayesian Analysis.* 6 (3), 457 – 474. https://doi.org/10.1214/11-BA618

Bravo, A. G., Sylvain B., Julie T., Erik B., Alejandro M-R, Stefan B. 2017. Molecular composition of organic matter controls methylmercury formation in boreal lakes. *Nature Communication.* 8, 14255. https://doi.org/10.1038/ncomms14255

Brindley, G.W. and Brown, G., eds., 1980. Crystal structures of clay minerals and their X-ray identification. Mineralogical Society of Great Britain and Ireland, 518pp

Broccoli, A. J., Dahl, K. A., and Stouffer, R. J. (2006). Response of the ITCZ to Northern Hemisphere cooling. *Geophysical Research Letters.* 33(1). http://doi.org/10.1029/2005GL024546

Caley, T., Malaizé, B., Revel, M., Ducassou, E., Wainer, K., Ibrahim, M., Shoeaib, D., Migeon, S., Marieu, V., 2011. Orbital timing of the indian, East Asian and African boreal monsoons and the concept of a 'global monsoon'. *Quatenary Science Reviews*. 30, 3705-3715. http://doi.org/10.1016/j.quascirev.2011.09.015

Castillo, V.M., Martinez-Mena, M., Albaladejo, J., 1997. Runoff and soil loss response to vegetation removal in a semiarid environment. *Soil Science Society of America Journal*. 61, 1116 – 1121. https://doi/.10.2136/sssaj1997.03615995006100040018x

Chakraborty, P., Sarkar, A., Vudamala, K., Naik, R., and Nath, B. N. (2015). Organic matter — A key factor in controlling mercury distribution in estuarine sediment. *Marine Chemistry, 173, 302–309.* https://doi.org/10.1016/j.marchem.2014.10.005

Corbitt E.S., Jacob D.J., Holmes C.D., Streets D.G., and Sunderland E.M., 2011. Global source-receptor relationships for mercury deposition under present-day and 2050 emissions. 45(24), 10477-84. https://doi.org/10.1021/es202496y

Cordeiro, R.C., Turcq, B., Sifeddine, A., Lacerda, L.D., Silva Filho, E.V., Gueiros, B., Potty, Y.P., Santelli, R.E., Pádua, E.O. and Pachinelam, S.R., 2011. Biogeochemical indicators of environmental changes from 50 ka to 10 ka in a humid region of the

Brazilian Amazon. *Palaeogeography, Palaeoclimatology, Paleaeoecology*. 299, 426-436. https://doi.org/10.1016/j.palaeo.2010.11.021

Dalibard, M., Popescu, S.-M., Maley, J., Baudin, F., Melinte-Dobrinescu, M.-C., Pittet, B., Marsset, T., Dennielou, B., Droz, L., Suc, J.-P., 2014. High-resolution vegetation history of West Africa during the last 145 ka. *Geobios*. 47, 183–198. https://doi.org/10.1016/j.geobios.2014.06.002

Davis J.C., 2002. Statistics and data analysis in geology, 3rd edn. Wiley, New York.

Deplazes, G., Lückge, A., Peterson, L.C., Timmermann, A., Hamann, Y., Hughen, K.A., Röhl, U., Laj, C., Cane, M.A., Sigman, D.M., Haug, G.H., (2013). Links between tropical rainfall and North Atlantic climate during the last glacial period. *Nature Geoscience*. 6, 1–5. https://doi.org/10.1038/ngeo1712

Driscoll C.T., Mason R.P., Chan H.M., Jacob D.J., and Pirrone N., 2013. Mercury as a global pollutant: Sources, pathways, and effects. *Environmental Science and Technology*. 47, 4967–4983. https://doi.org/10.1021/es305071v

Dupont, L., Schneider, R., Schmüser, A., Jahns, S., 1999. Marine-terrestrial interaction of climate changes in West Equatorial Africa of the last 190,000 years. *Paleoecology of Africa*. 26, 61– 84.

Dupont, L.M., Donner, B., Schneider, R.R. and Wefer, G. 2001. Mid-Pleistocene environmental change in tropical Africa. *Geology*. 29 (3): 195-198. https://doi.org/10.1130/0091-7613(2001)029<0195:MPECIT>2.0.CO;2

Dupont, Lydie M; Donner, Barbara; Schneider, Ralph R; Wefer, Gerold. 2001. Palynological records from the Congo fan analyzed on ODP Site 175-1077. *PANGAEA*. https://doi.org/10.1594/PANGAEA.872026

Eisma, D., and van Bennekom, A.J., 1978. The Zaire River and estuary and the Zaire outflow in the Atlantic Ocean. *Netherlands Journal of Sea Research*. 12, 255–272. https://doi.org/10.1016/0077-7579(78)90030-3

El Kateb, H., Zhang, H., Zhang, P., Mosandl, R., 2013. Soil erosion and surface runoff on different vegetation covers and slope gradients: a field experiment in Southern Shaanxi Province, China. *CATENA*. 105, 1-10. https://doi.org/10.1016/j.catena.2012.12.012

Engstrom, D. R., and E. B. Swain. 1997. Recent declines in atmospheric mercury deposition in the upper Midwest. *Environmental Science and Technology*, 312, 960–967. http://doi.org/10.1021/es9600892

Engstrom, D.R., Fitzgerald, W.F., Cooke, C.A., Lamborg, C.H., Drevnick, P.E., Swain, E.B., Balogh, S.J., Balcom, P.H., 2014. Atmospheric Hg emissions from preindustrial gold and silver extraction in the Americas: a re-evaluation from lake-sediment archives. *Environmental Science and Technology*. 48, 6533-6543. http://doi.org/10.1021/es405558e

Eriksen, C. C., Katz, E. J., 1987. Equatorial dynamics. Reviews of Geophysics 25(2), 217-226.

Fadini, P.S. and Jardim, W.F., 2001. Is the Negro River Basin (Amazon) impacted by naturally occurring mercury? *Science of the Total Environment*. 275, 71–82. https://doi.org/10.1016/S0048-9697(00)00855-X

Farias Castro A.A.J., 2003. Survey of the Vegetation in the State of Piaui. In: Gaiser T., Krol M., Frischkorn H., de Araújo J.C. (eds) Global Change and Regional Impacts. Springer, Berlin, Heidelberg, 117-123 https://doi.org/10.1007/978-3-642-55659-3_9

Figueiredo,T.S., Albuquerque, A.L.S., Sanders, C.J., Cordeiro, L.G., Silva-Filho, E.V., 2013. Mercury deposition during the previous century in an upwelling region; Cabo Frio, Brazil. *Marine Pollution Bulletin.* 76, 389 - 393. https://doi.org/10.1016/j.marpolbul.2013.07.049

Fitzgerald W.F. and Lamborg C.H., 2003. Geochemistry of Mercury in the Environment. In Treatise on Geochemistry: Second Edition, B. Sherwood Lollar, ed. (Elsevier), pp. 107–148

Fitzgerald W.F., Lamborg C.H., and Hammerschmidt C.R., 2007. Marine biogeochemical cycling of mercury. *Chemical Reviews.* 107, 641–662. https://doi.org/10.1021/cr050353m

Flügel, T.J., Eckardt, F.D., Cotterill, F.P.D., 2015. The present day drainage patterns of the Congo river system and their Neogene evolution. in: M.J. de Wit et al. (eds.), Geology and Resource Potential of the Congo Basin. Regional Geology Reviews, Springer-Verlag Berlin Heidelberg. https://doi.org/10.1007/978-3-642-29482-2_15

Forbes E.A., Posner A.M. and Quirk J.P., 1974. The specific adsorption of inorganic Hg(II) species and Co(III) complex ions on goethite. *Journal of Colloid and Interface Science*. 49, 403-409. https://doi.org/10.1016/0021-9797(74)90385-3

Fostier A.H., Melendez-Perez J.J. and Richter L., 2015. Litter mercury deposition in the Amazonian rainforest. *Environmental Pollution.* 206, 605–610. https://doi.org/10.1016/j.envpol.2015.08.010

Frédoux, A., 1994. Pollen analysis of a deep- sea core in the Gulf of Guinea: Vegetation and climatic changes during the last 225,000 years B. P. *Palaeogeography, Palaeoclimatology, Palaeoecology.* 109, 317–330. https://doi.org/10.1016/0031-0182(94)90182-1

Gasse F. 2000. Hydrological changes in the African tropics since the Last Glacial Maximum. *Quaternary Science Reviews.* 19, 189–211. https://doi.org/10.1016/S0277-3791(99)00061-X

Gasse, F., Stabell, B., Fourtanier, E., van Iperen, J., 1989. Freshwater diatom influx in intertropical Atlantic: Relationships with continental records from Africa. *Quaternary Research*. 32, 229 - 243. https://doi.org/10.1016/0033-5894(89)90079-3

Gingele, F.X., Müller, P.M., Schneider, R.R., 1998. Orbital forcing of freshwater input in the Zaire Fan area clay mineral evidence from the last 200 kyr. *Palaeogeography, Palaeoclimatology, Palaeoecology*. 138, 17–26. https://doi.org/10.1016/S0031-0182(97)00121-1

Giresse P. 1990. Paleoclimatic and structural environment at the end of the Cretaceous along the Western flank of the Congo Basin, with application of underground microdiamonds around Brazzaville. *Journal of African Earth Sciences*. 10, 399–408. https://doi.org/10.1016/0899-5362(90)90070-U

Govin, A., Holzwarth, U., Heslop, D., Ford Keeling, L., Zabel, M., Mulitza, S., Chiessi, C. M. 2012. Distribution of major elements in Atlantic surface sediments (36°N-49°S): Imprint of terrigenous input and continental weathering. *Geochemistry, Geophysics, Geosystems*, 13(1), 1525-2027. https://doi.org/10.1029/2011gc003785

Gradstein F, Ogg J, Smith A., 2004. A geologic time scale. Cambridge University Press, Cambridge

Grasby S.E., Sanei H., Beauchamp B. and Chen Z., 2013. Mercury deposition through the Permo-Triassic Biotic Crisis. *Chemical Geology*. 351, 209-216 https://doi.org/10.1016/j.chemgeo.2013.05.022

Grimaldi, M., Guédron, S. and Grimaldi, C., 2015. Impact of gold mining on mercury contamination and soil degradation in Amazonian ecosystems of French Guiana. In: Brearley, F.Q., Thomas, A.D. (Eds.), Land-use Change Impacts on Soil Processes: Tropical and Savannah Ecosystems. CABI, Wallingford, UK, 95–107.

Grinsted A, Moore JC, Jevrejeva S., 2004. Application of the cross wavelet transform and wavelet coherence to geophysical time series. Nonlinear Proc Geophys 11:561–566

Guillocheau, F., Chelalou, R., Linol, B., Dauteuil, O., Robin, C., Mvondo, F., Callec, Y., Colin, J.-P., 2015. Cenozoic Landscape Evolution in and Around the Congo Basin: Constraints from Sediments and Planation Surfaces. in: M.J. de Wit et al. (eds.), Geology and Resource Potential of the Congo Basin. Regional Geology Reviews, Springer-Verlag Berlin Heidelberg. https://doi.org/10.1007/978-3-642-29482-2_14

Gworek B., Bemowska-Kałabun O., Kijeńska M. and Wrzosek- Jakubowska J., 2016. Mercury in marine and oceanic waters - a review, *Water Air and Soil Pollution.* 227 (10) p. 371 https://doi.org/10.1007/s11270-016-3060-3

Gyssels, G., Poesen, J., Bochet, E., Li, Y., 2005. Impact of plant roots on the resistance of soils to erosion by water: a review. *Progress in Physical Geography.* 29(2), 189 – 217. https://doi.org/10.1191/0309133305pp443ra

Hall B., 1995. The gas phase oxidation of elemental mercury by ozone. In Mercury as a Global Pollutant. *Water Air and Soil Pollution*. 80(1), 301-315. https://doi.org/10.1007/BF01189680

Hammer, Ø., Harper, D. A. T. a. T., and Ryan, P. D., 2001. PAST: Paleontological Statistics Software Package for Education and Data Analysis. *Palaeontologia Electronica.* 4(1)(1), 1–9. http://doi.org/10.1016/j.bcp.2008.05.025

Hastenrath, S., and Merle, J., 1987. Annual cycle of subsurface thermal structure in the tropical Atlantic Ocean. *Journal of Physical Oceanography*. 17(9), 1518–1538. http://doi.org/10.1175/1520-0485(1987)017<1518:ACOSTS>2.0.CO;2

Hastenrath, S., 2012. Exploring the climate problems of Brazil's Nordeste: A review. *Climatic Change.* http://doi.org/10.1007/s10584-011-0227-1

Hatin, T., Crosta, X., Le Hérissé, A., Droz, L., Marsset, T., 2017. Diatom response to oceanographic and climatic changes in the Congo fan area, equatorial Atlantic Ocean, during the last 190 ka BP. *Palaeogeography, Palaeoclimatology, Palaeoecology. 469*, 47–59. http://dx.doi.org/10.1016/j.palaeo.2016.12.037

Hermanns Y.-M., Cortizas A.M., Arz H., Stein R., and Biester H., 2012. Untangling the influence of in-lake productivity and terrestrial organic matter flux on 4,250 years of mercury accumulation in Lake Hambre, Southern Chile. *Journal of Paleolimnology*. 49, 563–573. https://doi.org/10.1007/s10933-012-9657-7

Holmes C.D., Jacob D.J., Corbitt E.S., Mao J., Yang X., Talbot R., and Slemr F., 2010. Global atmospheric model for mercury including oxidation by bromine atoms. *Atmospheric Chemistry and Physics.* 10, 12037–12057. https://doi.org/10.5194/acp-10-12037-2010

Hopkins, J., Lucas, M.I., Dufau, C., Sutton, M., Stum, J., Lauret, O., Channelliere, C., 2013. Detection and variability of the Congo River plume from satellite derived sea surface temperature, salinity, ocean colour and sea-level. *Remote Sensing of Environment.* 139, 365-385. https://doi.org/10.1016/j.rse.2013.08.015

Horowitz H.M., Jacob D.J., Amos H.M., Streets D.G., and Sunderland E.M., 2014. Historical mercury releases from commercial products: Global environmental implications. *Environmental Science and Technology.* 48, 10242–10250. https://doi.org/10.1021/es501337j

Ikingura, J. R., Mutakyahwa, M. K. D., and Kahatano, J. M. J. (1997). Mercury and mining in africa with special reference to Tanzania. *Water, Air, and Soil Pollution*. 97(3-4), 223–232. https://doi.org/10.1007/bf02407460

Jaeschke, A., Rühlemann, C., Arz, H., Heil, G., and Lohmann, G., 2007. Coupling of millennial-scale changes in sea surface temperature and precipitation off northeastern Brazil with high-latitude climate shifts during the last glacial period. *Paleoceanography*. 22(4). http://doi.org/10.1029/2006PA001391

Jahn B., Schneider R. R., Mu¨ ller P. -J., Donner B. and Ro¨hl U. 2005. Response of tropical African and East Atlantic climates to orbital forcing over the last 1.7 Ma. *Geology*. 29(6), 65–84. https://doi.org/10.1130/0091-7613(2001)029<0499:ROTEAC>2.0.CO;2

Jahns, S., M. Hüls, and M. Sarnthein, 1998.Vegetation and climate history of west equatorial Africa based on a marine pollen record off Liberia (site GIK 16776) covering the last 400,000 years. *Review of Palaeobotany and Palynology.* 102, 277–288. https://doi.org/10.1016/S0034-6667(98)80010-9

Jansen, J.H.F., Ufkes, E., Schneider, R.R., 1996. Late Quaternary movements of the Angola- Benguela-Front, SE Atlantic, and implications for advection in the equatorial ocean. In Wefer, G., Berger, W.H., Siedler, G., and Webb, D. (Eds.), The South Atlantic: Present and Past Circulation: Berlin (Springer-Verlag), 553–575.

Jennerjahn, T.C. Venugopalan, I., Arz, H.W., Behling H., Pätzold J. and Wefer G., 2004. Asynchronous terrestrial and marine signals of climate change during Heinrich Events. Science. 306, 2236-2239. http://doi.org/10.1126/science.1102490

Jitaru, P., Gabrielli, P., Marteel, A., Plane, J.M.C., Planchon, F.A.M., Gauchard, P.A., Ferrari, C.P., Boutron, C.F., Adams, F.C., Hong, S., Cescon, P. and Barbante, C., 2009. Atmospheric depletion of mercury over Antarctica during glacial periods. *Nature Geoscience.* 2(7), 505-508. https://doi.org/10.1038/ngeo549

Johns, W. E., Lee, T. N., Beardsley, R. C., Candela, J., Limeburner, R., and Castro, B., 1998. Annual Cycle and Variability of the North Brazil Current. *Journal of Physical Oceanography.* 28(1), 103–128. http://doi.org/10.1175/1520-0485(1998)028<0103:ACAVOT>2.0.CO;2

Jolly, D., Harrison, S.P., Damnati, B., Bonnefille, R., 1998. Simulated climate and biomes of Africa during the Qauternary: comparison with pollen and Lake Status data. *Quaternary Science Reviews.* 17, 629-657. https://doi.org/10.1016/S0277-3791(98)00015-8

Kinniburgh, D.G. and Jackson, M.L., 1978. Adsorption of mercury (II) by iron hydrous oxide gel. *Soil Science Society of America Journal.* 42, 45-47. https://doi.org/10.2136/sssaj1978.03615995004200010010x

Kirk, J.L.; Muir, D.C.M.; Antoniades, D.; Douglas, M.S.V.; Evans, M.S.; Jackson, T.A.; Kling, H.; Amoureux, S.; Lim, D.S.S.; Pienitz, R.; et al., 2011. Climate change and mercury accumulation in canadian high and subarctic lakes. *Environmental Science and Technology*. 45(3), 964–970. https://doi.org/10.1021/es102840u

Kita I., Kojima M. and Hasegawa H., 2013. Mercury content as a new indicator of ocean stratification and primary productivity in Quaternary sediments off Bahama Bank in the Caribbean Sea. *Quaternary Research.* 80, 606–613. https://doi.org/10.1016/j.yqres.2013.08.006

Kita, I., T. Yamashita, S. Chiyonobu, H. Hasegawa, T. Sato and Y. Kuwahara, 2016. Mercury content in Atlantic sediments as a new indicator of the enlargement and reduction of Northern Hemisphere ice sheets. *Journal of Quaternary Science.* 31(3), 167–177. https://doi.org/10.1002/jqs.2854

Kumar, A., W. Abouchami, S. Galer, V. Garrison, E. Williams, and M. Andreae, 2014. A radiogenic isotope tracer study of transatlantic dust transport from Africa to the Caribbean. *Atmospheric Environment*. 82, 130–43. https://doi.org/10.1016/j.atmosenv.2013.10.021

Kuss, J. Zülicke, C. Pohl, C. and Schneider, B., 2011. Atlantic Mercury Emission Determined from Continuous Analysis of the Elemental Mercury Sea-Air Concentration Difference within Transects between 50º N and 50º S. *Global Biogeochemical Cycles.* 25, GB3021. https://doi.org/10.1029/2010GB003998

Lacerda L.D, Bruno Turcq, Abdel Sifeddine, Renato Campello Cordeiro, 2017. Mercury accumulation rates in Caço Lake, NE Brazil during the past 20.000 years. *Journal of South American Earth Sciences*, (77), 42- 50. https://doi.org/10.1016/j.jsames.2017.04.008

Lacerda, L. D., Ribeiro, M.G., Cordeiro, R.C., Sifeddine, A. and Turcq, B., 1999. Atmospheric mercury deposition over Brazil during the past 30,000 years. *Ciência e Cultura Journal of the Brazilian Association for the Advancement of Science.* 51, 363–371.

Lacerda, L.D., Campos, R.C., and Santelli, R.E., 2013. Metals in water, sediments and biota of an offshore oil exploration area in the Potiguar Basin, northeastern Brazil. *Environmental Monitoring and Assessment*. (185), 4427- 4447. http://doi.org/10.1007/s10661-012-2881-9

Lacerda, L.D.; Pfeiffer, W.C.; Silveira, E.G; Bastos, W.R. Souza; C.M.M., 1987. Contaminação por mercúrio na Amazônia; análise preliminar do rio Madeira, RO. In: Anais do II Congresso Brasileiro de Geoquímica. Sociedade Brasileira de Geoquímica. Rio de Janeiro, RJ, 295-299

Lambert, F., Delmonte, B., Petit, J.R., Bigler, M., Kaufmann, P.R., Hutterli, M.A., Stocker, T.F., Ruth, U., Steffensen, J.P., Maggi, V., 2008. Dust-climate couplings over the past 800,000 years from the EPICA Dome C ice core. *Nature*. 452, 616-619. https://doi.org/10.1038/nature06763

Laraque, A., Bricquet, J.P., Pandi, A., Olivry, J.C., 2009. A review of material transport by the Congo River and its tributaries. *Hydrological Processes.* 23, 3216–3224. https://doi.org/10.1002/hyp.7395

Laraque, A., Castellanos, B., Steiger, J., Lòpez, J.L., Pandi, A., Rodriguez, M., Rosales, J., Adèle, G., Perez, J., Lagane, C., 2013. A comparison of the suspended and dissolved matter dynamics of two large inter-tropical rivers draining into the Atlantic Ocean: the

Congo and the Orinoco. *Hydrological Processes.* 27, 2153–2170. https://doi.10.1002/hyp.9776

Laurier, F. J. G., Cossa, D., Gonzalez, J. L., Breviere, E. and Sarazin, G., 2003. Mercury transformations and exchanges in a high turbidity estuary: The role of organic matter and amorphous oxyhydroxides. *Geochimica et Cosmochimica Acta.* 67, 3329-3345. https://doi.org/10.1016/S0016-7037(03)00081-4

Leal I.R., Silva J.M.C., Tabarelli M., Lacher Jr. T.E. 2005. Changing the course of biodiversity conservation in the Caatinga of northeastern Brazil. *Conservation Biology*, 19 (3), 701–706. https://doi.org/ 10.1111/j.1523-1739.2005.00703.x

Lisiecki, L.E., Raymo, M.E., 2005. A Pliocene-Pleistocene stack of 57 globally distributed benthic d18O records. *Paleoceanography and Paleoclimatology.* 1003(1). https://doi.org/10.1029/2004PA001071

Lisiecki, L.E., Stern, J.V., 2016. Regional and global benthic d18O stacks for the last glacial cycle. *Paleoceanography.* 31, 1 – 27. https://doi.org/10.1002/2016PA003002

Lodenius M., Malm O. 1998. Mercury in the Amazon. In: Ware G.W. (eds) Reviews of Environmental Contamination and Toxicology. *Reviews of Environmental Contamination and Toxicology.* 157. https://doi.org/10.1007/978-1-4612-0625-5_2

Lucotte M. and d'Anglejan B., 1985. A comparison of several methods for the determination of iron hydroxides and associated orthophosphates in estuarine particulate matter. *Chemical Geology*. (48), 257-264. https://doi.org/10.1016/0009-2541(85)90050-6

Machado, W., C.J. Sanders, I.R. Santos, L.M. Sanders, E.V. Silva-Filho, and W. Luiz-Silva. 2016. Mercury dilution by autochthonous organic matter in a fertilized mangrove wetland. *Environmental Pollution.* 213: 30 – 35. https://doi.org/10.1016/j.envpol.2016.02.002

Maley J, Brenac P. 1998. Vegetation dynamics, palaeoenvironments and climatic changes in the forests of Western Cameroon during the last 28 000 years B.P. *Review of Palaeobotany and Palynology.* 99, 157–187. https://doi.org/10.1016/S0034-6667(97)00047-X

Mallas, J. and Benedito, N., 1986. Mercury and gold mining in the Brazilian Amazon. *AMBIO: A Journal of the Human Environment.* (15), 248–249.

Marins R. V., Lacerda L. D., Paraquetti H. H. M., de Paiva E. C. and Villas Boas Bull R. C., 1998. Geochemistry of Mercury in Sediments of a Sub-Tropical Coastal Lagoon, Sepetiba Bay, Southeastern Brazil. *Environmental Contamination and Technology.* 61, 57-64

Marques, M., da Costa, M. F., Mayorga, M. I. de O., and Pinheiro, P. R. C., 2004. Water Environments: Anthropogenic Pressures and Ecosystem Changes in the Atlantic Drainage Basins of Brazil. *AMBIO: A Journal of the Human Environment.* 33(1), 68–77. https://doi.org/10.1579/0044-7447-33.1.68

Marret, F., Scourse, J., Versteegh, G., Jansen, J., Fred, S. and Ralph, R., 2001, Integrated marine and terrestrial evidence for abrupt Congo River palaeodischarge fluctuations during the last deglaciation. *Journal of Quaternary Science.* 16, 761–766. https://doi.org/10.1002/jqs.646

Martínez Cortizas, A.; Pontevedra-Pombal, X.; García-Rodeja, E.; Nóvoa-Muñoz, J.C. and Shotyk, W., 1999. Mercury in a Spanish Peat Bog: Archive of Climate Change and

Atmospheric *Metal Deposition. Science.* 284(516), 939–942. https://doi.org/10.1126/science.284.5416.939

Mason R., Fitzgerald W., and Morel F., 1994. The biogeochemical cycling of elemental mercury: Anthropogenic influences. *Geochimica et Cosmochimica Acta.* 58, 3191–3198. https://doi.org/10.1016/0016-7037(94)90046-9

Mason R.P. and Sheu G.R., 2002. Role of the ocean in the global mercury cycle. *Global Biogeochemical Cycles*. 16 (4), 1- 14. https://doi.org/10.1029/2001gb001440

Mason R.P., Choi A.L., Fitzgerald W.F., Hammerschmidt C.R., Lamborg C.H., Soerensen A.L., and Sunderland E.M., 2012. Mercury biogeochemical cycling in the ocean and policy implications. *Environmental Research.* 119, 101–117. https://doi.org/10.1016/j.envres.2012.03.013

McIntyre, A., Ruddiman, W.F., Karlin, K., Mix, A.C., 1989. Surface water response of the equatorial Atlantic Ocean to orbital forcing. *Paleoceanography and Paleoclimatology*. 4(1), 19-55. https://doi.org/10.1029/PA004i001p00019

Meeuwis, J.M. and Lutjeharms, J.R.E. 1990. Surface thermal characteristics of the Angola-Benguela front. *South African Journal of Marine Science.* 9(1), 261-279. https://doi.org/10.2989/025776190784378772

Menviel, L., Timmermann, A., Mouchet, A. and Timm, O., 2008. Meridional reorganizations of marine and terrestrial productivity during Heinrich events. *Paleoceanography.* 23 PA1203 http://doi.org/10.1029/2007PA001445

Meyers, P. A. (1994). Preservation of elemental and isotopic source identification of sedimentary organic matter. *Chemical Geology, 114(3-4), 289–302.* http://doi.org/10.1016/0009-2541(94)90059-0

Morel F.M.M., Kraepiel A.M.L., and Amyot M., 1998. The Chemical Cycle and Bioaccumulation of Mercury. *Annual Review of Ecology and Systematics*. 29, 543–566. https://doi.org/10.1146/annurev.ecolsys.29.1.543

Morgan, R P. C. 2005. Soil erosion and conservation. Blackwell, Oxford, UK.

Moura, R.L.; Amado-Filho, G.M.; Moraes, F.C.; Brasileiro, P.S.; Salomon, P.S.; Mahiques, M.M.; et al. 2016. An extensive reef system at the Amazon River mouth. *Science Advances*, 2, 1501252. http://doi.org/10.1126/sciadv.1501252

Mulitza, S., Chiessi, C.M., Schefuß, E., Lippold, J., Wichmann, D., Antz, B., Mackensen, A., Paul, A., Prange, M., Rehfeld, K., Werner, M., Bickert, T., Frank, N., Kuhnert, H., Lynch-Stieglitz, J., Portilho-Ramos., R.C., Sawakuchi, A.O., Schulz, M., Schwenk, T., Tiedemann, R., Vahlenkamp, M. and Zhang, Y., 2017. Synchronous and proportional deglacial changes in Atlantic meridional overturning and northeast Brazilian precipitation. *Paleoceanography.* 32(6), 622–633. http://doi.org/10.1002/2017PA003084

Nace, T. E., Baker, P. A., Dwyer, G. S., Silva, C. G., Rigsby, C. A., Burns, S. J., … Zhu, J., 2014. The role of North Brazil Current transport in the paleoclimate of the Brazilian Nordeste margin and paleoceanography of the Western tropical Atlantic during the late Quaternary. *Palaeogeography, Palaeoclimatology, Palaeoecology.* 415, 3–13. http://doi.org/10.1016/j.palaeo.2014.05.030

Nicholson, 2000. The nature of rainfall variability over Africa on time scales of decades to millennia. *Global and Planetary Change.* 26, 137-158. https://doi.org/10.1016/S0921-8181(00)00040-0

Ning, S., and L. M. Dupont, 1997. Vegetation and climatic history of southwest Africa: A marine palynological record of the last 300,000 years. *Vegetation History and Archaeobotany*. 6(2), 17–131. https://doi.org/10.1007/BF01261959

North Greenland Ice Core Project members, 2004. High-resolution record of Northern Hemisphere climate extending into the last interglacial period. Nature, 431(7005), 147–151. http://doi.org/10.1038/nature02805

Nriagu, J.O., Pfeiffer, W.C., Malm, O., Souza, C.M.M. and Mierle, G., 1992. Mercury pollution in Brazil. *Nature.* 356, 389. http://dx.doi.org/10.1038/356389a010.1038/356389a0

Oliveira, S.M.B., Melfi, A.J., Fostier, A.H., Forti, M.C., Favaro, D.I.T., and Boulet, R., 2001. Soils as an important sink for mercury in the Amazon. *Water, Air and Soil Pollution*. 26, 321–337. https://doi.org/10.1007/s12665-018-7471-x

Outridge, P.M., Sanei, H., Stern, G.A., Hamilton, P.B. and Goodarzi, F., 2007. Evidence for control of mercury accumulation in sediments by variations of aquatic primary productivity in Canadian High Arctic lakes. *Environmental Science and Technology*. 41, 5259–5265. https://doi.org/10.1021/es070408x

Padberg, S. (1990). Mercury determinations in samples from Tapajós (Itaituba). Institut für angewandte Physikalische Chemie, Jülich, Germany,13.

Paula Filho, Marins R.V. and Lacerda L.D., 2015. Natural and anthropogenic emissions of N and P to the Parnaíba River Delta in NE Brazil. *Estuarine, Coastal and Shelf Science*. 166 (A), 34-44. https://doi.org/10.1016/j.ecss.2015.03.020

Pérez-Rodríguez, M., Horák-Terra, I., Rodríguez-Lado, L., Aboal, J. R., and Martínez Cortizas, A. 2015. Long-Term (~57 ka) Controls on Mercury Accumulation in the Souther Hemisphere Reconstructed Using a Peat Record from Pinheiro Mire (Minas Gerais, Brazil). *Environmental Science and Technology*, 49(3), 1356–1364. https://doi.org/10.1021/es504826d

Pfeiffer, W. C., and de Lacerda, L. D., 1988. Mercury inputs into the Amazon Region, Brazil. *Environmental Technology Letters.* 9(4), 325–330. https://doi.org/10.1080/09593338809384573

Pfeiffer, W.C., Lacerda, L.D., Malm, O., Souza, C.M.M., Silveira, E.G. and Bastos, W.R., 1989. Mercury concentrations in inland waters of gold mining areas in Rondonia, Brazil. *Science of the Total Environment.* (87/88), 233–240. https://doi.org/10.1016/0048-9697(89)90238-6

Pirrone N., Cinnirella S., Feng X., Finkelman R.B., Friedli H.R., Leaner J., Mason R., Mukherjee A.B., Stracher G.B., Streets D.G., et al., 2010. Global mercury emissions to the atmosphere from anthropogenic and natural sources. *Atmospheric Chemistry and Physics.* 10, 5951–5964. https://doi.org/10.5194/acp-10-5951-2010

Pirrone N., Cinnirella S., Feng X., Finkelman R.B., Friedli H.R., Leaner J., Mason R., Mukherjee A.B., Stracher G.B., Streets D.G., et al., 2010. Global mercury emissions to the atmosphere from anthropogenic and natural sources. *Atmospheric Chemistry and Physics*. 10, 5951–5964. https://doi.org/10.5194/acp-10-5951-2010

Prokoph, A., El Bilali, H., 2008. Cross-wavelet analysis: a tool for detection of relationships between paleoclimate proxy records. *Mathematical Geosciences.* 40, 575–586. https://doi.org/10.1007/s11004-008-9170-8

Pufahl, P.K., Maslin, M.A., Anderson, L., Brüchert, V., Jansen, F., Lin, H., Perez, M., Vidal, L., and Shipboard Scientific Party, 1998. Lithostratigraphic summary for Leg 175: Angola–Benguela upwelling system. In Wefer, G., Berger, W.H., and Richter, C., et al., Proc. ODP, Init. Repts., 175: College Station, TX (Ocean Drilling Program), 533–542. https://doi.org/10.2973/odp.proc.ir.175.118.1998

Ramlal, P. S., Bugenyi, F. W. B., Kling, G. W., Nriagu, J. O., Rudd, J. W. M., and Campbell, L. M. (2003). Mercury Concentrations in Water, Sediment, and Biota from Lake Victoria, East Africa. Journal of Great Lakes Research, 29, 283–291. https://doi.org/10.1016/s0380-1330(03)70555-3

Ramos, T.P.A., Ramos, R.T.C. and Ramos, S.A.Q.A., 2014. Ichthyofauna of the Parnaíba river Basin, Northeastern Brazil. *Biota Neotropica*. (14), 1–8. http://dx.doi.org/10.1590/S1676-06020140039

Ratter, J.A., Ribeiro, J.F., Bridgewater, S. 1997. The Brazilian Cerrado vegetation and threats to its biodiversity. *Annals of Botany*. 80: 223–230. http://doi.org/10.1006/anbo.1997.0469

Richardson, P. L., and Reverdin, G., 1987. Seasonal cycle of velocity in the Atlantic North Equatorial Countercurrent as measured by surface drifters, current meters, and ship drifts. *Journal of Geophysical Research: Oceans.* 92(C4), 3691–3708. http://doi.org/10.1029/JC092iC04p03691

Richey, J. E., Hedges, J. I., Devol, A. H., Quay, P. D., Victoria, R., Martinelli, L., Bruce, R. 1990. Biogeochemistry of carbon in the Amazon River. *Limnology and Oceanography*, 35, 352–371. http://doi.org/10.4319/lo.1990.35.2.0352

Rodrigues, R. R., Rothstein, L. M., and Wimbush, M., 2007. Seasonal Variability of the South Equatorial Current Bifurcation in the Atlantic Ocean: A Numerical Study. *Journal of Physical Oceanography.* 37(1), 16–30. http://doi.org/10.1175/JPO2983.1

Rolfhus, K.R., Fitzgerald, W.F., 1995. Linkages between atmospheric mercury deposition and the methylmercury content of marine fish. *Water, Air, Soil Pollution.* 80, 291–297. https://doi.org/10.1007/BF01189679

Roller, S., Wittmann, H., Kastowski, M., Hinderer, M., 2012. Erosion of the Rwenzori Mountains, East African Rift, from in situ-produced cosmogenic 10Be. *Journal of Geophysical Research*. 117, F03003. https://doi.org/10.1029/2011JF002117

Rommerskirchen, F., Eglinton, G., Dupont, L., Rullkötter, J., 2006. Glacial/interglacial changes in southern Africa: Compound-specific d13C land plant biomarker and pollen records from southeast Atlantic continental margin sediments. *Geochemistry, Geophysics, Geosystems.* 7, Q08010. https://doi.org/10.1029/2005GC001223

Roos-Barraclough, F., Martinez-Cortizas, A., García-Rodeja, E. and Shotyk,W., 2002. A 14500 year record of the accumulation of atmospheric mercury in peat: volcanic signals, anthropogenic influences and a correlation to bromine accumulation. *Earth and Planetary Science Letters.* 202(2), 435 – 451. https://doi.org/10.1016/S0012-821X(02)00805-1

Rosa, R.S., Menezes, N.A., Britski, H.A., Costa, W.J.E.M. and Groth, F., 2003. Diversidade, padro˜es de distribuic¸a˜o e conservac¸a˜ o dos peixes da Caatinga. In: Leal, I.R., Tabarelli, M. andSilva, J.M.C. Ecologia e Conservac¸a˜o da Caatinga. Recife: Editora Universita´ria da UFPE. p.135-162.

Roulet M., Lucotte M., Saint-Aubin A., Tran S., Rhéault I., Farell N., De Jesus Da Silva E., Dezencourt J., Sousa Passos C. J., Santos Soares G., Guimaraesc J. R. D., Mergler D., Amorime M., 1998. The geochemistry of mercury in central Amazonian soils developed on the Alter-do-Chão formation of the lower Tapajos River Valley, Para state, Brazil. *Science of the Total Environment.*, 223, 1-24.

Roulet, M. and Lucotte, M., 1995. Geochemistry of mercury in pristine and flooded ferralitic soils of a tropical rain forest in French Guiana, South America. *Water, Air and Soil Pollution.* 80, 1079–1088.

Roulet, M., Lucotte, M., Rheault, I., Tran, S., Farella, N., Canuel, R., Mergler, D. and Amorim, M., 1996. Mercury in Amazonian soils: accumulation and release. In: IV International Conference on the Geochemistry of the Earth's Surface. *Internatioal Association of Geochemistry and Cosmochemistry, Ilkley, Yorkshire, England*. 453–457.

Runge, J., 2008. The Congo River, Central Africa. In: Gupta, A. (Ed.), Large Rivers: Geomorphology and Management. Wiley and Sons, London, UK.

Ruth, U., Bigler, M., Röthlisberger, R., Siggaard-Andersen, M., Kipfstuhl, S., Goto-Azuma, K., Hansson, M. E., Johnsen, S. J., Lu, H. and Steffensen, J.P., 2007. Ice core evidence for a very tight link between North Atlantic and east Asian glacial climate. *Geophysical Research Letters.* 34, L03706, https://doi.org/10.1029/2006GL027876

Sachs, J. P., and R. F. Anderson, 2005. Increased productivity in the Subantarctic Ocean during Heinrich events. *Nature.* 434(7037), 1118–1120. http://doi.org/10.1038/nature03544

Salmond, J. A., 2005. Wavelet analysis of intermittent turbulence in a very stable nocturnal boundary layer: implications for the vertical mixing of ozone. *Boundary-Layer Meteorology*, 114(3), 463–488. https://doi.org/10.1007/s10546-004-2422-3

Santos, G.M., Cordeiro, R.C., Silva Filho, E.V., Turcq, B., Lacerda, L.D., Fifield, L.K., Gomes, P.R.S., Hausladen, P.A. and Sifeddine, A., 2001. Chronology of atmospheric mercury in Lagoa da Pata Lake, upper Rio Negro region of Brazilian Amazon. *Radiocarbon*. 43, 801- 808. http://doi.org/10.1017/S0033822200041473

Savoye, B., Babonneau, N., Dennielou, B., Bez, M., 2009. Geological overview of the Angola–Congo margin, the Congo deep-sea fan and its submarine valleys. *Deep-Sea Research II Topical Studies in Oceanography.* 56, 2169–2182. http://doi.org/10.1016/j.dsr2.2009.04.001

HatimSchneider, R.R., Price, B., Müller, P.J., Kroon, D., Alexander, I., 1997. Monsoon related variations in Zaire (Congo) sediment load and influence of fluvial silicate supply on marine productivity in the east 896 equatorial Atlantic during the last 200,000 years. *Paleoceanography.* 12, 463–481. https://doi.org/10.1029/96PA03640

Sholupov, S., Pogarev, S., Ryzhov, V., Mashyanov, N., Stroganov, A., 2004. Zeeman atomic absorption spectrometer RA-915+ for direct determination of mercury in air and complex matrix samples. *Fuel Processing Technology*, 85, 473 – 485. https://doi.org/10.1016/j.fuproc.2003.11.003

Schroeder, W. H. and Munthe, J., 1998. Atmospheric mercury: An overview. *Atmospheric Environment.* 32, 809–822. https://doi.org/10.1016/S1352-2310(97)00293-8

Schulz, M., and Mudelsee, M., 2002. REDFIT: Estimating red-noise spectra directly from unevenly spaced paleoclimatic time series. *Computers and Geosciences.* 28(3), 421–426. http://doi.org/10.1016/S0098-3004(01)00044-9

Schuster, E., 1991. The behavior of mercury in the soil with special emphasis on complexation and adsorption processes--A review of the literature. *Water, Air and Soil Pollution.* 56, 667-680, https://doi.org/10.1007/BF00342308

Selim H.M., ed., 2013. Competitive Sorption and Transport of Heavy Metals in Soils and Geological Media. CRC Press Taylor and Francis Group, 420pp

Selin N.E., Jacob D.J., Yantosca R.M., Strode S., Jaeglé L., and Sunderland E.M., 2008. Global 3-D land-ocean-atmosphere model for mercury: Present-day versus preindustrial cycles and anthropogenic enrichment factors for deposition. *Global Biogeochemical Cycles*. 22, 1–13. https://doi.org/10.1029/2007GB003040

Servain, J., Legler, D.M., 1986. Empirical orthogonal function analysis of tropical Atlantic sea surface temperature and wind stress. *Journal of Geophysical Research Atmospheres*. 91(C12), 181 - 191. https://doi.org/10.1029/JC091iC12p14181

Shackleton, N.J., Berger, A., Peltier, W.R., 1990. An alternative astronomical calibration of the lower Pleistocene time-scale based on ODP Site 677. *Transactions of the Royal Society of Edinburgh Earth Sciences*. 81, 252 – 261. https://doi.org/10.1017/S0263593300020782

Shannon, L.V., Boyd, A.J., Brundrit, G.B., Taunton-Clark, J., 1986. On the existence of an El Nino-type phenomenon in the Benguela system. *Journal of Marine Research.* 44, 495-520. https://doi.org/10.1357/002224086788403105

Shannon, L.V., Nelson, G., 1996. The Benguela: large scale features and processes and system variability. In: Wefer, G., Berger, W.H., Siedler, G., Webb, D. (Eds). The South Atlantic Ocean, Present and Past Circulation, Springer, Berlin, pp.163-217.

Silveira C.S., Brandão V.S., Bernedo A.V.B. and Mantovano J.L., 2016. Geochemistry of river suspended sediments in tropical watersheds: anthropogenic and granite-gneiss sources, SE Brazil. *International Journal of River Basin Management.* 14(4), 385–391. http://dx.doi.org/10.1080/15715124.2016.1213271

Skonieczny, C. McGee, D. Winckler, G. Bory, A. Bradtmiller, L.I. Kinsley, C.W. Polissar, P.J. De Pol-Holz, R. Rossignol, L. Malaizé, B., 2019. Monsoon-driven Saharan dust variability over the past 240,000 years. *Science Advances.* 5(1), eaav1887. https://doi.org/10.1126/sciadv.aav1887

Smith-Downey N. V., Sunderland E.M., and Jacob D.J., 2010. Anthropogenic impacts on global storage and emissions of mercury from terrestrial soils: Insights from a new global model. *Journal of Geophysical Research: Biogeosciences*. 115, 1–11. https://doi.org/10.1029/2009JG001124

Soerensen A.L., Sunderland E.M., Holmes C.D., Jacob D.J., Yantosca R.M., Skov H., Christensen J.H., Strode S.A., and Mason R.P., 2010. An improved global model for air-sea exchange of mercury: High concentrations over the North Atlantic. *Environmental Science and Technology.* 44, 8574–8580. https://doi.org/10.1021/es102032g

Soerensen, A. L.; Mason, R. P.; Balcom, P. H.; Jacob, D. J.; Zhang, Y.; Kuss, J.; Sunderland, E. M., 2014. Elemental mercury concentrations and fluxes in the tropical

atmosphere and ocean. *Environmental Science and Technology*. 48, 11312–11319. https://doi.org/10.1021/es503109p

Steffen A., Lehnherr I., Cole A., Ariya P., Dastoor A., Durnford D., Kirk J., and Pilote M., 2015. Atmospheric mercury in the Canadian Arctic. Part I: A review of recent field measurements. *Science of the Total Environment.* (509–510), 3–15. https://doi.org/10.1016/j.scitotenv.2014.10.109

Stern, G.A., Sanei, H., Roach, P., Delaronde, J. and Outridge, P.M., 2009. Historical interrelated variations of mercury and aquatic organic matter in lake sediment cores from a subarctic lake in Yukon, Canada: further evidence toward the algal-mercury scavenging hypothesis. *Environmental Science and Technology*. 43, 7684–7690. https://doi.org/10.1021/es902186s

Stouffer, R.J., Yin J., Gregory J.M., Kamenkovich I.V. and Sokolov A., 2006. Investigating the causes of the response of the thermohaline circulation to past and future climate changes. *Journal of Climate.* 19(8), 1365 – 1387. https://doi.org/10.1175/JCLI3689.1

Stramma, L., Fischer, J., and Reppin, J., 1995. The North Brazil Undercurrent. *Deep-Sea Research Part I.* 42(5), 773–795. http://doi.org/10.1016/0967-0637(95)00014-W.

Stramma, L.; England, M., 1999. On the water masses and mean circulation of the South *Atlantic Ocean. Journal of Geophysical Research.* 104(C9), 20863-20.

Sunderland E.M. and Mason R.P., 2007. Human impacts on open ocean mercury concentrations. *Global Biogeochemical Cycles.* 21(4) https://doi.org/10.1029/2006GB002876

Torrence C, Webster P.G., 1999. Interdecadal changes in the ENSO-Monsoon System. Journal of Climate. 12:2679–2690. https://doi.org/10.1175/1520-0442(1999)012<2679:ICITEM>2.0.CO;2

Uliana, E., Lange C.B., Wefer G. 2002. Evidence for Congo River freshwater load in Late Quaternary sediments of ODP Site 1077 (5°S, 10°E). Palaeogeography, Palaeoclimatology, Palaeoecology, 187(1-2), 137-150, https://doi.org/10.1016/S0031-0182(02)00514-X

Uliana, E., Lange, C.B., Donner, B. and Wefer, G. 2001. Siliceous phytoplankton productivity fluctuations in the Congo Basin over the past 460,000 years: marine vs. riverine influence, ODP Site 1077. In: WEFER, G., BERGER, W.H. and RICHTER, C. (eds) Proceedings of the Ocean Drilling Program, Scientific Results, 175. http://www-odp.tarnu.edu/ publications/175_SRfVOLUME/CHAPTERS/SR175_11.PDF

UNEP, 2013. Global Mercury Assessment (2013). Sources, Emissions, Releases and Environmental Transport. UNEP Chemicals Branch, Geneva, Switzerland.

van Bennekom, A.J., and Berger, G.W., 1984. Hydrography and silica budget of the Angola Basin. *Netherlands Journal of Sea Research.* 17, 149 –200. https://doi.org/10.1016/0077-7579(84)90047-4

van Iperen, J.M., van Weering, T.C.E., Jansen, J.H.F., and van Bennekom, A.J., 1987. Diatoms in surface sediments of the Zaire deep-sea fan (SE Atlantic Ocean) and their relation to overlying water masses. *Netherlands Journal of Sea Research.* 21:203–217. https://doi.org/10.1016/0077-7579(87)90013-5

Vandal, G.M., Fitzgerald, W.F., Boutron, C.F. and Candelone, J.P., 1993. Variations in mercury deposition to Antarctica over the past 34,000 years. *Nature.* 362 (6421), 621–623. https://doi.org/10.1038/362621a0

Venancio I. M., Mulitza S., Govin A., Santos T. P., Lessa D. O., Albuquerque A. L. S., Chiessi C. M., Tiedemann R., Vahlenkamp M., Bickert T., and Schulz M., 2018. Millennial- to orbital-scale responses of Western equatorial Atlantic thermocline depth to changes in the trade wind system since the Last Interglacial. *Paleoceanography and Paleoclimatology*. 33. https://doi.org/ 10.1029/2018PA003437

Wang, X., Auler, A. S., Edwards, L. L., Cheng, H., Cristalli, P. S., Smart, P. L., Shen, C. C., 2004. Wet periods in northeastern Brazil over the past 210 kyr linked to distant climate anomalies. *Nature.* 432(7018), 740–743. http://doi.org/10.1038/nature03067

Wasserman J.C., Hacon S. and Wasserman M.A., 2003. Biogeochemistry of Mercury in the Amazonian Environment. *AMBIO: A Journal of the Human Environment*. 32(5), 336-342. https://doi.org/10.1579/0044-7447-32.5.336

WHO, 1989. Environmental Health Criteria 86: Mercury - Environmental Aspects (Geneva).

Williams R.H., McGee D., Kinsley C.W., Ridley D.A., Hu S., Fedorov A., Tal I., Murray R.W. and deMenoca P.B., 2006. Glacial to Holocene changes in trans-Atlantic Saharan dust transport and dust-climate feedbacks. *Science Advances.* 2(11)1600445-1600445. https://doi/10.1126/sciadv.1600445

Xin ZB, Yu XX,and Lu X. X. 2010. Factors controlling sediment yield in China's Loess Plateau. *Earth Surface Processes and Landforms.* 36(6):816 – 826. https://doi.org/10.1002/esp.2109

Xinxiao Y,Henian W, Zhongbao X, Xizhi Lv. 2013. Effect of forest on sediment yield in North China. *International Soil and Water Conservation Research.* 1 (1), 58-64. https://doi.org/10.1016/S2095-6339(15)30050-2

Yang, H., Engstrom, D. R., and Rose, N. L. (2010). Recent Changes in Atmospheric Mercury Deposition Recorded in the Sediments of Remote Equatorial Lakes in the Rwenzori Mountains, Uganda. *Environmental Science and Technology.* 44(17), 6570–6575. https://doi.org/10.1021/es101508p

Zabel, M., Schneider, R.R., Wagner, T., Adegbie, A.T., de Vries, U., Kolonic, S., 2001. Late Quaternary climate changes in Central Africa as inferred from terrigenous input to the Niger Fan. *Quaternary Research.* 56(2), 207- 217. https://doi.org/10.1006/qres.2001.2261

Zhang, Y., Chiessi, C.M., Mulitza, S., Zabel, M., Trindade, R.I.F., Hollanda, M.H.B.M., Dantas, E.L., Govin, A., Tiedemann, R., Wefer, G., 2015. Origin of increased terrigenous supply to the NE South American continental margin during Heinrich Stadial 1 and the Younger Dryas. *Earth and Planetary Science Letters*. 432, 493–500. http://doi.org/10.1016/j.epsl.2015.09.054

Sediment core	Depth (cm)	Sample type	Lab. No.	Alignment to reference curve	Uncalibrated ages (yr BP)	Calibrated ages (yr BP)	Tie-point ages (yr)
GL-1248	1	*G. ruber; T. sacculifer*	Beta 423071		1140 ±30	679 (658-724)	
GL-1248	27	*G. ruber; T. sacculifer*	Beta 423082		5120 ±30	5460 (5331-5575)	
GL-1248	63	*G. ruber; T. sacculifer*	Beta 423072		9150 ±30	9728 (9599-9887)	
GL-1248	126	*G. ruber; T. sacculifer*	Beta 423073		10910 ±40	12478 (12260-12577)	
GL-1248	170	*G. ruber; T. sacculifer*	Beta 423074		12910 ±40	14776 (14372-15039)	
GL-1248	218	*G. ruber; T. sacculifer*	Beta 423075		25430 ±110	29062 (28769-29432)	
GL-1248	278	*G. ruber; T. sacculifer*	Beta 423076		27430 ±120	age reversal	
GL-1248	322	*G. ruber; T. sacculifer*	Beta 423083		29220 ±150	age reversal	
GL-1248	338	*G. ruber; T. sacculifer*	Beta 423077		27020 ±120	30861 (30661-31057)	
GL-1248	386	*G. ruber; T. sacculifer*	Beta 423085		29000 ±140	32666 (31959-33196)	
GL-1248	414	*G. ruber; T. sacculifer*	Beta 423078		31130 ±170	34661 (34303-35032)	
GL-1248	446	*G. ruber; T. sacculifer*	Beta 423084		32350 ±200	35857 (35401-36252)	
GL-1248	550	*G. ruber; T. sacculifer*	Beta 423079		35120 ±250	39227 (38675-39821)	
GL-1248	630	*G. ruber; T. sacculifer*	Beta 423080		40860 ±400	44035 (43335-44812)	
GL-1248	504	Ti/Ca		*to NGRIP-GICC05δ^{18}Oice*			38240/±2962
GL-1248	726	Ti/Ca		*to NGRIP-GICC05δ^{18}Oice*			46860/±3872
GL-1248	782	Ti/Ca		*to NGRIP-GICC05δ^{18}Oice*			48840/±4072
GL-1248	901	Ti/Ca		*to NGRIP-GICC05δ^{18}Oice*			54780/±4700
GL-1248	932	Ti/Ca		*to NGRIP-GICC05δ^{18}Oice*			55740/±4816

GL-1248	1008	Ti/Ca	*to NGRIP-GICC05δ^{18}Oice*	59320/±5176
GL-1248	1105	Ti/Ca	*to NGRIP-GICC05modelext δ^{18}Oice*	71060/±3966
GL-1248	1138	Ti/Ca	*to NGRIP-GICC05modelext δ^{18}Oice*	72340/±3550
GL-1248	1149	Ti/Ca	*to NGRIP-GICC05modelext δ^{18}Oice*	74440/±3862
GL-1248	1229	Ti/Ca	*to NGRIP-GICC05modelext δ^{18}Oice*	76460/±3636
GL-1248	1268	Ti/Ca	*to NGRIP-GICC05modelext δ^{18}Oice*	78280/±3452
GL-1248	1355	Ti/Ca	*to NGRIP-GICC05modelext δ^{18}Oice*	85160/±3572
GL-1248	1402	Ti/Ca	*to NGRIP-GICC05modelext δ^{18}Oice*	87960/±3466
GL-1248	1532	Ti/Ca	*to NGRIP-GICC05modelext δ^{18}Oice*	108300/±3646
GL-1248	1562	Ti/Ca	*to NGRIP-GICC05modelext δ^{18}Oice*	111140/±3528
GL-1248	1666	Ti/Ca	*to EDC-AICC2012 CH4*	128726/±3504

Supplementary Table 1